

1 Impact of PØD NuMu Samples in BANFF

2 Hogan, Matthew¹ and Toki, Walter¹

3 June 13, 2019

4 ¹Colorado State University, Fort Collins, USA

5 **Abstract**

6 This is the abstract

7 **Contents**

8	1 Introduction	10
9	1.1 ND280	10
10	1.1.1 The PØD	11
11	1.2 Usage of ND280 Psyche Software	12
12	2 ND280 Binned Likelihood	14
13	2.1 Motivation	14
14	2.2 Introduction to Conditional PDFs and Likelihoods	15
15	2.3 BANFF Fit Test Statistic	16
16	2.3.1 Flux, Cross Section, and Detector Systematics	20
17	3 PØD Selections and Data Samples	24
18	3.1 Global Reconstruction	24
19	3.2 PØD Selection Cuts	26
20	3.2.1 Pre-Selection Cuts	26
21	3.2.2 ν_μ CC Inclusive in FHC Cut	29
22	3.2.3 $\bar{\nu}_\mu$ CC Inclusive in RHC Cuts	29
23	3.2.4 ν_μ Background CC Inclusive in RHC Cuts	31
24	3.3 Sample Kinematics and Validation	31
25	3.4 PØD Water-Out Samples	32
26	3.4.1 CC Inclusive	33
27	3.4.1.1 ν_μ Selection in FHC Mode:	33
28	3.4.1.2 $\bar{\nu}_\mu$ Selection in RHC Mode:	40
29	3.4.1.3 ν_μ Background Selection in RHC Mode:	47
30	3.4.2 CC 1-Track (CCQE Enhanced)	54

31	3.4.2.1	ν_μ Selection in FHC Mode:	54
32	3.4.2.2	$\bar{\nu}_\mu$ Selection in RHC Mode:	61
33	3.4.2.3	ν_μ Background Selection in RHC Mode:	68
34	3.4.3	CC N-Tracks (CCnQE Enhanced)	68
35	3.4.3.1	ν_μ Selection in FHC Mode:	68
36	3.4.3.2	$\bar{\nu}_\mu$ Selection in RHC Mode:	75
37	3.4.3.3	ν_μ Background Selection in RHC Mode:	82
38	3.5	PØD Water-In Samples	82
39	3.5.1	CC Inclusive	83
40	3.5.1.1	ν_μ Selection in FHC Mode:	83
41	3.5.1.2	$\bar{\nu}_\mu$ Selection in RHC Mode:	90
42	3.5.1.3	ν_μ Background Selection in RHC Mode:	97
43	3.5.2	CC 1-Track (CCQE Enhanced)	97
44	3.5.2.1	ν_μ Selection in FHC Mode:	97
45	3.5.2.2	$\bar{\nu}_\mu$ Selection in RHC Mode:	104
46	3.5.2.3	ν_μ Background Selection in RHC Mode:	111
47	3.5.3	CC N-Tracks (CCnQE Enhanced)	111
48	3.5.3.1	ν_μ Selection in FHC Mode:	111
49	3.5.3.2	$\bar{\nu}_\mu$ Selection in RHC Mode:	112
50	3.5.3.3	ν_μ Background Selection in RHC Mode:	112
51	3.5.4	Differences Between Water-Out and Water-In Samples	112
52	4	PØD-Only BANFF Parameterization	113
53	4.1	PØD Samples Fit Binning	113
54	4.1.1	Fit Binning Determination	114
55	5	Detector Systematics	117

56	5.1 Detector Systematic Uncertainties	117
57	5.1.1 Efficiency-like Systematics	117
58	5.1.2 Observable Variation Systematics	118
59	5.1.3 Normalization Systematics	118
60	6 Fitter Validation	120
61	7 Fitter Results	121
62	8 Discussion	122
63	References	123
64	Nomenclature	125

65 **List of Figures**

66	1.1 Exploded view of the off-axis detectors of ND280	10
67	1.2 Cartoon of the PØD	11
68	1.3 Cartoon of an Individual PØDule	12
69	1.4 Fluxing Tuning Histogram for FHC Events	13
70	2.1 BANFF Pre-fit Flux Covariance Matrix	20
71	2.2 BANFF ND280 NuMu and ANuMu Flux Binning Parameters	21
72	2.3 Cross Section Parameters Pre-fit Correlation Matrix	21
73	3.1 PØD Air FHC ν_μ CC Inc. Lepton Cand. Reco. Momentum by True Particle	34
74	3.2 PØD Air FHC ν_μ CC Inc. Lepton Cand. Reco. $\cos\theta$ by True Particle . . .	35
75	3.3 PØD Air FHC ν_μ CC Inc. Lepton Cand. Reco. Momentum by NEUT Mode	36
76	3.4 PØD Air FHC ν_μ CC Inc. Lepton Cand. Reco. $\cos\theta$ by NEUT Mode . . .	37
77	3.5 PØD Air FHC ν_μ CC Inc. Lepton Cand. Reco. Momentum by True Topology	38
78	3.6 PØD Air FHC ν_μ CC Inc. Lepton Cand. Reco. $\cos\theta$ by True Topology . .	39
79	3.7 PØD Air FHC ν_μ CC Inc. Lepton Cand. True E_ν by NEUT Mode	40
80	3.8 PØD Air RHC $\bar{\nu}_\mu$ CC Inc. Lepton Cand. Reco. Momentum by True Particle	41
81	3.9 PØD Air RHC $\bar{\nu}_\mu$ CC Inc. Lepton Cand. Reco. $\cos\theta$ by True Particle . . .	42
82	3.10 PØD Air RHC $\bar{\nu}_\mu$ CC Inc. Lepton Cand. Reco. Momentum by NEUT Mode	43
83	3.11 PØD Air RHC $\bar{\nu}_\mu$ CC Inc. Lepton Cand. Reco. $\cos\theta$ by NEUT Mode . . .	44
84	3.12 PØD Air RHC $\bar{\nu}_\mu$ CC Inc. Lepton Cand. Reco. Momentum by True Topology	45
85	3.13 PØD Air RHC $\bar{\nu}_\mu$ CC Inc. Lepton Cand. Reco. $\cos\theta$ by True Topology . .	46
86	3.14 PØD Air FHC $\bar{\nu}_\mu$ CC Inc. Lepton Cand. True E_ν by NEUT Mode	47
87	3.15 PØD Air RHC ν_μ CC Inc. Lepton Cand. Reco. Momentum by True Particle	48
88	3.16 PØD Air RHC ν_μ CC Inc. Lepton Cand. Reco. $\cos\theta$ by True Particle . . .	49
89	3.17 PØD Air FHC ν_μ CC Inc. Lepton Cand. Reco. Momentum by NEUT Mode	50

90	3.18 PØD Air FHC ν_μ CC Inc. Lepton Cand. Reco. $\cos\theta$ by NEUT Mode	51
91	3.19 PØD Air FHC ν_μ CC Inc. Lepton Cand. Reco. Momentum by True Topology	52
92	3.20 PØD Air FHC ν_μ CC Inc. Lepton Cand. Reco. $\cos\theta$ by True Topology	53
93	3.21 PØD Air FHC ν_μ CC Inc. Lepton Cand. True E_ν by NEUT Mode	54
94	3.22 PØD Air FHC ν_μ CC Inc. Lepton Cand. Reco. Momentum by True Particle	55
95	3.23 PØD Air FHC ν_μ CC Inc. Lepton Cand. Reco. $\cos\theta$ by True Particle	56
96	3.24 PØD Air FHC ν_μ CC Inc. Lepton Cand. Reco. Momentum by NEUT Mode	57
97	3.25 PØD Air FHC ν_μ CC Inc. Lepton Cand. Reco. $\cos\theta$ by NEUT Mode	58
98	3.26 PØD Air FHC ν_μ CC Inc. Lepton Cand. Reco. Momentum by True Topology	59
99	3.27 PØD Air FHC ν_μ CC Inc. Lepton Cand. Reco. $\cos\theta$ by True Topology	60
100	3.28 PØD Air FHC ν_μ CC Inc. Lepton Cand. True E_ν by NEUT Mode	61
101	3.29 PØD Air RHC $\bar{\nu}_\mu$ CC Inc. Lepton Cand. Reco. Momentum by True Particle	62
102	3.30 PØD Air RHC $\bar{\nu}_\mu$ CC Inc. Lepton Cand. Reco. $\cos\theta$ by True Particle	63
103	3.31 PØD Air RHC $\bar{\nu}_\mu$ CC Inc. Lepton Cand. Reco. Momentum by NEUT Mode	64
104	3.32 PØD Air RHC $\bar{\nu}_\mu$ CC Inc. Lepton Cand. Reco. $\cos\theta$ by NEUT Mode	65
105	3.33 PØD Air RHC $\bar{\nu}_\mu$ CC Inc. Lepton Cand. Reco. Momentum by True Topology	66
106	3.34 PØD Air RHC $\bar{\nu}_\mu$ CC Inc. Lepton Cand. Reco. $\cos\theta$ by True Topology	67
107	3.35 PØD Air FHC $\bar{\nu}_\mu$ CC Inc. Lepton Cand. True E_ν by NEUT Mode	68
108	3.36 PØD Air FHC ν_μ CC N-Tracks Lepton Cand. Reco. Momentum by True	
109	Particle	69
110	3.37 PØD Air FHC ν_μ CC N-Tracks Lepton Cand. Reco. $\cos\theta$ by True Particle	70
111	3.38 PØD Air FHC ν_μ CC N-Tracks Lepton Cand. Reco. Momentum by NEUT	
112	Mode	71
113	3.39 PØD Air FHC ν_μ CC N-Tracks Lepton Cand. Reco. $\cos\theta$ by NEUT Mode	72
114	3.40 PØD Air FHC ν_μ CC N-Tracks Lepton Cand. Reco. Momentum by True	
115	Topology	73

116	3.41 PØD Air FHC ν_μ CC N-Tracks Lepton Cand. Reco. $\cos\theta$ by True Topology	74
117	3.42 PØD Air FHC ν_μ CC N-Tracks Lepton Cand. True E_ν by NEUT Mode . . .	75
118	3.43 PØD Air RHC $\bar{\nu}_\mu$ CC N-Tracks Lepton Cand. Reco. Momentum by True	
119	Particle	76
120	3.44 PØD Air RHC $\bar{\nu}_\mu$ CC N-Tracks Lepton Cand. Reco. $\cos\theta$ by True Particle .	77
121	3.45 PØD Air RHC $\bar{\nu}_\mu$ CC N-Tracks Lepton Cand. Reco. Momentum by NEUT	
122	Mode	78
123	3.46 PØD Air RHC $\bar{\nu}_\mu$ CC N-Tracks Lepton Cand. Reco. $\cos\theta$ by NEUT Mode .	79
124	3.47 PØD Air RHC $\bar{\nu}_\mu$ CC N-Tracks Lepton Cand. Reco. Momentum by True	
125	Topology	80
126	3.48 PØD Air RHC $\bar{\nu}_\mu$ CC N-Tracks Lepton Cand. Reco. $\cos\theta$ by True Topology	81
127	3.49 PØD Air FHC $\bar{\nu}_\mu$ CC N-Tracks Lepton Cand. True E_ν by NEUT Mode . .	82
128	3.50 PØD Water FHC ν_μ CC Inc. Lepton Cand. Reco. Momentum by True Particle	84
129	3.51 PØD Water FHC ν_μ CC Inc. Lepton Cand. Reco. $\cos\theta$ by True Particle .	85
130	3.52 PØD Water FHC ν_μ CC Inc. Lepton Cand. Reco. Momentum by NEUT Mode	86
131	3.53 PØD Water FHC ν_μ CC Inc. Lepton Cand. Reco. $\cos\theta$ by NEUT Mode .	87
132	3.54 PØD Water FHC ν_μ CC Inc. Lepton Cand. Reco. Momentum by True Topology	88
133	3.55 PØD Water FHC ν_μ CC Inc. Lepton Cand. Reco. $\cos\theta$ by True Topology .	89
134	3.56 PØD Water FHC ν_μ CC Inc. Lepton Cand. True E_ν by NEUT Mode . . .	90
135	3.57 PØD Water RHC $\bar{\nu}_\mu$ CC Inc. Lepton Cand. Reco. Momentum by True Particle	91
136	3.58 PØD Water RHC $\bar{\nu}_\mu$ CC Inc. Lepton Cand. Reco. $\cos\theta$ by True Particle .	92
137	3.59 PØD Water RHC $\bar{\nu}_\mu$ CC Inc. Lepton Cand. Reco. Momentum by NEUT Mode	93
138	3.60 PØD Water RHC $\bar{\nu}_\mu$ CC Inc. Lepton Cand. Reco. $\cos\theta$ by NEUT Mode .	94
139	3.61 PØD Water RHC $\bar{\nu}_\mu$ CC Inc. Lepton Cand. Reco. Momentum by True	
140	Topology	95
141	3.62 PØD Water RHC $\bar{\nu}_\mu$ CC Inc. Lepton Cand. Reco. $\cos\theta$ by True Topology .	96

142	3.63 PØD Water FHC $\bar{\nu}_\mu$ CC Inc. Lepton Cand. True E_ν by NEUT Mode	97
143	3.64 PØD Water FHC ν_μ CC 1-Track Lepton Cand. Reco. Momentum by True	
144	Particle	98
145	3.65 PØD Water FHC ν_μ CC 1-Track Lepton Cand. Reco. $\cos\theta$ by True Particle	99
146	3.66 PØD Water FHC ν_μ CC 1-Track Lepton Cand. Reco. Momentum by NEUT	
147	Mode	100
148	3.67 PØD Water FHC ν_μ CC 1-Track Lepton Cand. Reco. $\cos\theta$ by NEUT Mode	101
149	3.68 PØD Water FHC ν_μ CC 1-Track Lepton Cand. Reco. Momentum by True	
150	Topology	102
151	3.69 PØD Water FHC ν_μ CC 1-Track Lepton Cand. Reco. $\cos\theta$ by True Topology	103
152	3.70 PØD Water FHC ν_μ CC 1-Track Lepton Cand. True E_ν by NEUT Mode . .	104
153	3.71 PØD Water RHC $\bar{\nu}_\mu$ CC Inc. Lepton Cand. Reco. Momentum by True Particle	105
154	3.72 PØD Water RHC $\bar{\nu}_\mu$ CC Inc. Lepton Cand. Reco. $\cos\theta$ by True Particle . .	106
155	3.73 PØD Water RHC $\bar{\nu}_\mu$ CC Inc. Lepton Cand. Reco. Momentum by NEUT Mode	107
156	3.74 PØD Water RHC $\bar{\nu}_\mu$ CC Inc. Lepton Cand. Reco. $\cos\theta$ by NEUT Mode . .	108
157	3.75 PØD Water RHC $\bar{\nu}_\mu$ CC Inc. Lepton Cand. Reco. Momentum by True	
158	Topology	109
159	3.76 PØD Water RHC $\bar{\nu}_\mu$ CC Inc. Lepton Cand. Reco. $\cos\theta$ by True Topology .	110
160	3.77 PØD Water FHC $\bar{\nu}_\mu$ CC Inc. Lepton Cand. True E_ν by NEUT Mode	111
161	4.1 PØD Momenta Resolutions Used for Fit Binning	115
162	4.2 PØD Angular Residuals Used for Fit Binning	116

163 **List of Tables**

164 3.1 PØD WT FV and Corridor Definition	28
165 3.2 POT Used in This Analysis	32
166 5.1 [2]	119

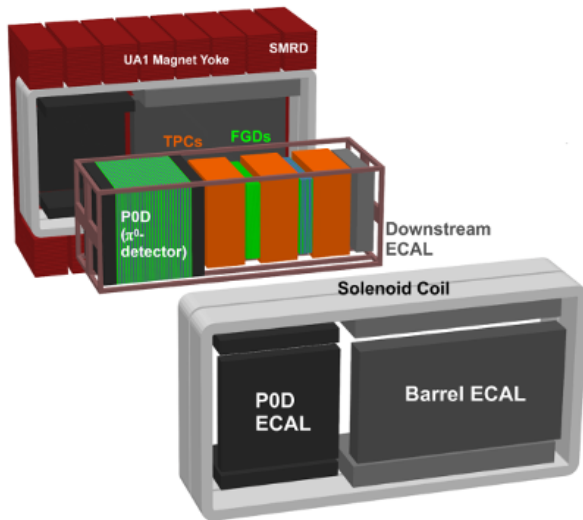


Figure 1.1: Exploded view of the off-axis detectors of ND280. The neutrino beam is directed from left to right along the figure.

167 1 Introduction

168 The primary goal of an oscillation experiment is to measure the parameters in a neutrino
 169 mixing matrix. All other parameters, with some having some theoretical importance to
 170 fundamental physics, are nuisance parameters. To understand the methodology of Beam
 171 and Near detector Flux task Force (BANFF) fit, it is relevant to understand how likelihood
 172 fitting works.

173 1.1 ND280

174 The T2K near detector (ND) complex consists of on-axis and off-axis detectors at 280m away
 175 from the secondary beamline proton target. The off-axis detector is used in this analysis
 176 which consists of several subdetectors housed inside the UA1/NOMAD magnet yoke as
 177 shown in figure 1.1. A similar analysis was also performed with the on-axis detector and is
 178 available in T2K-TN-335[14]. . The magnet provides a 0.2T magnetic field which is designed
 179 to provide momentum and particle identification for the tracker region.

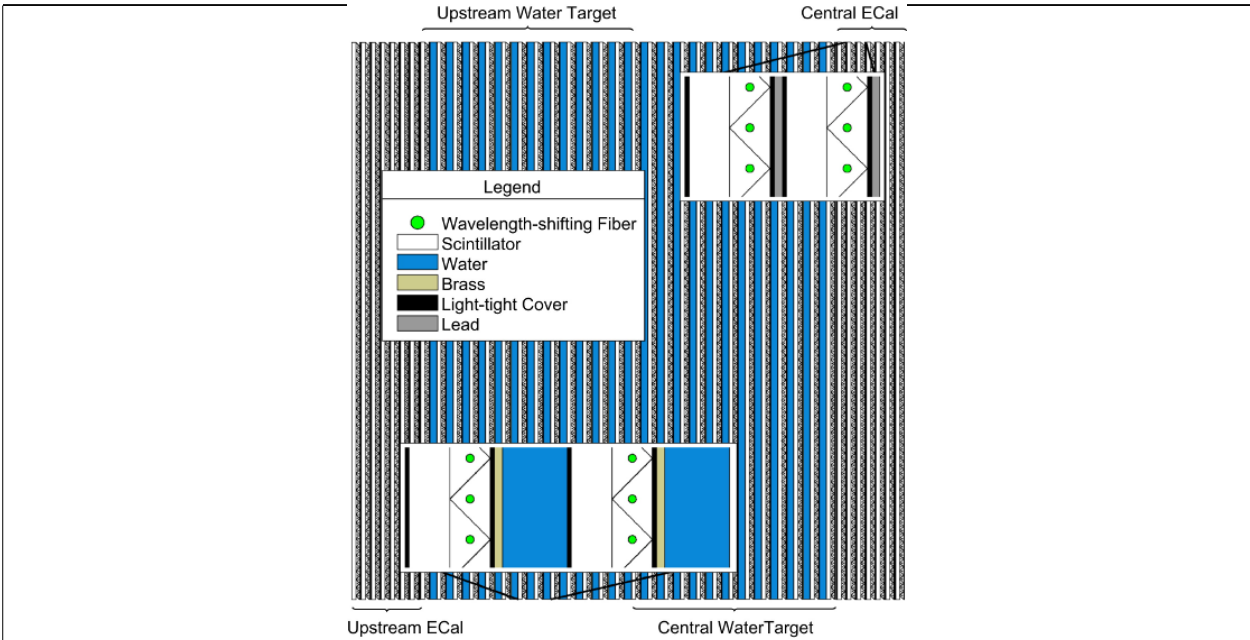


Figure 1.2: This cartoon illustrates the concept design of the PØD where the neutrino beam is approaching from the left.

180 1.1.1 The PØD

181 The PØD, short for π^0 Detector, is a plastic scintillator based tracking calorimeter inside the
182 ND280 basket. The PØD is constructed as many sandwiches of active and inactive materials
183 designed to fully contain π^0 decay photons. The four primary regions inside the PØD in
184 order of upstream to downstream of the neutrino beam are the upstream ECal (USECal),
185 upstream water target (WT), central WT, and central ECal (CECal). A representation of
186 the entire PØD can be seen in Figure 1.2. Each active module, also called a PØDule, consists
187 of two orthogonally oriented sheets of triangular, scintillator-doped plastic bars as shown in

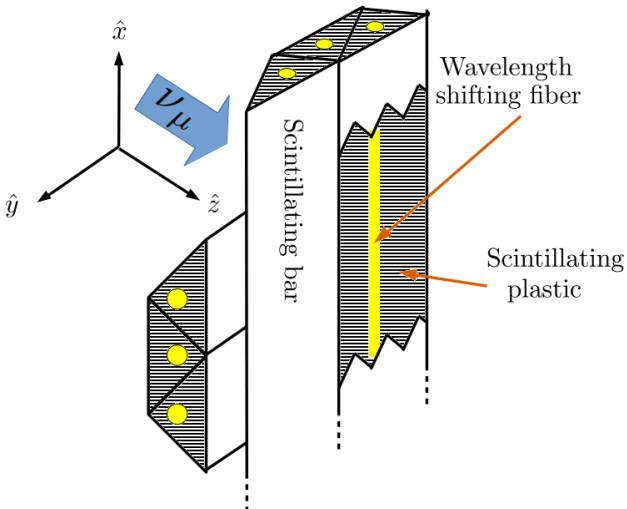


Figure 1.3: This cartoon illustrates the design of a PØDule with orthogonal layers of scintillating, triangular bars. When a charged particle travels through the bar such as a muon from CC interaction, the scintillation light is captured and wavelength shifted inside a fiber bored in the center of each bar. The wavelength shifted light is later observed by a photon counter.

188 Figure 1.3. The ECal regions are designed to contain decay photons inside the PØD by
 189 alternating the scintillator planes with lead sheets. The WT regions, as compared to the lead
 190 sheets in the ECals, alternate a thin brass sheet and water filled bags between the PØDules.
 191 A unique feature of the PØD is that the water can be drained out resulting in two detector
 192 configurations: water-in and water-out.

193 1.2 Usage of ND280 Psyche Software

194 Psyche is a general framework for data handling, event selections, and systematic evaluations
 195 with toy experiments. Psyche is a “lean” package from the perspective of analyzing MC
 196 events since that functionality is built heavily into Highland2. The analysis performed in
 197 this technical note required making additions to psyche in order replicate features available
 198 in Highland2. It would be wise for future analyses to build a selection in Highland2 and
 199 migrate that psyche once mature.

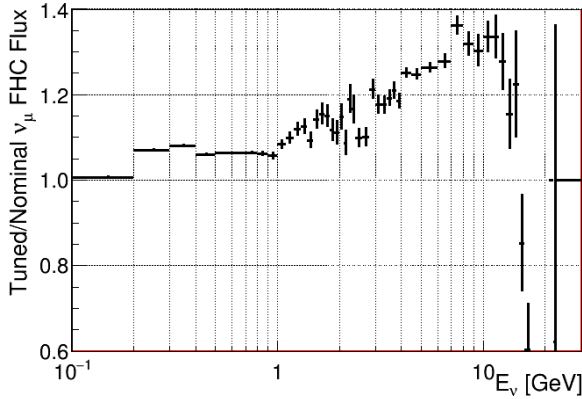


Figure 1.4: Fluxing tuning histogram for ν_μ FHC events taken from the 13av3 flux release.

BANFF uses a psyche package called psycheSteering that interfaces with all the psyche tools to manage the migration of samples into its analysis code. New PØD selections were added to the psycheSelections package and validated using the psycheSteering AnalysisManager class. The AnalysisManager provides the functionality to get the true and reconstructed detector observables from each reconstructed event along with the flux tuning and detector systematic weights.

Flux tuning is the process of applying an event weight based on the true neutrino energy, flavor, and run period. Since the ND280 MC uses a series of models to describe the expected neutrino flux, it cannot perfectly model the true flux nor know the beam conditions at run time. The beam group is responsible for releasing the expected and measured neutrino flux in order to account for these differences. To flux tune an event, the relevant neutrino flavor flux histogram must be referenced. The weight is extracted by taking the ratio of the tuned flux to the nominal flux in the MC for a given neutrino energy. As an example Figure 1.4 shows the flux tuning weights for true ν_μ FHC events.

214 **2 ND280 Binned Likelihood**

215 The BANFF likelihood maximization procedure is a binned likelihood maximization of the
216 ND280 data. In a ND280 and Super-Kamiokande (SK) joint fit, the measurements from both
217 detectors are considered along with their respective nuisance parameters. This approach
218 is more computationally expensive compared to the Markov Chain Monte Carlo analysis
219 (MaCh3) which will not be explained here. The BANFF likelihood maximization, hitherto
220 referred to as the “BANFF-fit”, includes nuisance parameters that affect the measurement of
221 the oscillation parameters, but are not physics goals of the T2K experiment. The BANFF-
222 fit parameters and their respective covariances are then used as inputs in the oscillation
223 analysis. This “divide-and-conquer” approach allows for more rapidly completed studies
224 on the effects of model parameters and biases present. Also this approach should provide
225 the same result with a joint ND280 and SK analysis as is performed in MaCh3. However,
226 information encoded in the ND280 measurements for shared nuisance parameters like the
227 neutrino flux is inevitably lost in the BANFF-fit.

228 The modern BANFF-fit likelihood is described in detail in TN-220[11]. It uses a fre-
229 quentist approach to find the best nuisance parameter set to maximize a binned likelihood.
230 Subsequent updates to the BANFF analysis[12, 5, 4] increase the sample sizes and systematic
231 parameterizations.

232 **2.1 Motivation**

233 Curve fitting is commonly found in the particle physics community literature due to the
234 need to compare two models or constrain unknown model parameters using one or more
235 histograms. For the first case, this involves two competing models, H_0 and H_1 , in order to
236 establish if the data supports new Physics (H_1) not predicted in the Standard Model (H_0).
237 The second case finds the “best” set of the model predictions, θ , that match the data as is the

case for the BANFF-fit. In both cases, chi-squared tests are performed to provide goodness of fit, parameter estimation (also referred to as “best fit parameters”), and error/confidence estimation.

2.2 Introduction to Conditional PDFs and Likelihoods

Consider the problem of extracting physics parameters \vec{y} given some data vector \vec{N} . The conditional probability density function (PDF) \mathcal{P} to measure these parameters is given as

$$\mathcal{P}(\vec{y}|\vec{N}) = \frac{\mathcal{L}(\vec{N}|\vec{y})\mathcal{P}(\vec{y})}{\int \mathcal{L}(\vec{N}|\vec{x})\mathcal{P}(\vec{x})d\vec{x}}, \quad (2.1)$$

where anything right of a vertical line represents a condition on the probability, $\mathcal{L}(\vec{N}|\vec{y})$ is the likelihood of the model with parameters \vec{y} , $\mathcal{P}(\vec{y})$ is the probability for the model, and the denominator is the normalization over all possible constraints on the observations. A frequentist interpretation of a PDF is a proportion of outcomes of repeated trials or experiments. A likelihood function is an expression of the probability of observing data as a function of the model parameters in their appropriate ranges.

One arrives at (2.1) by using the definition of compound probabilities

$$\mathcal{P}(A, B) = \mathcal{P}(B|A)\mathcal{P}(A) \quad (2.2)$$

to evaluate $\mathcal{P}(\vec{y}|\vec{N})$ as

$$\mathcal{P}\left(\underbrace{\vec{y}}_B \middle| \underbrace{\vec{N}}_A\right) = \frac{\mathcal{P}(\vec{N}, \vec{y})}{\mathcal{P}(\vec{N})} \quad (2.3)$$

with the denominator here is recognized as the normalization of the PDF. The compound

253 PDF $\mathcal{P}(\vec{N}, \vec{y})$ can expanded using Bayes' theorem which states

$$\mathcal{P}(A|B)\mathcal{P}(B) = \mathcal{P}(B|A)\mathcal{P}(A), \quad (2.4)$$

254 and combined with (2.2) yielding

$$\mathcal{P}\left(\underbrace{\vec{N}}_A, \underbrace{\vec{y}}_B\right) = \mathcal{P}(\vec{N}|\vec{y}) \times \mathcal{P}(\vec{y}), \quad (2.5)$$

255 where the PDFs to the left and right of the \times operator are recognized as the likelihoods and
256 priors, respectively. Combining resulting in (2.3) and (2.5) reproduces the original expression
257 of (2.1).

258 2.3 BANFF Fit Test Statistic

259 For the BANFF fit, one considers the problem of trying to maximize the agreement between
260 measured and predicted data histograms. This is equivalent to maximizing a binned likeli-
261 hood function \mathcal{L} of the data given the a set of parameters that predict the measured rate.
262 The use of likelihood functions in fits to histogram is explained further in reference [3] and
263 the PDG review on Statistics. By invoking Wilks' theorem, also known as the likelihood ratio
264 theorem, the likelihood maximization procedure is converted into a minimization problem
265 involving a test statistic denoted as a chi-squared. Below is an explanation of the BANFF
266 test statistic, $\Delta\chi^2$, and its systematic model terms.

267 Consider many binned samples that select different charged current topologies. A conve-
268 nient choice of observables for all the samples are the outgoing charged lepton l momentum P_l
269 and angle $\cos\theta_l$ as measured in ND280. Much of this is also documented in TN-220[11] where
270 additional details can be found. For each $(P_l, \cos\theta_l)$ analysis bin $i = 1, 2, \dots, M - 1, M$, the

271 likelihood is given by

$$\mathcal{L}(\vec{N}^d | \vec{N}^p) = \left(\prod_{i=1}^M \left(\vec{N}_i^p \right)^{\vec{N}_i^d} \frac{e^{-\vec{N}_i^p}}{\vec{N}_i^d!} \right) \quad (2.6)$$

272 where \vec{N}_i^d is the number of observed data events in the i th bin and \vec{N}_i^p is the number of
 273 predicted events as a function of nuisance parameters in the i th bin. One recognizes the
 274 likelihood function in (2.6) as a product of Poisson distributions with each corresponding
 275 to bins $i = 1, 2, \dots, M - 1, M$. The sets of dependent nuisance parameters, also sometimes
 276 called systematics, that affect the predicted event rate are

- 277 • cross section physics models, labeled as “xsec”,
- 278 • neutrino flux, and
- 279 • detector biases and inefficiencies.

280 Given these three sets of systematics, the number of predicted CC events from any neutrino
 281 flavor ν_l at ND280 is calculated using the general formula

$$N_{\nu_l} = \Phi_{\nu_l} \sum_t (\sigma_{\nu_l}^t M_t) \epsilon_{\nu_l}, \quad (2.7)$$

282 where Φ_{ν_l} is the flux of l flavor neutrinos, $\sigma_{\nu_l}^t$ is the cross section of the interaction for
 283 neutrino flavor l on target t , M_t is the number of t targets, and ϵ_{ν_l} is the total efficiency
 284 to reconstruct and properly identify the event as ν_l CC interactions. Each term in (2.7) is
 285 modeled carefully and the efficiency term is estimated using Monte Carlo (MC) simulations
 286 and control samples. The number of predicted events from the MC for a given analysis bin
 287 i is given by

$$\vec{N}_i^p(\vec{b}, \vec{x}, \vec{d}) = w_i^{\text{POT}} (\vec{d})_i^{\text{Det}} \sum_{j=1}^{N_i^{\text{MC}}} \left[\sum_{k=1}^{N^{\text{Flux}}} \left(\delta_{j,k}^{\text{Flux}} (\vec{b})_k^{\text{Flux}} \right) \prod_{l=1}^{N^{\text{xSyst}}} w_{j,l}((\vec{x})_l^{\text{xsec}}) \right]. \quad (2.8)$$

288 Here w_i^{POT} is the protons on target (POT) weight for the i th analysis which normalizes
 289 the MC statistics to expected data statistics. To account for the detector inefficiencies, the
 290 $(\vec{d})_i^{\text{Det}}$ parameters are normalization parameters that vary the total number of predicted
 291 events in the i th bin. Each $(\vec{d})_i^{\text{Det}}$ is determined prior to the fit by surveying over a large
 292 number of toy experiments with the detector systematics varied in each. The sum over
 293 $j = 1, 2, \dots, N_i^{\text{MC}} - 1, N_i^{\text{MC}}$ considers the contribution of all MC events in the i th analysis
 294 bin. The $(\vec{b})_k^{\text{Flux}}$ parameters, out of a total of N^{Flux} , are flux normalization systematics
 295 for each flux bin. Since the flux bins are categorized not only by neutrino energy, but also
 296 by flavor and horn current, the $\delta_{j,k}^{\text{Flux}}$ term in the sum over k selects the correct flux bin.
 297 The parameters $w_{j,l}$ are pre-calculated weights as a function for the l th cross section model,
 298 $(\vec{x})_l^{\text{xsec}}$, with a total of N^{xSyst} cross section model terms. Different t target materials have
 299 separate cross section parameters. Also the number of targets M_t can vary via detector
 300 systematics.

301 Using the likelihood ratio test theorem, a test statistic is defined as taking -2 times the
 302 natural logarithm of the ratio of predicted to observed likelihoods

$$\Delta\chi_{\text{LLR}}^2 = -2 \log \frac{\mathcal{L}(\vec{N}^d | \vec{N}^p)}{\mathcal{L}(\vec{N}^d | \vec{N}^d)}, \quad (2.9)$$

303 where this test statistic $\Delta\chi_{\text{LLR}}^2$ obeys a true chi-squared distribution for asymptotically
 304 large statistics and the likelihood functions are of the form (2.6). The denominator in (2.9)
 305 is the MC predicted probability which assumes the best maximum likelihood estimate is
 306 the number of observed events. Penalty terms from the cross section, flux, and detector
 307 systematics are included in order to prevent overfitting of the data. The new test statistic

308 for all of ND280, $\Delta\chi^2_{\text{ND280}}$, is given by

$$\Delta\chi^2_{\text{ND280}} = \Delta\chi^2_{\text{LLR}} + \Delta\chi^2_{\text{xsec}} + \Delta\chi^2_{\text{Flux}} + \Delta\chi^2_{\text{Det}} \\ - 2 \left(\log \frac{\mathcal{L}(\vec{N}^d | \vec{N}^p)}{\mathcal{L}(\vec{N}^d | \vec{N}^d)} + \underbrace{\log \pi(\vec{x})}_{\text{xsec}} + \underbrace{\log \pi(\vec{b})}_{\text{Flux}} + \underbrace{\log \pi(\vec{d})}_{\text{Det}} \right), \quad (2.10)$$

309 where each of the PDFs $\pi(\vec{y} = \vec{x}, \vec{b}, \vec{d})$ are assumed multivariate normal distributions

$$\pi(\vec{y}) = C_y e^{\left(-\frac{1}{2}\Delta\vec{y} \cdot V_y^{-1} \cdot \Delta\vec{y}^T\right)}, \quad (2.11)$$

310 $\Delta\vec{y}$ is a vector with the difference between the current/explored and nominal set of vector
 311 parameters \vec{y} , T corresponds to the transpose operator, and the normalization is given by

$$C_y = ((2\pi)^{k_y} \det(V_y))^{-\frac{1}{2}} \quad (2.12)$$

312 with V_y being the covariance matrix for a vector \vec{y} with k_y rows. The expanded form of the
 313 test statistic $\Delta\chi^2_{\text{ND280}}$ is given by

$$\Delta\chi^2_{\text{ND280}} = 2 \sum_{i=1}^M \left[\vec{N}_i^p - \vec{N}_i^d + \vec{N}_i^d \log \left(\frac{\vec{N}_i^d}{\vec{N}_i^p} \right) \right] \\ + \Delta\vec{x} \cdot (V_x^{-1}) \cdot \Delta\vec{x}^T + \Delta\vec{b} \cdot (V_b^{-1}) \cdot \Delta\vec{b}^T + \Delta\vec{d} \cdot (V_d^{-1}) \cdot \Delta\vec{d}^T \quad (2.13)$$

314 where the “ \cdot ” is the matrix multiplication operator. It must be stated that the test statistic
 315 (2.13) purposefully *excludes normalization terms*. Once the global minimum of the test
 316 statistic is found, the postfit covariance matrix V is calculated as the inverse of the Hessian
 317 matrix H

$$V_{i,j}(\hat{\vec{y}}) = (H_{i,j})^{-1} = \left(\frac{\partial^2}{\partial y_i \partial y_j} (\Delta\chi^2_{\text{ND280}}) \Big|_{\vec{y}=\hat{\vec{y}}} \right)^{-1} \quad (2.14)$$

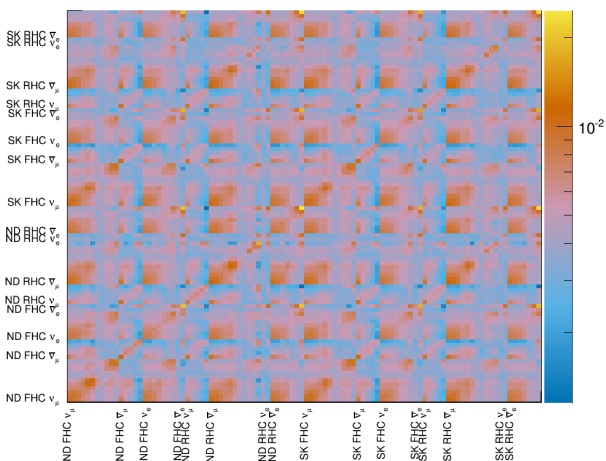


Figure 2.1: BANFF pre-fit flux covariance matrix shown with respective detector, horn current, and neutrino flavor.

318 where $y_i, y_j \in \vec{y}$ and $\hat{\vec{y}}$ is the maximum likelihood estimate for the parameters \vec{y} .

319 2.3.1 Flux, Cross Section, and Detector Systematics

320 Below is a description for each of the systematics in the BANFF likelihood and test statistic
 321 penalty terms. First is a description of flux, followed by the cross section, and finally the
 322 detector systematics.

323 **Flux:** The flux weight is binned as a function of neutrino energy, horn current/polarity
 324 (FHC and RHC), and neutrino flavor ($\nu_\mu, \bar{\nu}_\mu, \nu_e$, and $\bar{\nu}_e$). There are 50 ND280 and 50 SK
 325 parameters with an associated covariance matrix as shown in Figure 2.1. The binning and
 326 covariance matrix is provided by the T2K flux group prior to the BANFF analysis. Each
 327 flux bin is assigned a normalization parameter with initial value of one (1) for all events in
 328 that neutrino energy bin. A value of 1.1 indicates that any event in that energy bin has an
 329 additional weight of 1.1, or 10% increase in events. An example of the flux normalizations
 330 and uncertainties used in the 2017 analysis are shown in Figure 2.2.

331 **Cross Section:** There are a number of cross section model systematics implemented in
 332 BANFF to account for the uncertainties in cross section measurements. The cross section

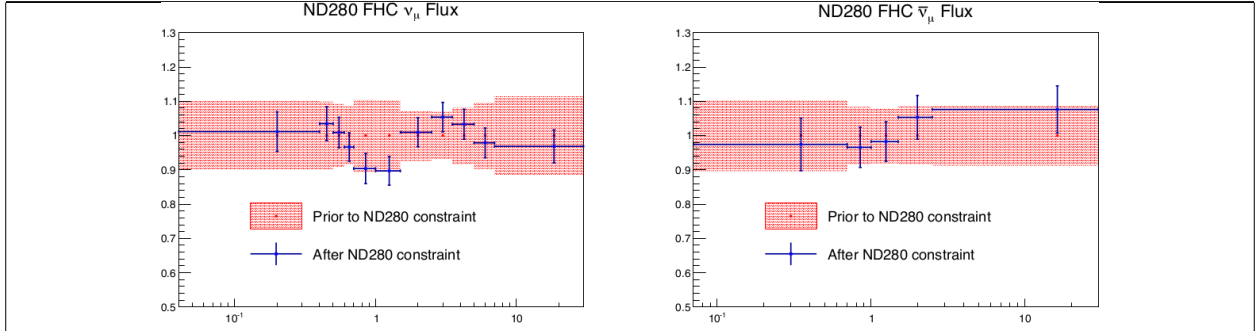


Figure 2.2: BANFF ND280 flux ν_μ and $\bar{\nu}_\mu$ binning parameters from T2K-TN-324 data post-fit results. The uncertainties are extracted from the pre-fit and post-fit covariance matrices.

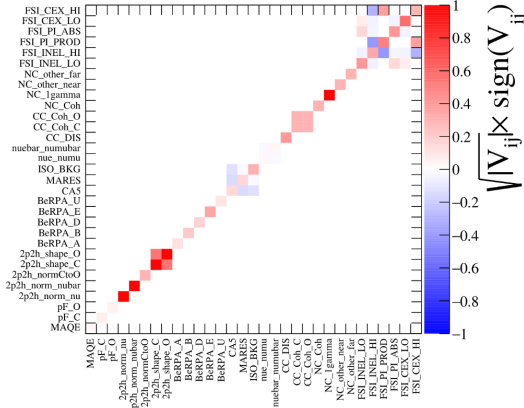


Figure 2.3: Cross section parameters pre-fit correlation matrix from the 2017 BANFF analysis.

models used in this analysis are the 2017 Neutrino Interactions Working Group (NIWG) parameterization, which is a canonical set of parameters and covariance matrix shared among all analyses in T2K. A technical description of the 2017 parameterization is given in TN-315[6] and TN-307[15]. There are a total of 25 cross section parameters for interactions like meson exchange current that affect the shape and normalization of the cross section. The cross section correlation matrix is shown in Figure 2.3[5].

Detector Systematic Errors: Detector systematics are implemented in BANFF to account for uncertainties in detector efficiencies. Since neutrino interaction events can migrate from sample-to-sample, bin-to-bin, or both depending on the relevant systematics, numerous toy experiments are performed by varying parameters that model known detector

343 systematics.

344 After many toy experiments, a covariance matrix among the bins is constructed con-
345 sidering correlations and statistical errors. This detector covariance matrix is fractional to
346 be consistent with the definitions for the flux and cross section covariance matrices. The
347 detector covariance matrix, σ_{Det}^2 , between bins x and y given explicitly as

$$\sigma_{\text{Det}}^2(x, y) = \frac{1}{x_{\text{Nom}}} \frac{1}{y_{\text{Nom}}} (\sigma_{\text{Cov}}^2(x, y) + \sigma_{\text{Stat}}^2(x, y)), \quad (2.15)$$

348 where ‘‘Nom’’, ‘‘Cov’’, and ‘‘Stat’’ refer to the nominal MC prediction, covariance, and sta-
349 tistical uncertainties for bins x and y , respectively. The nominal bin expectation for bin x
350 is

$$x_{\text{Nom}} = \sum_{k=1}^{N_x^{\text{MC}}} w_k, \quad (2.16)$$

351 where N_x^{MC} being the number of predicted MC events in the bin and w_k being the product
352 of all the weights applied to the k th event (see (2.8) for all possible weights). The covariance
353 and statistical terms are given by

$$\begin{aligned} \sigma_{\text{Cov}}^2(x, y) &= \frac{1}{N_{\text{Toy}}} \sum_{t=1}^{N_{\text{Toy}}} (x_t - \bar{x})(y_t - \bar{y}) \\ \sigma_{\text{Stat}}^2(x, y) &= \delta(x, y) \sum_{k=1}^{N_x^{\text{MC}}} w_k^2, \end{aligned} \quad (2.17)$$

354 where N_{Toy} is the number of toy experiments, \bar{x} is the mean of the all the toy experiments
355 in bin x , and $\delta(x, y)$ is the Kronecker delta function. Additional uncertainties like fake data
356 contributions are added to the covariance in quadrature.

357 While there could be one detector systematic normalization for each analysis bin, also
358 called a observable normalization, a single one can be assigned to multiple analysis bins to
359 reduce the number of fit parameters. This procedure requires careful consideration of the

360 shared detector systematics among analysis bins. A considerable drawback to designing nor-
361malizations in this way is that not all detector systematics are Gaussian with respect to the
362observables ($P_l, \cos \theta_l$), and so the covariance matrix may not be an accurate representation
363of the detector systematics.

364 **3 PØD Selections and Data Samples**

365 This section describes the development of ν_μ and $\bar{\nu}_\mu$ CC Inclusive selections in both FHC
366 and RHC beam configuration for PØD-based analyses. These selections are the continuation
367 of previous works that developed ν_μ CC Inclusive selections between the PØD and TPC1.
368 The first such analyses were T2K-TN-80 and T2K-TN-100 which described the ν_μ CC In-
369 clusive event selection and, later, cross-section analysis using ND280 Production 5 software,
370 respectively[8, 9]. These analyzes relied on each sub-detector’s reconstruction software and
371 developed a track matching algorithm since the ND280 “Global” reconstruction matching
372 was problematic in Production 5. As the inter-detector matching reconstruction improved in
373 “Global”, two CC-0 π cross section analyzes, T2K-TN-258 and T2K-TN-328, were developed
374 that also used the CC Inclusive selection as pre-selection cuts[17, 7]. The selections described
375 in this technical note also employ the same pre-selection cuts. What follows from here in
376 this section is a layout of the following topic discussions.

377 The first topic discussed in this section is a description of the π^0 Detector (PØD). The
378 next topic is the event reconstruction using the “Global” reconstruction software. Following
379 that is the pre-selection cut flow. With the pre-selection cuts established, each of the three
380 CC Inclusive selection’s cut flow is described. Concluding this section is a discussion of the
381 three samples in the following order: ν_μ in FHC mode, $\bar{\nu}_\mu$ in RHC, and ν_μ background in
382 RHC.

383 **3.1 Global Reconstruction**

384 The task of the Global reconstruction is to combine all the ND280 information into a com-
385 bined reconstructed object. It was originally designed to analyze “CCQE-like” events in the
386 Tracker region and has been extended to operate with all of ND280. A brief description
387 of the Global reconstruction is described below. First the specific detector technologies and

388 electronics of ND280 are explained. That is followed by the calibration procedure to properly
389 tune each detector’s response. And finally a general outline of the reconstruction algorithms
390 to form tracks and vertices in ND280 is presented.

391 ND280 events are first collected in the form of electronic signals from either multipixel
392 photon counters (MPPCs) in the scintillator-based sub-detectors or charge collection planes
393 of the time projection chambers (TPCs). MPPCs were chosen for the scintillator-based sub-
394 detectors since they are insensitive to the strong 0.2T magnetic field present in ND280. The
395 PØD, ECals, and SMRD all share the same “Trip-T” frontend board (TFB) electronics of
396 which collect the photoelectrons released when photons interact with a pixel in the MPPCs.
397 The FGDs operate with the same MPPC technology while using different frontend electron-
398 ics. The TPCs utilize a locally strong electric field to collect ionization electrons from an
399 Argon-based gas. Collected charge in the TPCs are collected and enhanced using micromega
400 technology[1]. With the collected information from each sub-detector, the next step is the
401 data calibration.

402 Data calibration in ND280 is the process where the charge and timing information col-
403 lected from each sub-detector is adjusted to match with expected parameters. This is an
404 important process that takes into account environmental changes, aging effects, and other
405 behavior that might be present. Calibration data is collected frequently before and during
406 operational runtime and is stored in a database for later use. A common calibration is to
407 measure the detector’s cosmic ray response since most cosmic rays deposit the same energy
408 per unit length. After the data has been calibrated, reconstruction algorithms now attempt
409 to find charged particle tracks in the data.

410 The Global reconstruction is a software package that attempts to recognize patterns of
411 data to form tracks and find vertices for those tracks. Particle shower reconstruction in
412 Global will not be discussed in this TN since no shower objects are used. Each sub-detector
413 reconstruction is run to seeds Global’s track matching algorithms. Global attempts to then

414 re-fit sub-detector tracks using a Kalman filter while correcting for particle energy loss as a
415 function of length (dE/dx) and multi-scattering processes. A vertex is then associated with
416 the re-fit track using another Kalman filter algorithm. A further detailed description of the
417 track matching and vertex finding algorithms for Global is described in T2K-TN-46[16].

418 **3.2 PØD Selection Cuts**

419 The selection of CC Inclusive events use a series of cuts to select the primary lepton. The
420 pre-selection cuts (“precuts”) are applied first to extract events that start in the PØD FV.
421 A MIP is more likely to reach TPC1 from the PØD FV since the PØD is constructed out
422 of heavy materials especially in the CECal. So the main track each selection is designed to
423 select a muon.

424 This following sections will describe the precuts common to all CC Inclusive selections
425 and the branching of different cuts, after the precuts, to select the main track.

426 **3.2.1 Pre-Selection Cuts**

427 The pre-selection (“precuts”) were initially developed to select ν_μ CC Inclusive using the PØD
428 and TPC sub-detector reconstruction softwares separately[8]. They were then used with the
429 Global reconstruction software for the ν_μ CC-0 π selection in the FHC beam configuration as
430 described in technical note T2K-TN-258[17]. The description and flow of the precuts are
431 described here as well since there is an incomplete description of the selection precuts.

432 The precuts are performed on each bunch per beam spill as follows

- 433 1. The event has a “good” data quality flag.
 - 434 • An event is rejected if any sub-detector or electronics in ND280 reported as “bad”
435 during that bunch.
- 436 2. There is at least one (1) track reconstructed in TPC1.

- 437 • There are no restrictions on the number of tracks fully contained in the PØD or
438 exiting into other sub-detectors.

439 3. The track in TPC1 must have more than 18 nodes.

- 440 • The TPC reconstruction gathers vertical and horizontal hits into clusters of hits.
441 The charge distribution of the cluster is used to get a vertical (horizontal) position
442 that is more accurate than the individual readout pads. A node is constructed
443 out of each cluster with associated track state information. The set of nodes are
444 used to fit the track helix[13].

445 4. The reconstructed vertex is within the PØD WT FV.

- 446 • The PØD FV is defined to include as much as the WT regions as possible. Its
447 X and Y borders are 25 cm away from the PØDule edges while its Z borders
448 intersect the last and first half downstream PØDule in the USECal and CECal,
449 respectively. The enumerated volume edges are shown in table 3.1. This volume,
450 while used for track-based analyzes in the past, was optimized for π^0 and ν_e
451 analyzes[10].

452 5. All tracks that enter TPC1 pass the veto cut

- 453 • An event is rejected if any PØD track enters TPC1 from outside the “corridor”
454 volume. This cut was designed to eliminate broken tracks between the PØD and
455 TPC1 when the separate sub-detector reconstructions were used[8]. In practice,
456 this cut ensures that Global tracks entering TPC1 away from its X and Y edges.
457 The corridor definition is the same as defined in T2K-TN-208 and shown in Ta-
458 ble 3.1.

PØD WT FV			Corridor Volume		
-836	< X <	764	-988	< X <	910
-871	< Y <	869	-1020	< Y <	1010
-2969	< Z <	1264	-3139	< Z <	-900

Table 3.1: The PØD WT FV (left) and veto corridor volume (right) in the ND280 coordinate system. The corridor spans from the 5th (8th) to 40th (80th) PØDule (scintillator layer). All the units are given in millimeters.

459 After passing all the precuts, a single, global track, which is observed in TPC1, is assigned
460 as the lepton candidate or “main track” of a selection.

461 The momentum of the main track, P , is sum of its momentum in the TPC, P_{TPC} , with
462 the estimate momentum lost in the PØD, $\Delta P_{\text{PØD}}$

$$P = P_{\text{TPC}} + \Delta P_{\text{PØD}}. \quad (3.1)$$

463 Momentum lost in the PØD is estimated by summing the energy loss (dT/dx) in along the
464 track path dx

$$\Delta T = \int \left(\frac{dT}{dx} \right) dx. \quad (3.2)$$

465 Using the chain rule, we can convert the energy loss into momentum loss

$$\begin{aligned} \frac{dT}{dx} &= \left(\frac{dT}{dP} \right) \left(\frac{dP}{dx} \right) \\ &= \left(\frac{Pc^2}{E} \right) \left(\frac{dP}{dx} \right) \\ &= \beta c \left(\frac{dP}{dx} \right), \end{aligned} \quad (3.3)$$

466 where β is the particle velocity as a ratio of the speed of light c . The fundamental theorem

467 of Calculus permits the us to write the energy loss now as a momentum loss

$$\Delta P_{\text{P}\emptyset\text{D}} = \int \left(\frac{dP}{dx} \right) dx = \frac{1}{c} \int \left[\left(\frac{dT}{dx} \right) \frac{1}{\beta} \right] dx.$$

468 Since we cannot take infinitesimally small steps along the track, we must replace the integral
469 with a sum and $dx \rightarrow \Delta x$ to arrive at the expression of the momentum loss estimate in the
470 P \emptyset D

$$P = P_{\text{TPC}} + \frac{1}{c} \sum_t \left[\left(\frac{dT}{dx} \right) \left(\frac{\Delta x}{\beta} \right) \right]_t. \quad (3.4)$$

471 For most tracks entering the TPC, they will be highly relativistic in the P \emptyset D ($\beta(x) \approx 1$),
472 and (3.4) becomes

$$P = P_{\text{TPC}} + \frac{1}{c} \sum_t \left[\left(\frac{dT}{dx} \right) \Delta x \right]_t \quad (3.5)$$

473 The next sections describe the selection cuts. irst in FHC mode and then RHC mode.

474 **ν_μ CC Inclusive in FHC Cut**

- 475 • The highest momentum negatively charged track (HMNT) is the lepton candidate

476 As discussed in Section section 3.2.1 on page 26, this selection is the basis for the ν_μ CC-0 π
477 P \emptyset D+TPC1 analysis. In FHC mode, the vast majority of neutrino interactions are ν_μ CC
478 events producing an outgoing, negatively charged muon. So if there is no negatively charged
479 track in the TPC, the event is rejected.

480 **$\bar{\nu}_\mu$ CC Inclusive in RHC Cuts**

- 481 • The highest momentum positively charged track (HMPT) is the lepton candidate
482 • The HMPT must be the highest momentum track (HMT)

483 In RHC, the majority of neutrinos in the beam is $\bar{\nu}_\mu$ since the horn focuses negatively charged
484 pions. To select $\bar{\nu}_\mu$ CC interaction events by selecting positively charged muons, the lepton

candidate is the HMPT in the TPC. The event is rejected if there is no positively charged track. However, since the RHC mode beam is not as $\bar{\nu}_\mu$ pure as the FHC beam, another cut was added to reduce this effect.

Since RHC neutrino beam can be described as a $\bar{\nu}_\mu$ -enhanced beam, the HMPT must also be the HMT due to the significant “wrong-sign” ν_μ background. This effect is two fold due to the nature of the neutrino source and the cross section between neutrinos and antineutrinos.

Firstly the neutrino flux is larger in RHC mode due to neutrino production at the target. The source of neutrinos are from protons, which have positive charge, on a graphite target. This method is more likely to produce positively charged pions in the target than negatively charged one. While the horns are designed to select the negatively charged pions in RHC mode, the excess amount of positively charged pions will penetrate the horns’ filter. Therefore there are many more $\pi^+ \rightarrow \mu^+ + \nu_\mu$ decays in RHC compared to FHC mode.

Secondly, antineutrino interactions on matter are suppressed compared to neutrinos due to helicity considerations. Consider neutrino-electron scattering, the cross section for $\nu_e + e^-$ is given by

$$\frac{d\sigma}{d\Omega} = \left(\frac{G \hbar c}{2\pi} \right)^2 s, \quad (3.6)$$

where G is the Fermi constant and s is the center of mass energy squared. The outgoing particles are isotropic since the initial and final spin state of the system is $J = 0$. Compare (3.6) with the cross section for $\bar{\nu}_e + e^-$

$$\frac{d\sigma}{d\Omega} = \left(\frac{G \hbar c}{4\pi} \right)^2 (1 - \cos \theta)^2 s, \quad (3.7)$$

where θ is the observed scattering angle of the electron. Since the total spin of the $\bar{\nu}_e + e^-$ system is $J = 1$ with the $J_z = 1$, the antineutrino is preferentially forward scattered.

506 Integrating over all angles, the cross sections come out to

$$\sigma(\bar{\nu}_e + e^-) = \frac{1}{3}\sigma(\nu_e + e^-).$$

507 The factor 1/3 arises from the fact that angular momentum conservation forbids the $J_z = -1$
508 and 0 states for $\bar{\nu}_e + e^-$ scattering. The same 1/3 factor arises with e^- replaced with quarks.
509 Therefore the cross sections for neutrinos are larger than antineutrinos.

510 **ν_μ Background CC Inclusive in RHC Cuts**

- 511 • The highest momentum negative track (HMNT) is the lepton candidate
- 512 • The HMNT must be the highest momentum track (HMT)

513 As discussed in section 3.2.3 on page 29, the RHC neutrino beam has a significant wrong-
514 sign ν_μ background. The selection of the HMNT is designed to select the negatively charged
515 muons. To prevent selecting the antineutrino events, the HMNT must also be the HMT.
516 The event is rejected if there is no negatively charged track. If there are both positively and
517 negatively charged tracks, the HMT cut discriminates if the event originates from a ν_μ or
518 $\bar{\nu}_\mu$.

519 **3.3 Sample Kinematics and Validation**

520 This section examines the kinematics for each of selections while differentiating between
521 water-in and water-out mode. The selection cuts were implemented in Psyche which is the
522 software interface that BANFF uses to select events. An analysis of the kinematics are care-
523 fully cross validated with the same selection cuts in the T2K high level analysis framework
524 called Highland. Comparing the results between Highland and Psyche is important since
525 they are complementary frameworks within T2K. The data sets used in this analysis are

Run Period	Horn Current	PØD Status	Data POT ($\times 10^{20}$)	MC POT ($\times 10^{20}$)
2	+250 kA	Water	0.4339	12.03
		Air	0.3591	9.239
3b	+205 kA		0.2172	4.478
3c	+250 kA		1.364	26.32
4			1.782	34.99
		Water	1.642	34.97
5c	-250 kA		0.4346	22.77
6b		Air	1.288	14.17
6c			0.5058	5.275
6d			0.7753	6.884
6e			0.8479	8.594
7b		Water	2.436	33.70
8	+250 kA		1.580	26.46
		Air	4.148	36.06
Sand	FHC		-	11.19
Sand	RHC		-	12.92
2, 3b, 3c, 4, 8	FHC	Air	7.872	79.18
		Water	3.657	73.47
6b, 6c, 6d, 6e	RHC	Air	3.417	34.92
		Water	2.871	56.48

Table 3.2: T2K MC and data POT divided by run periods. The bottom four rows are the aggregated periods grouped by horn current and PØD status which is how the data analysis is performed.

526 runs 2-8 in both PØD water-in and water-out (air) modes as shown in Table 3.2.

527 3.4 PØD Water-Out Samples

528 This section shows the kinematic distributions for the PØD water-out samples. First an
 529 examination of the CC Inclusive samples and the effects of the systematic weights will be
 530 explored. The samples are then examined as CC 1-track and CC N-tracks.

531 **3.4.1 CC Inclusive**

532 The CC Inclusive sample cuts are discussed 3.2.1. Since both flux and systematic weights
533 are applied to all MC events in BANFF, it is important to validate the event weights. Using
534 neither set of weights is referred to as the nominal MC.

535 **3.4.1.1 ν_μ Selection in FHC Mode:** Shown in Figures 3.1 to 3.7 are the momentum
536 and $\cos\theta$ distributions for ν_μ CC Inclusive events in FHC mode. There are three pairs of
537 P, θ figures with the same truth information break down accompanied by one of neutrino
538 energy. The truth information categories are lepton candidate particle, NEUT reaction, and
539 topology. Each figure consists of a set of four sub-figures which illustrate the application of
540 flux and detector systematic weights.

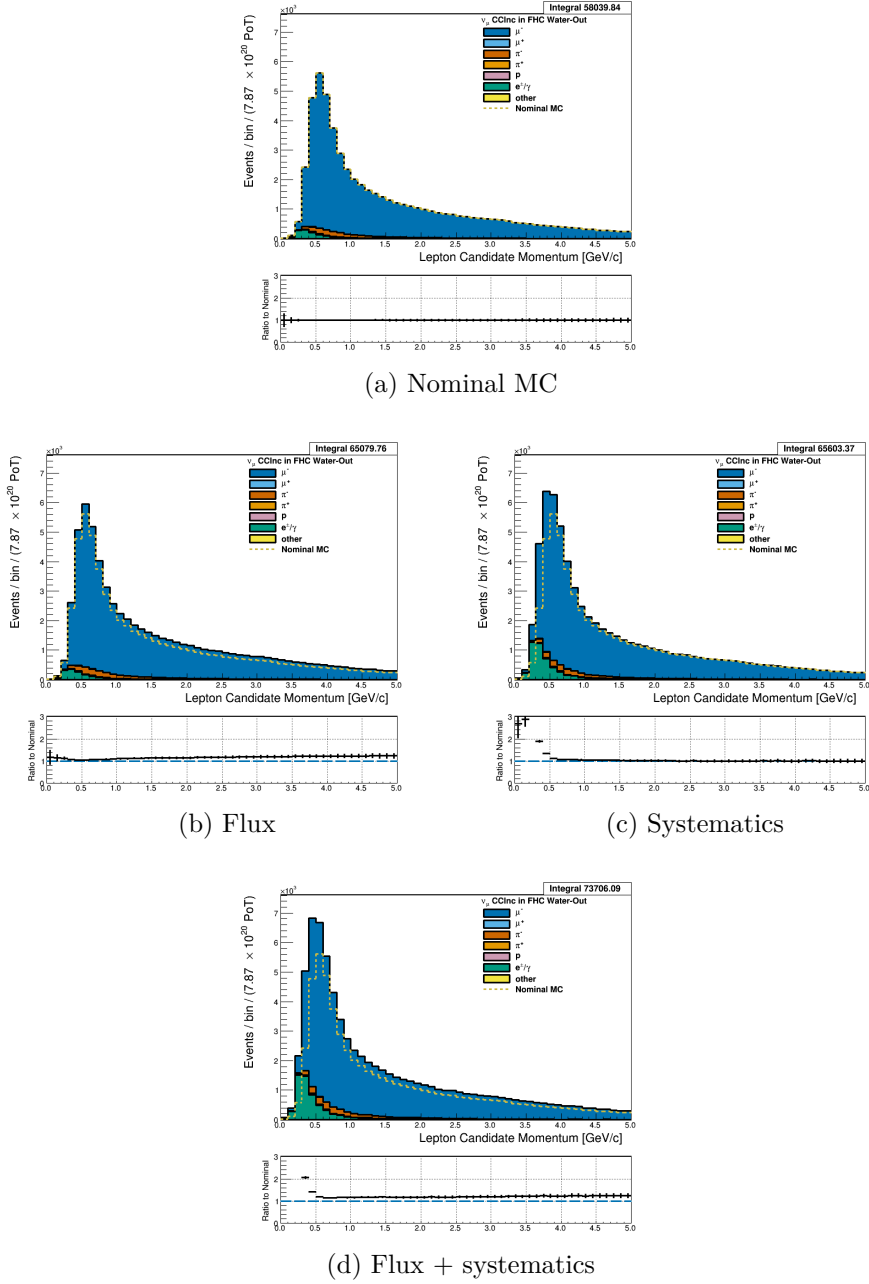


Figure 3.1: Reconstructed lepton candidate momentum separated by true particle species for FHC ν_μ CC Inc. events occurring in the PØD in water-out mode. (a) The nominal MC prediction without any weights applied. (b) The flux tuning are applied. (c) The systematic weighting are applied. (d) Both flux and systematic weighting are applied.

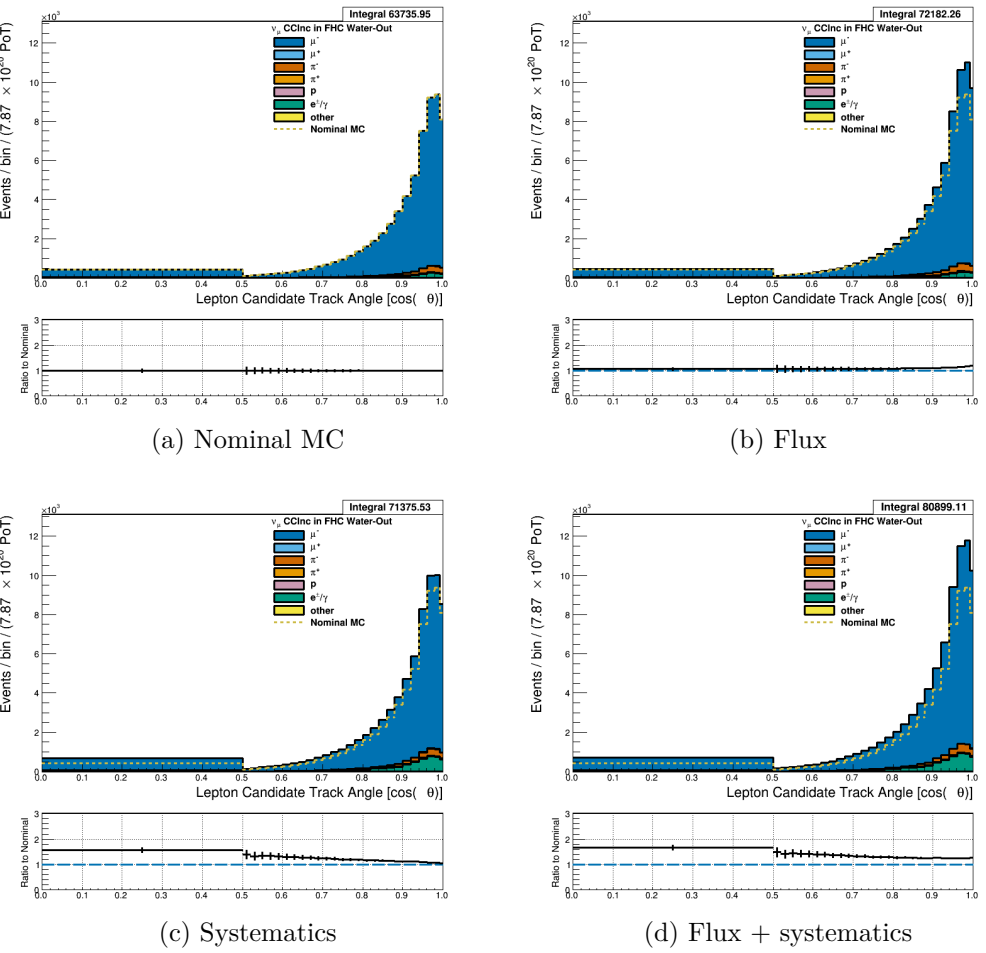


Figure 3.2: Reconstructed lepton candidate angle separated by true particle species for FHC ν_μ CC Inc. events occurring in the PØD in water-out mode. (a) The nominal MC prediction without any weights applied. (b) The flux tuning are applied. (c) The systematic weighting are applied. (d) Both flux and systematic weighting are applied.

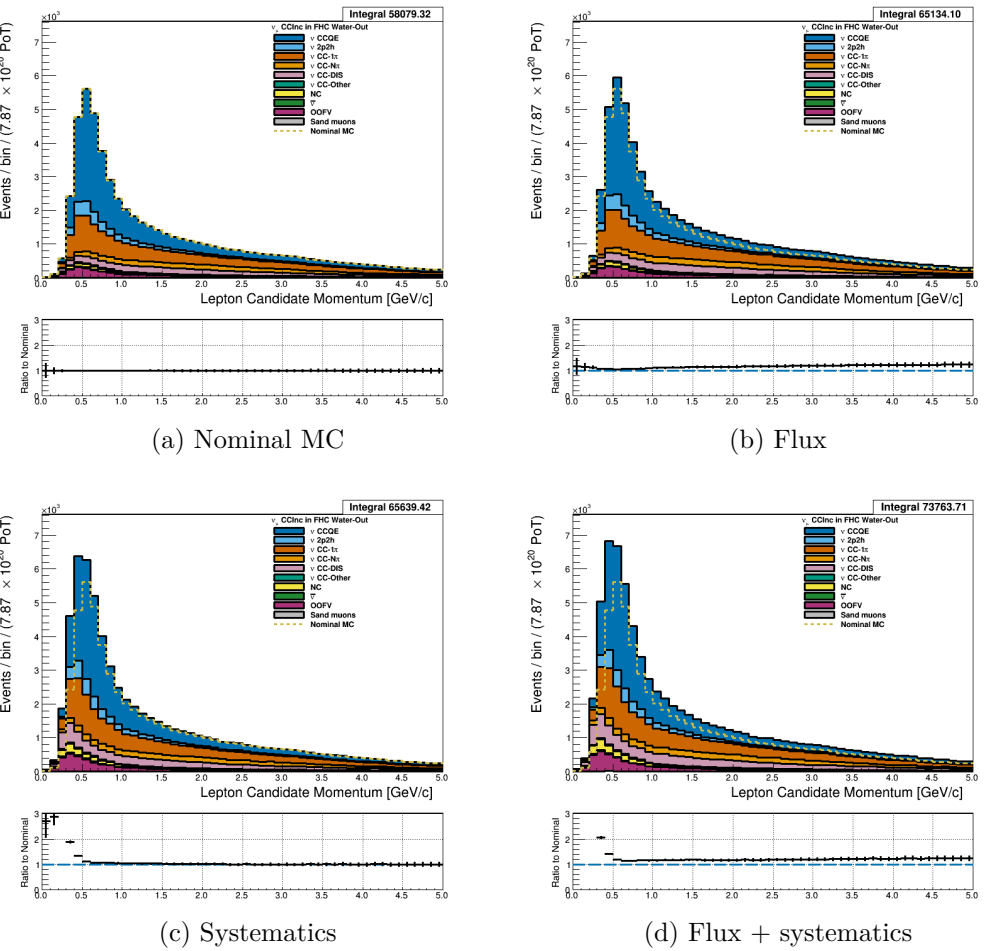


Figure 3.3: Reconstructed lepton candidate momentum separated by NEUT model interaction mode for FHC ν_μ CC Inc. events occurring in the PØD in water-out mode. (a) The nominal MC prediction without any weights applied. (b) The flux tuning are applied. (c) The systematic weighting are applied. (d) Both flux and systematic weighting are applied.

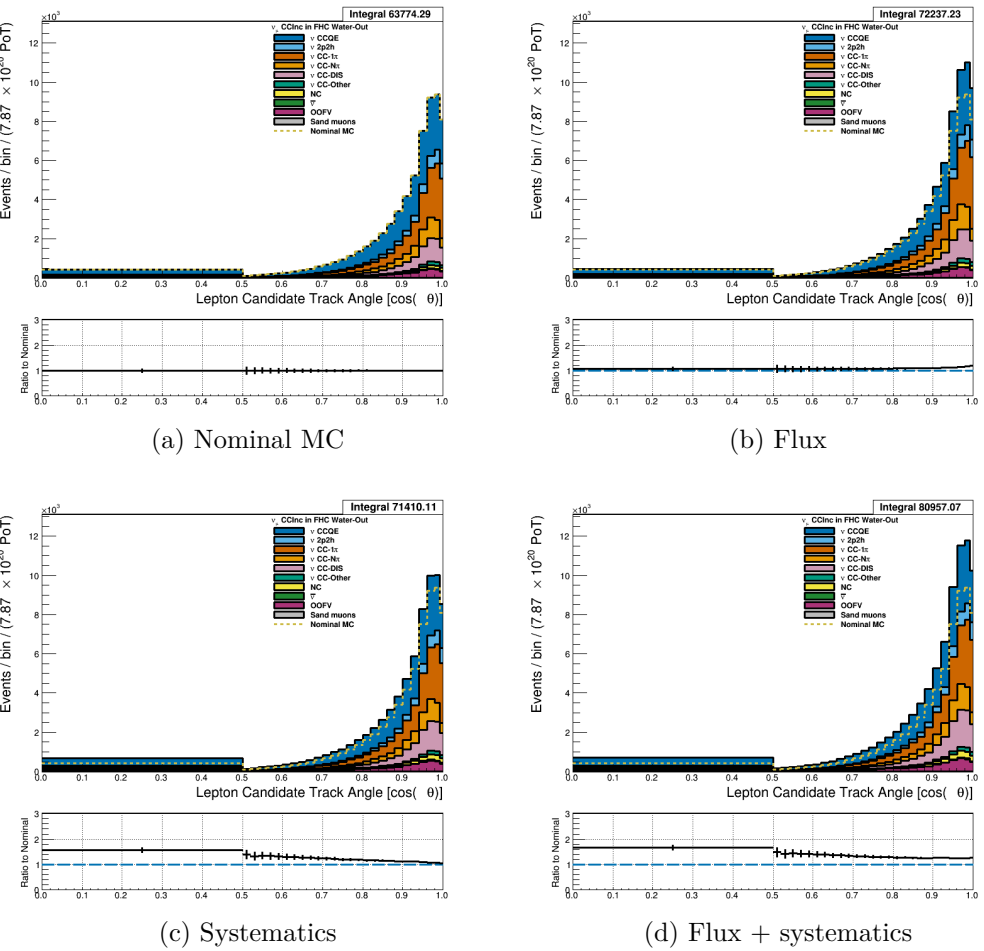


Figure 3.4: Reconstructed lepton candidate $\cos\theta$ separated by NEUT model interaction mode for FHC ν_μ CC Inc. events occurring in the PØD in water-out mode. (a) The nominal MC prediction without any weights applied. (b) The flux tuning are applied. (c) The systematic weighting are applied. (d) Both flux and systematic weighting are applied.

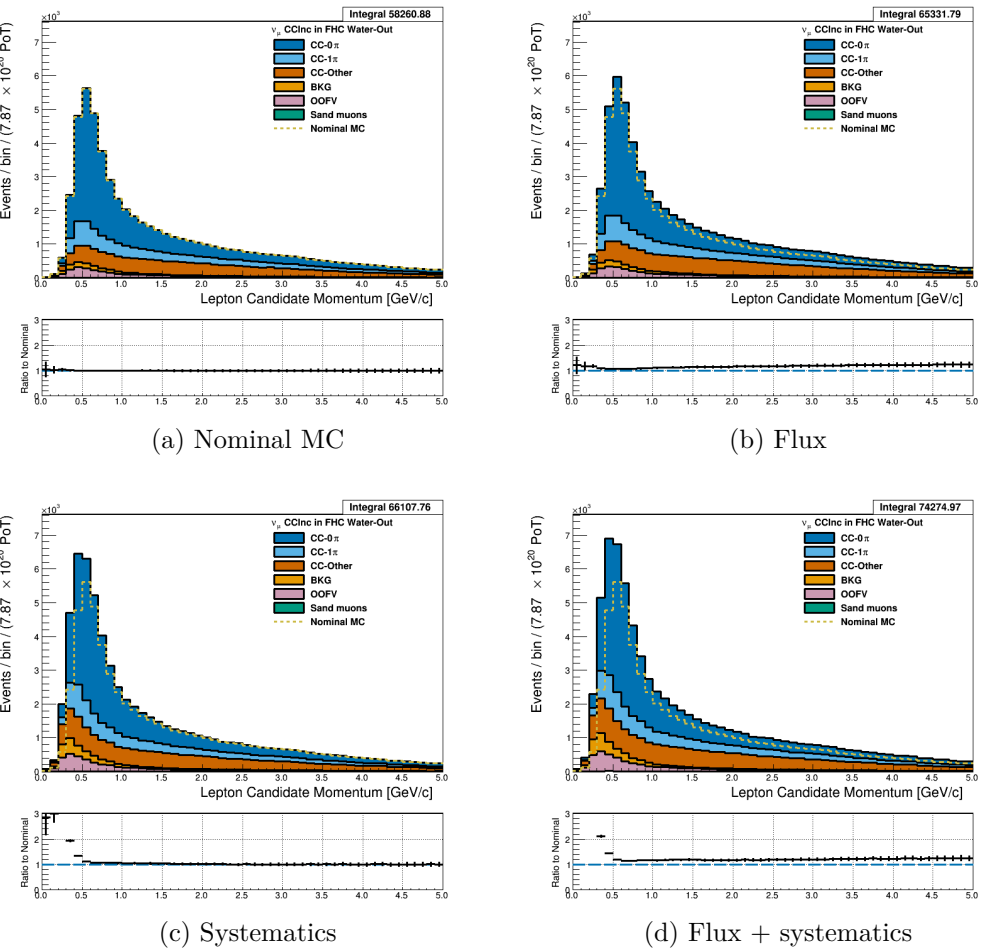


Figure 3.5: Reconstructed lepton candidate momentum separated by topology for FHC ν_μ CC Inc. events occurring in the PØD in water-out mode. (a) The nominal MC prediction without any weights applied. (b) The flux tuning are applied. (c) The systematic weighting are applied. (d) Both flux and systematic weighting are applied.

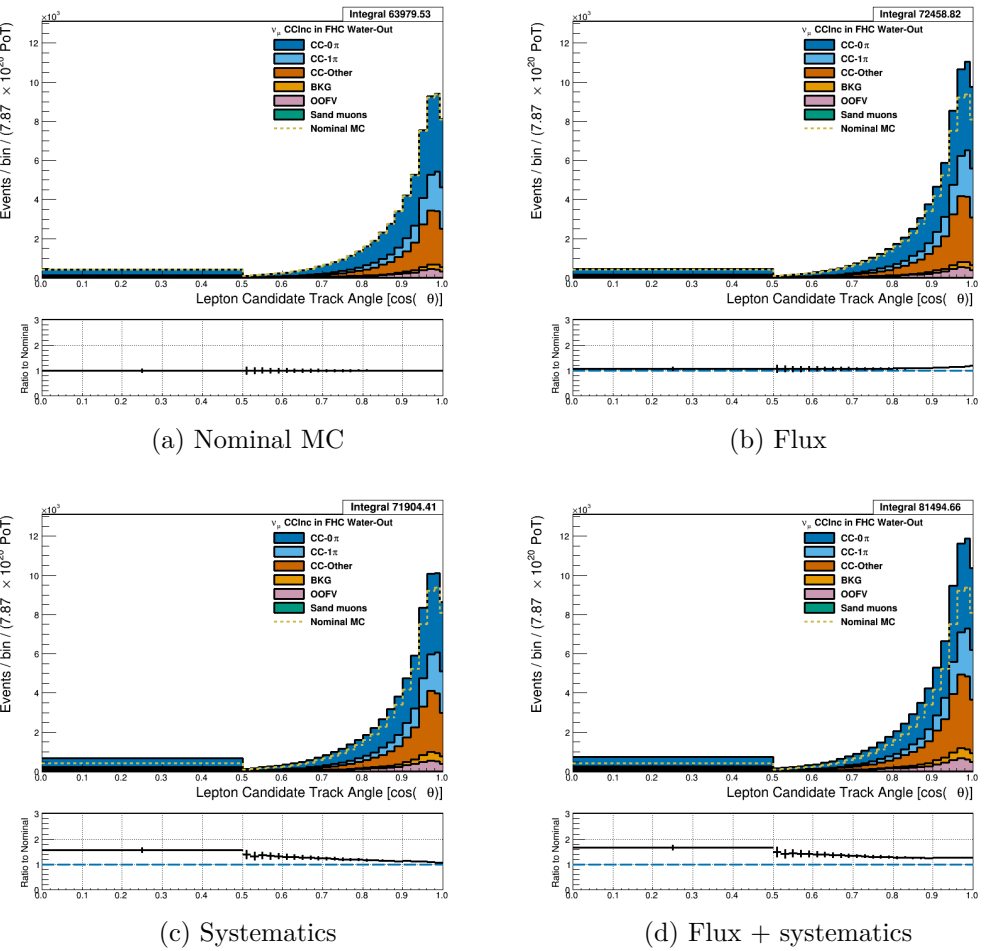


Figure 3.6: Reconstructed lepton candidate $\cos \theta$ separated by topology for FHC ν_μ CC Inc. events occurring in the PØD in water-out mode. (a) The nominal MC prediction without any weights applied. (b) The flux tuning are applied. (c) The systematic weighting are applied. (d) Both flux and systematic weighting are applied.

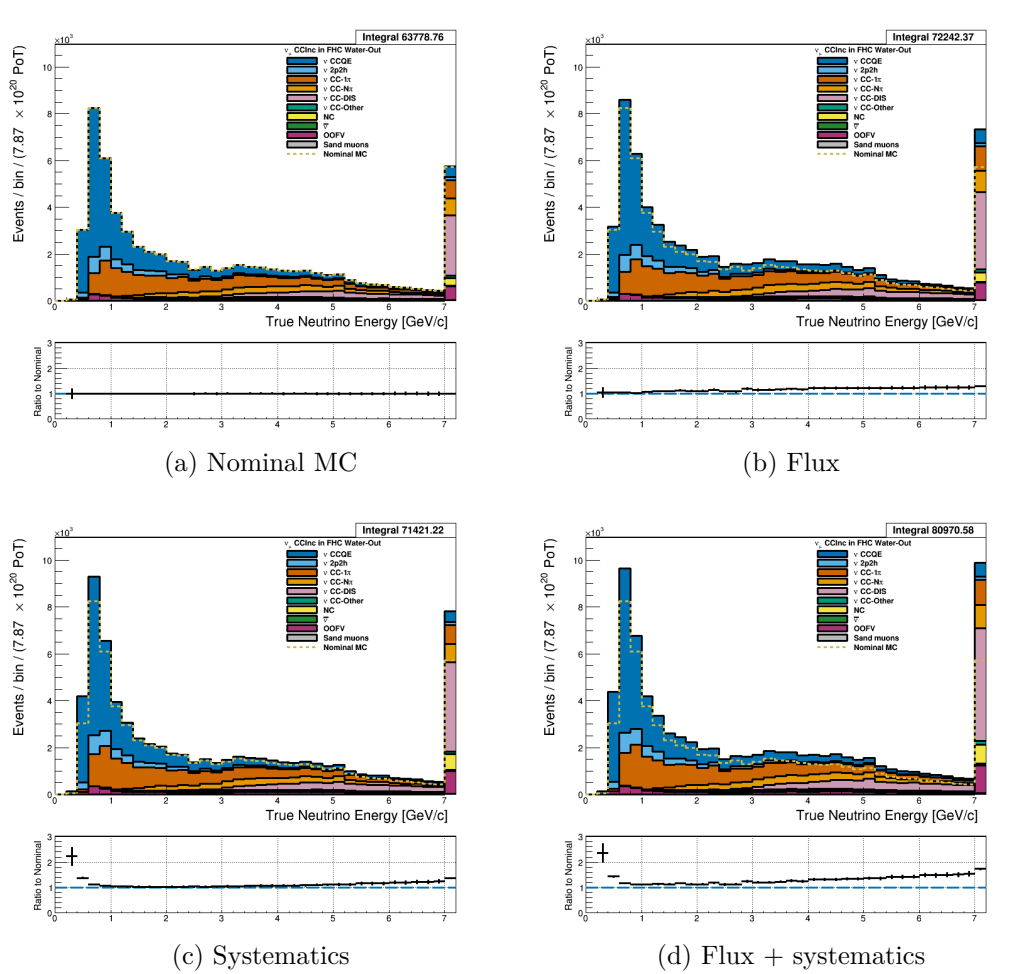


Figure 3.7: True neutrino energy associated with the lepton candidate separated by NEUT model interaction mode for FHC ν_μ CC Inc. events occurring in the PØD in water-out mode. (a) The nominal MC prediction without any weights applied. (b) The flux tuning are applied. (c) The systematic weighting are applied. (d) Both flux and systematic weighting are applied.

541 **3.4.1.2 $\bar{\nu}_\mu$ Selection in RHC Mode:** Shown in Figures 3.8 to 3.14 for $\bar{\nu}_\mu$ CC Inclusive
 542 events in RHC mode. There are three pairs of P, θ figures with the same truth information
 543 break down accompanied by one of neutrino energy. The truth information categories are
 544 lepton candidate particle, NEUT reaction, and topology. Each figure consists of a set of four
 545 sub-figures which illustrate the application of flux and detector systematic weights.

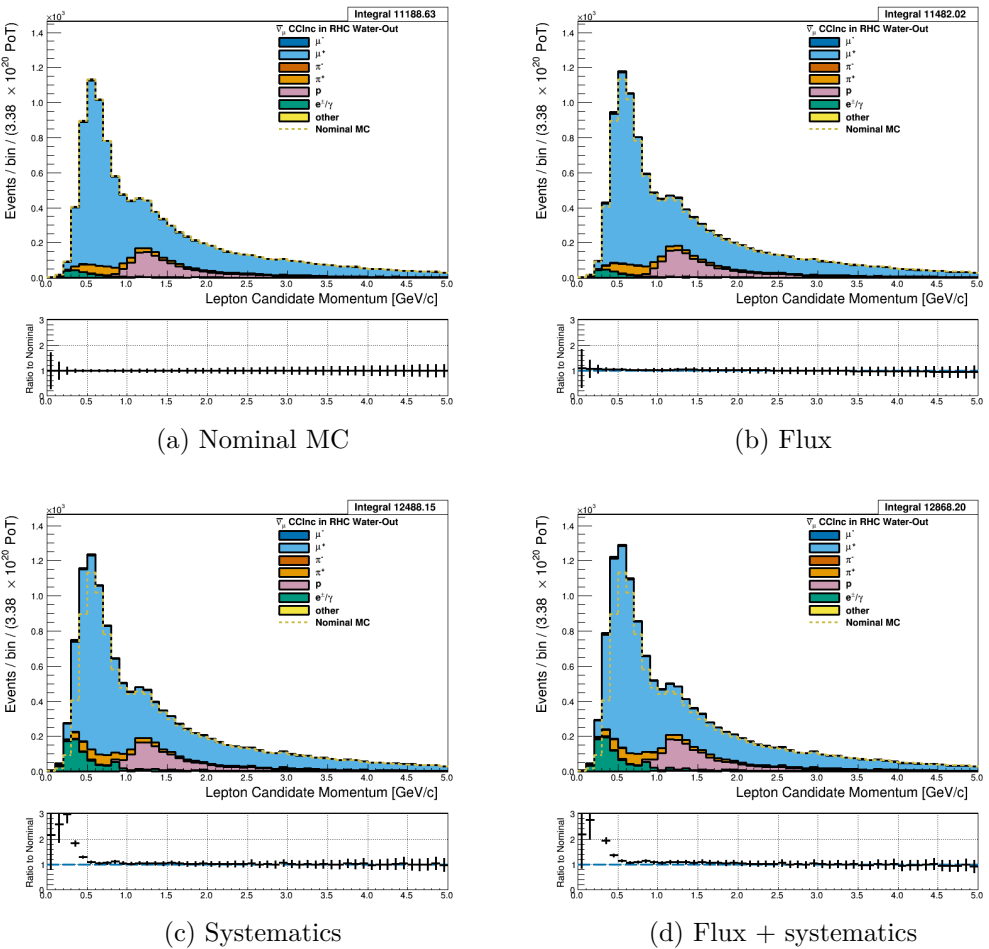


Figure 3.8: Reconstructed lepton candidate momentum separated by true particle species for RHC $\bar{\nu}_\mu$ CC Inc. events occurring in the PØD in water-out mode. Reconstructed lepton candidate angle separated by true particle species for RHC $\bar{\nu}_\mu$ CC Inc. events occurring in the PØD in water-in mode. (a) The nominal MC prediction without any weights applied. (b) The flux tuning are applied. (c) The systematic weighting are applied. (d) Both flux and systematic weighting are applied.

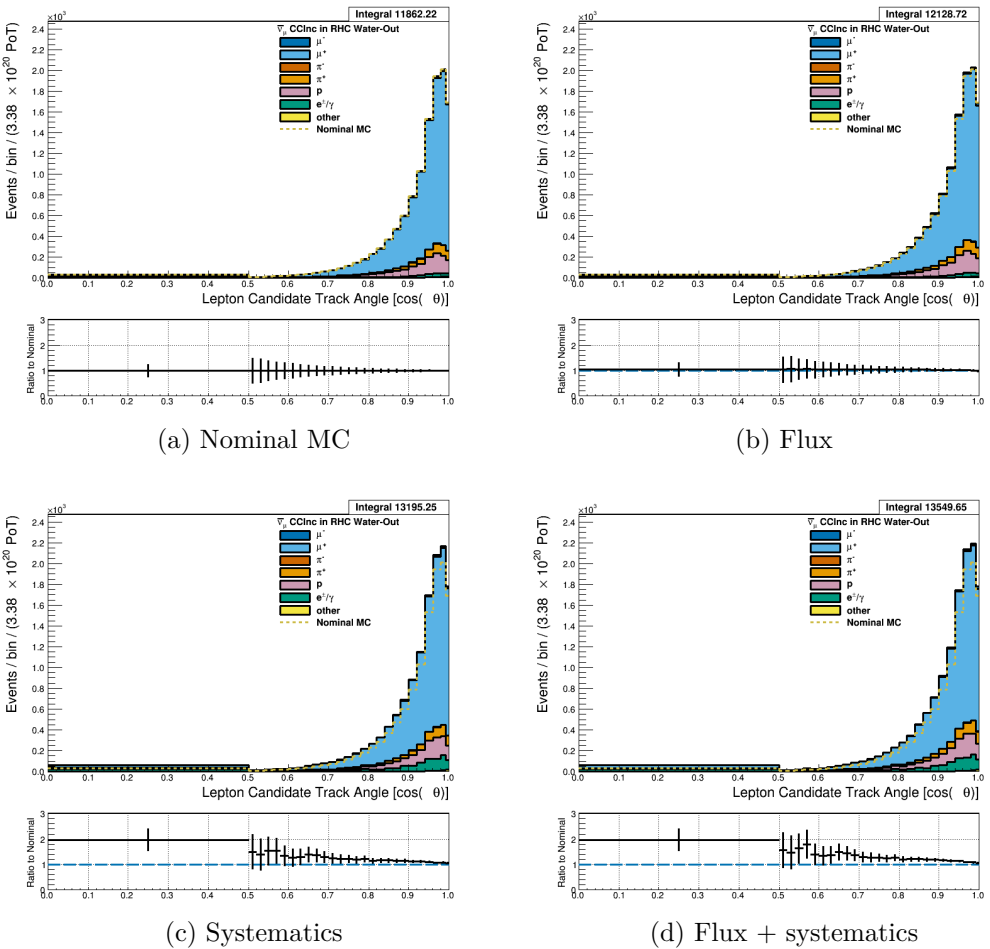


Figure 3.9: Reconstructed lepton candidate angle separated by true particle species for RHC $\bar{\nu}_\mu$ CC Inc. events occurring in the PØD in water-out mode. (a) The nominal MC prediction without any weights applied. (b) The flux tuning are applied. (c) The systematic weighting are applied. (d) Both flux and systematic weighting are applied.

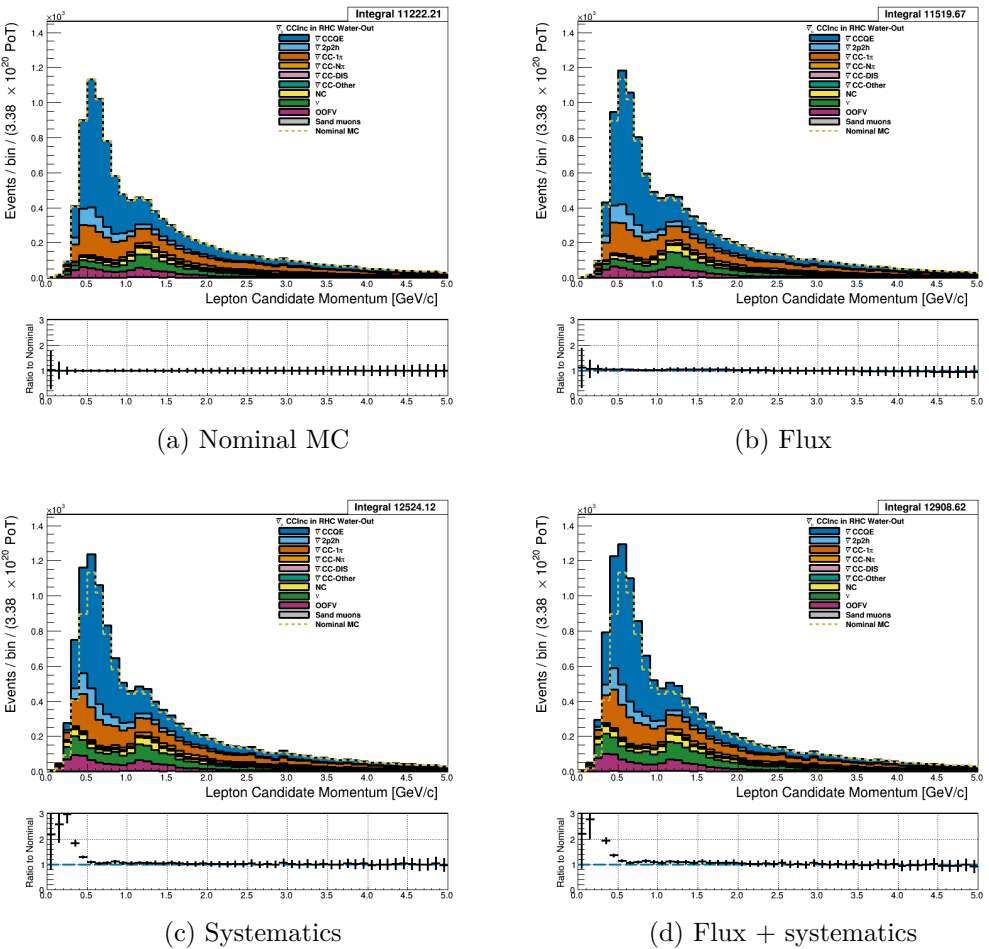


Figure 3.10: Reconstructed lepton candidate momentum separated by NEUT model interaction mode for RHC $\bar{\nu}_\mu$ CC Inc. events occurring in the PØD in water-out mode. (a) The nominal MC prediction without any weights applied. (b) The flux tuning are applied. (c) The systematic weighting are applied. (d) Both flux and systematic weighting are applied.

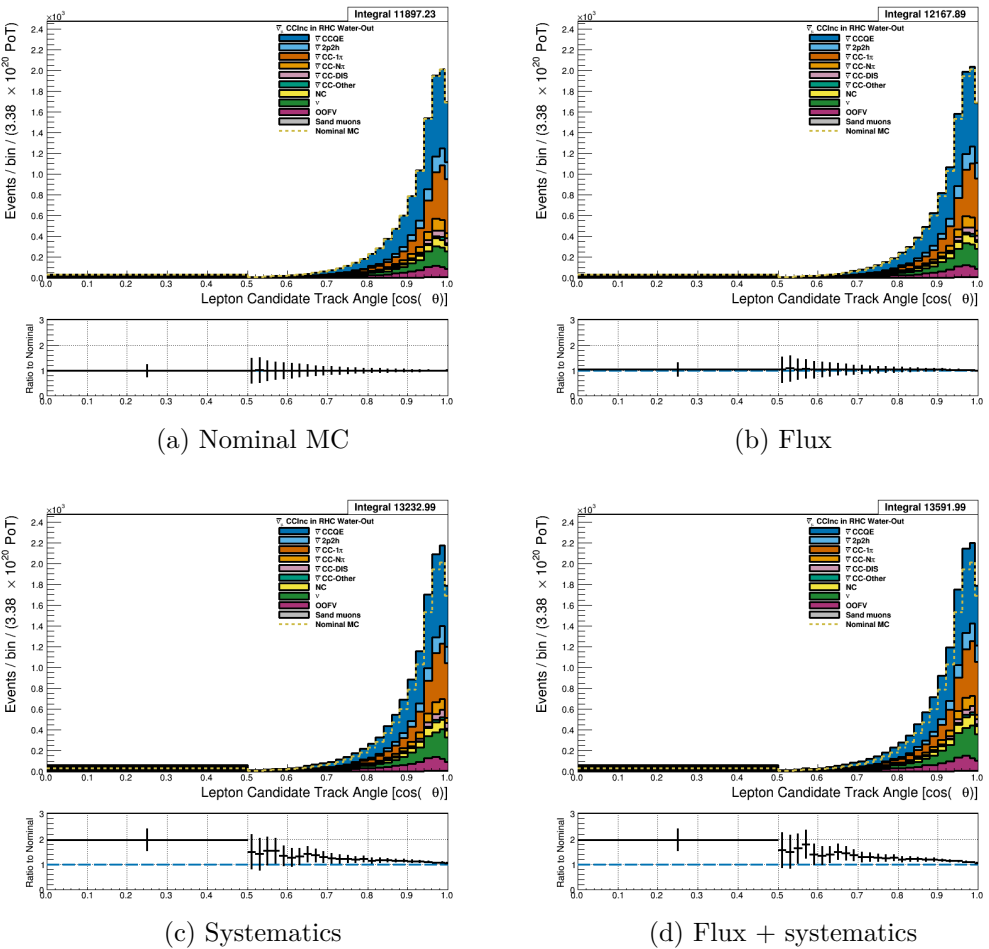


Figure 3.11: Reconstructed lepton candidate $\cos \theta$ separated by NEUT model interaction mode for RHC $\bar{\nu}_\mu$ CC Inc. events occurring in the PØD in water-out mode. (a) The nominal MC prediction without any weights applied. (b) The flux tuning are applied. (c) The systematic weighting are applied. (d) Both flux and systematic weighting are applied.

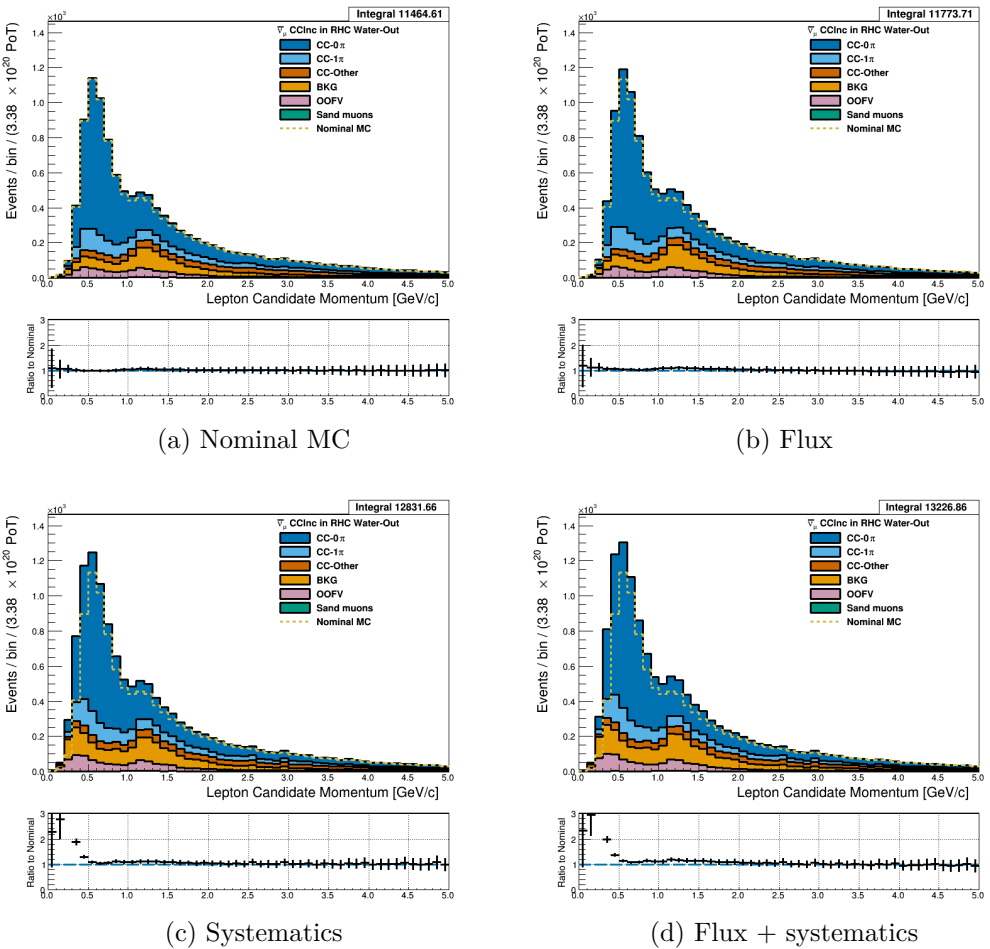


Figure 3.12: Reconstructed lepton candidate momentum separated by topology for RHC $\bar{\nu}_\mu$ CC Inc. events occurring in the PØD in water-out mode. (a) The nominal MC prediction without any weights applied. (b) The flux tuning are applied. (c) The systematic weighting are applied. (d) Both flux and systematic weighting are applied.

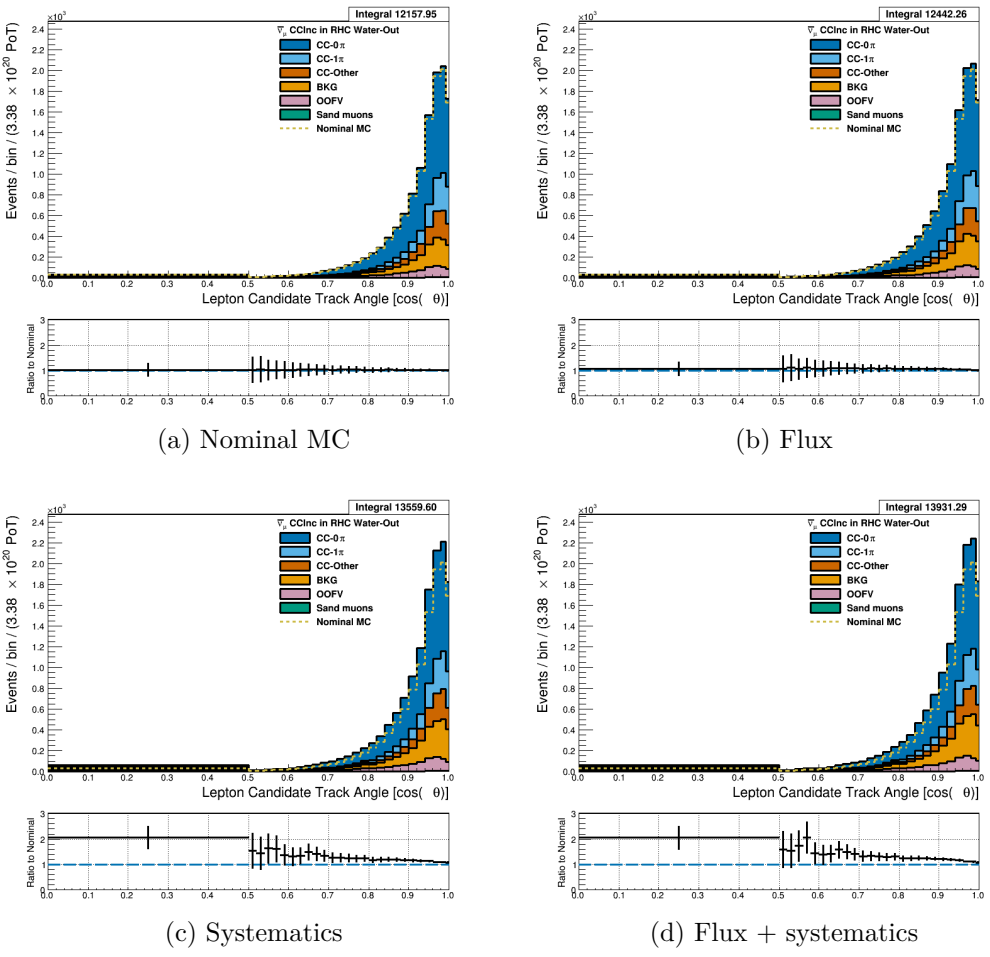


Figure 3.13: Reconstructed lepton candidate $\cos \theta$ separated by topology for RHC $\bar{\nu}_\mu$ CC Inc. events occurring in the PØD in water-out mode. (a) The nominal MC prediction without any weights applied. (b) The flux tuning are applied. (c) The systematic weighting are applied. (d) Both flux and systematic weighting are applied.

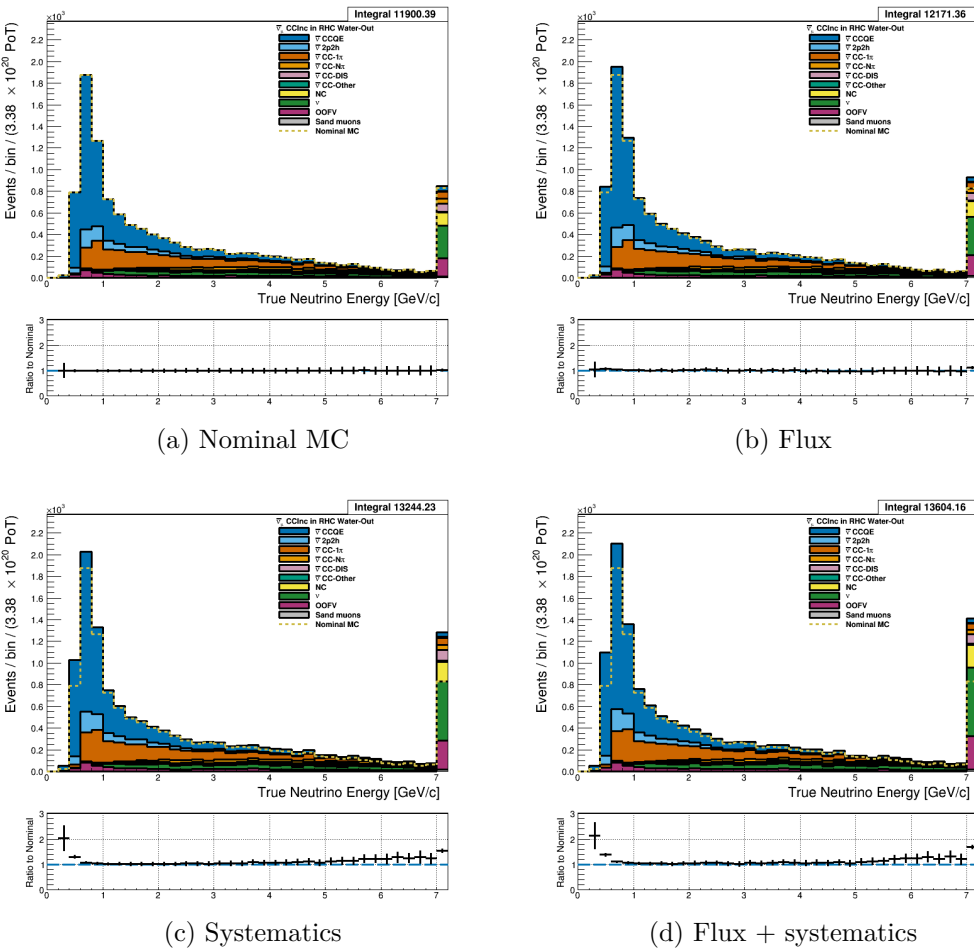


Figure 3.14: True neutrino energy associated with the lepton candidate separated by NEUT model interaction mode for RHC $\bar{\nu}_\mu$ CC Inc. events occurring in the PØD in water-out mode. (a) The nominal MC prediction without any weights applied. (b) The flux tuning are applied. (c) The systematic weighting are applied. (d) Both flux and systematic weighting are applied.

546 **3.4.1.3 ν_μ Background Selection in RHC Mode:** Shown in Figures 3.15, 3.16 and 3.19

547 to 3.21 and ????

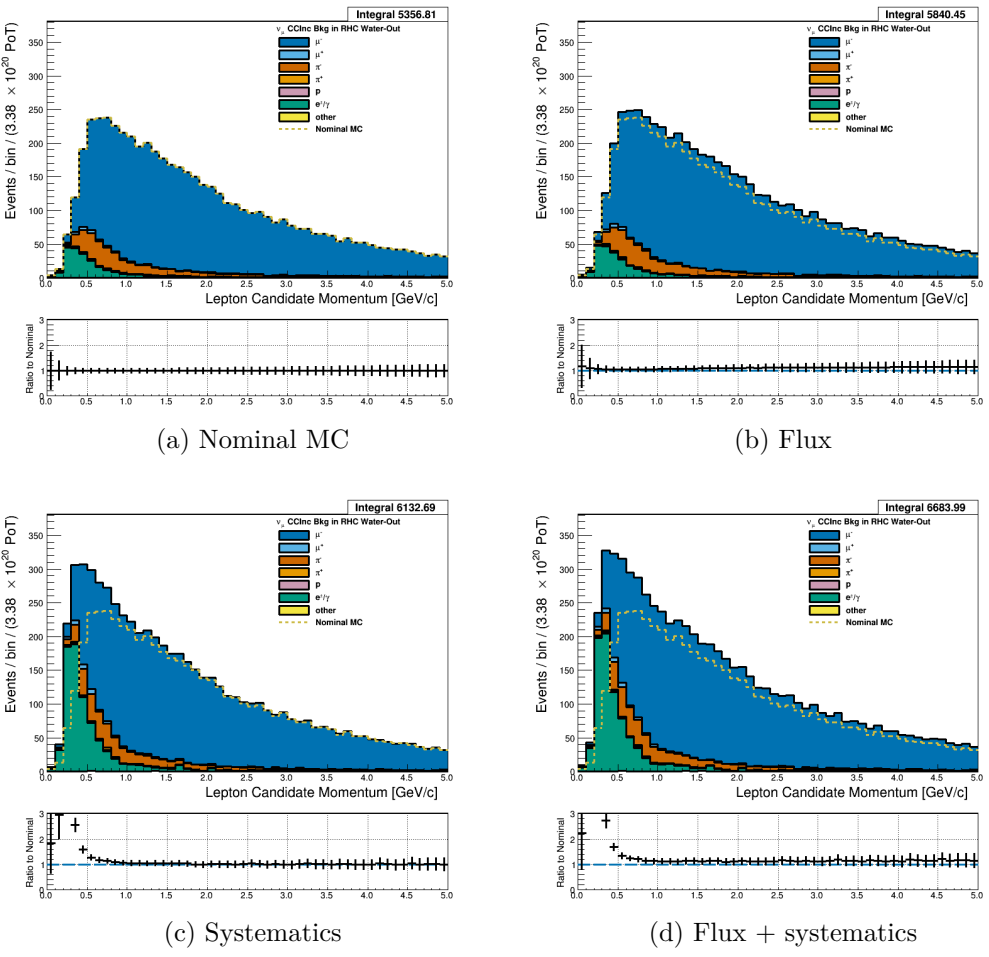


Figure 3.15: Reconstructed lepton candidate momentum separated by true particle species for RHC ν_μ CC Inc. events occurring in the PØD in water-out mode. (a) The nominal MC prediction without any weights applied. (b) The flux tuning are applied. (c) The systematic weighting are applied. (d) Both flux and systematic weighting are applied.

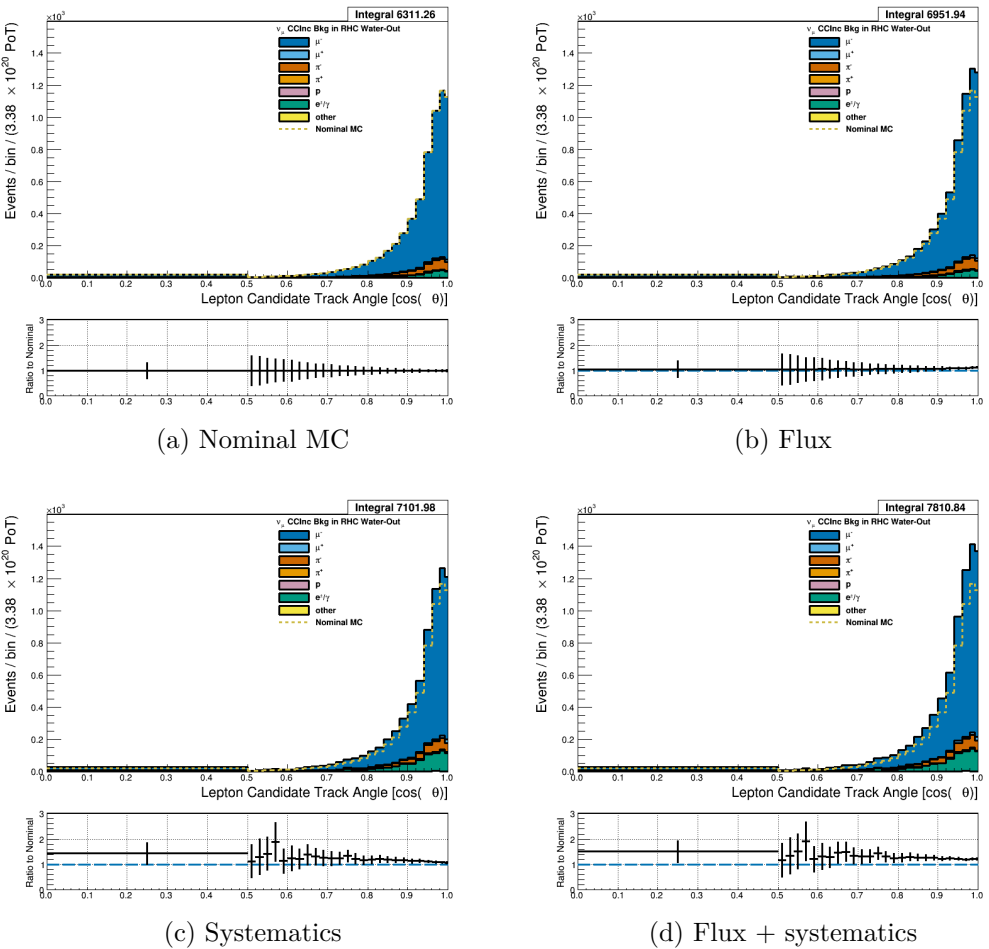


Figure 3.16: Reconstructed lepton candidate angle separated by true particle species for RHC ν_μ CC Inc. events occurring in the PØD in water-out mode. (a) The nominal MC prediction without any weights applied. (b) The flux tuning are applied. (c) The systematic weighting are applied. (d) Both flux and systematic weighting are applied.

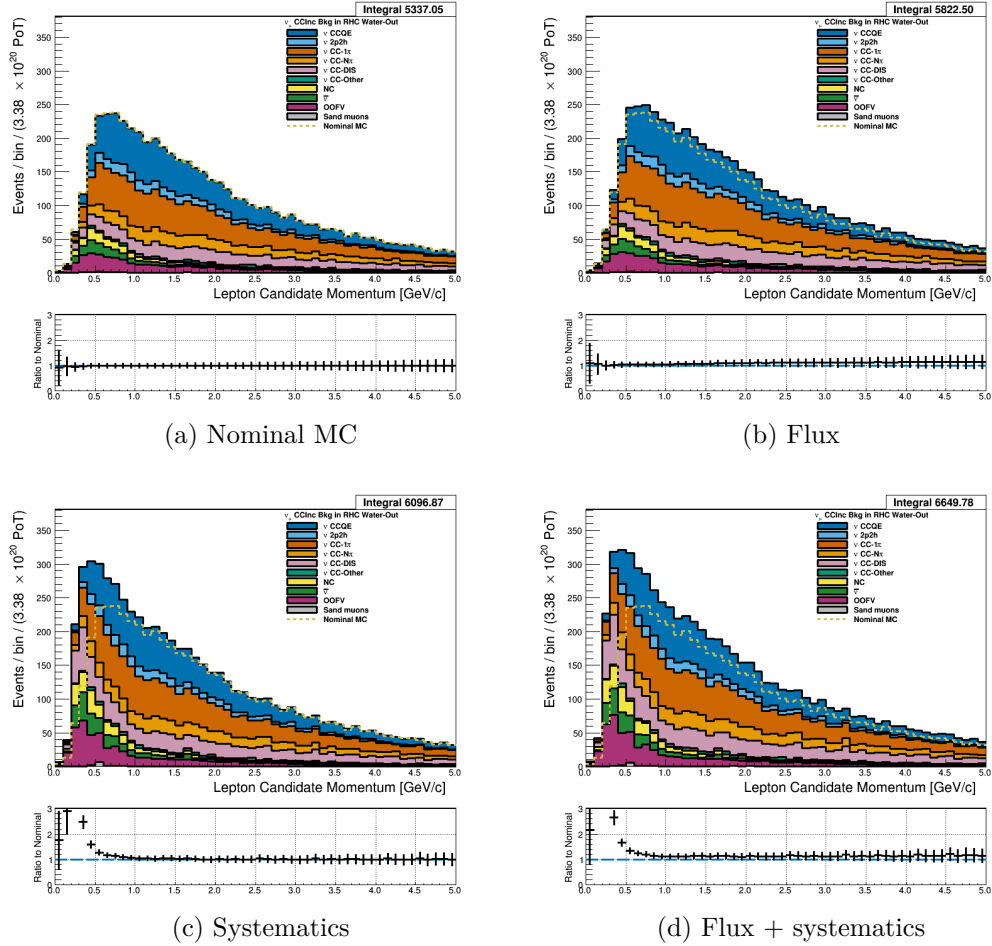


Figure 3.17: Reconstructed lepton candidate momentum separated by NEUT model interaction mode for RHC ν_μ CC Inc. events occurring in the PØD in water-out mode. (a) The nominal MC prediction without any weights applied. (b) The flux tuning are applied. (c) The systematic weighting are applied. (d) Both flux and systematic weighting are applied.

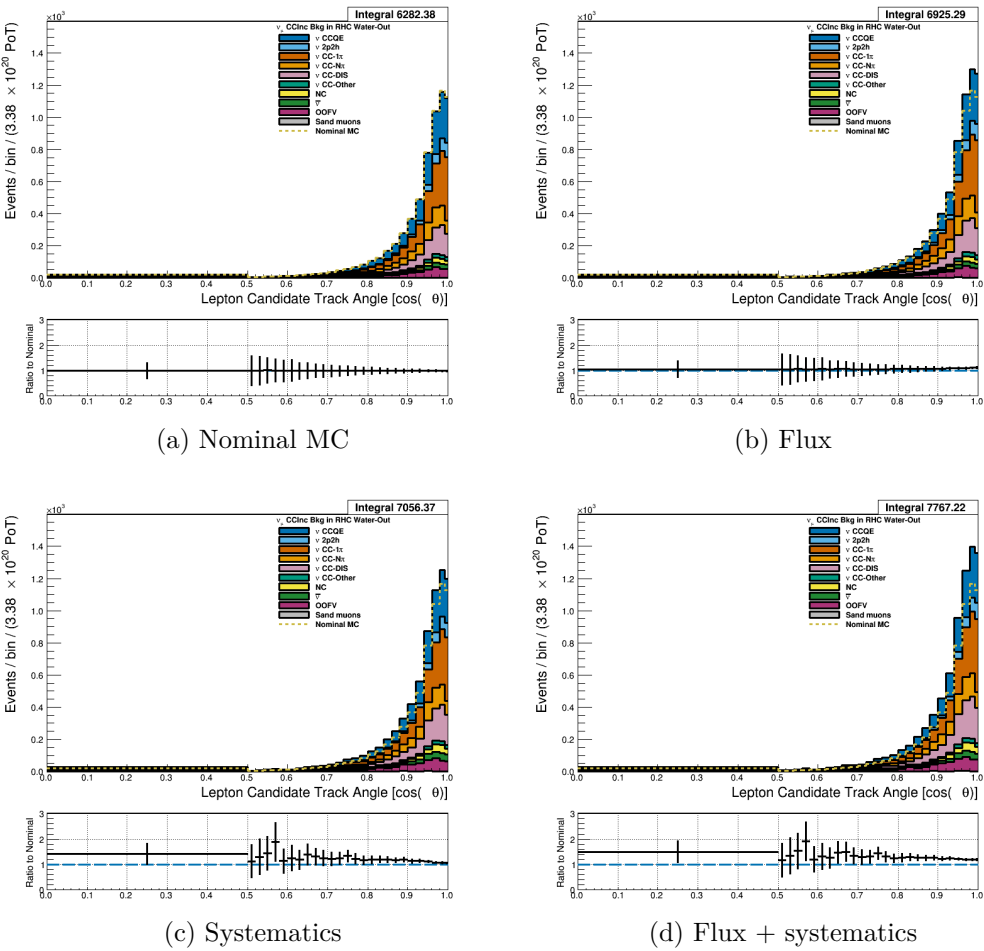


Figure 3.18: Reconstructed lepton candidate $\cos \theta$ separated by NEUT model interaction mode for FHC ν_μ CC Inc. events occurring in the PØD in water-out mode. (a) The nominal MC prediction without any weights applied. (b) The flux tuning are applied. (c) The systematic weighting are applied. (d) Both flux and systematic weighting are applied.

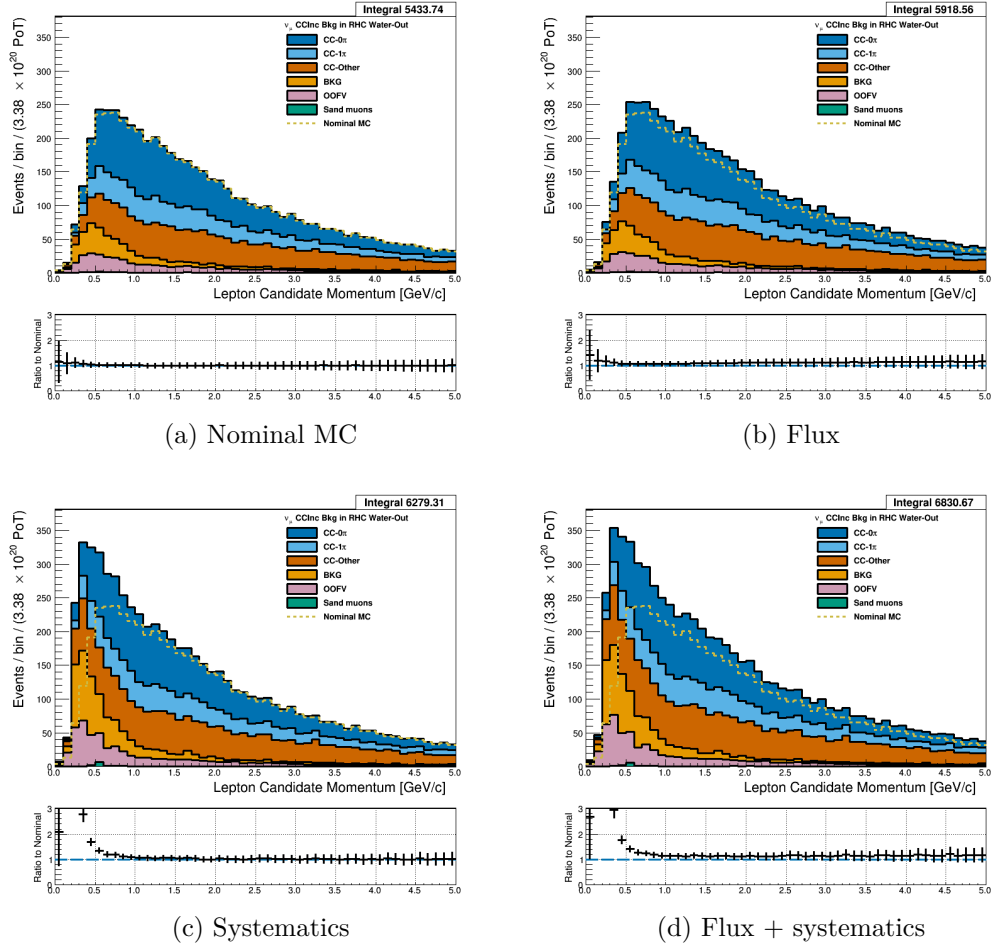


Figure 3.19: Reconstructed lepton candidate momentum separated by topology for FHC ν_μ CC Inc. events occurring in the PØD in water-out mode. (a) The nominal MC prediction without any weights applied. (b) The flux tuning are applied. (c) The systematic weighting are applied. (d) Both flux and systematic weighting are applied.

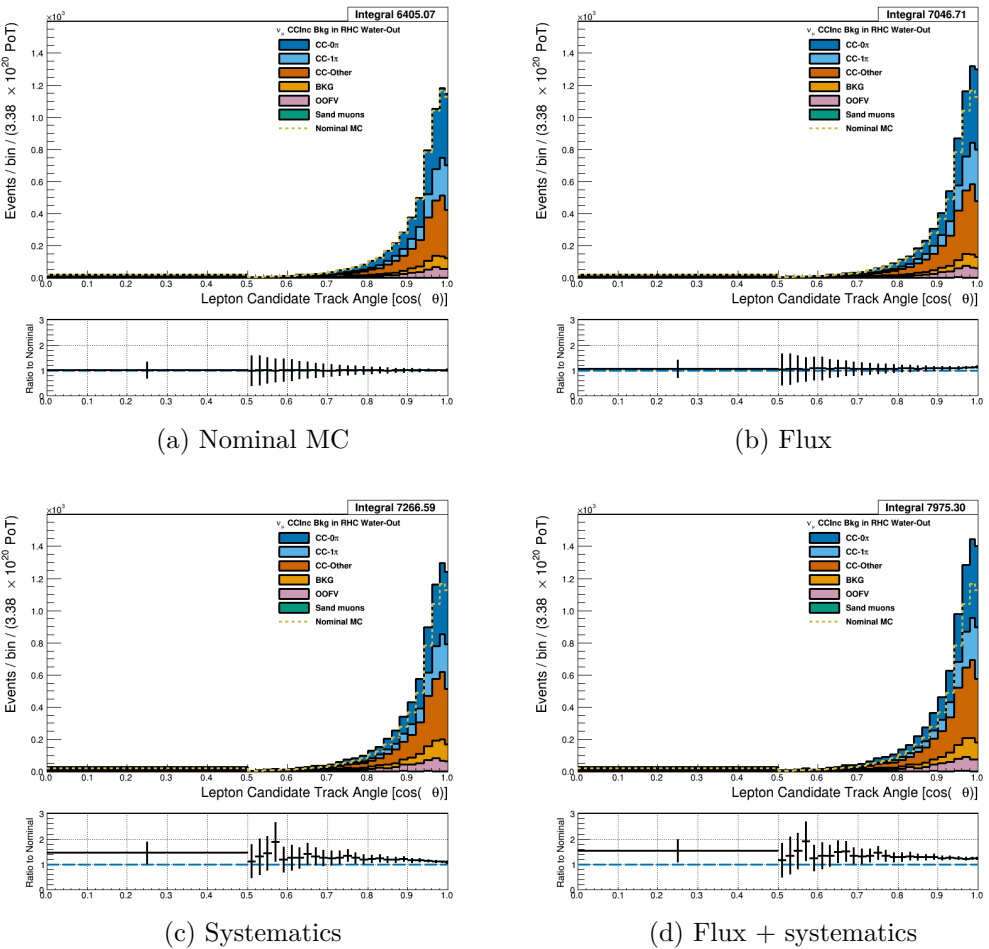


Figure 3.20: Reconstructed lepton candidate $\cos \theta$ separated by topology for FHC ν_μ CC Inc. events occurring in the PØD in water-out mode. (a) The nominal MC prediction without any weights applied. (b) The flux tuning are applied. (c) The systematic weighting are applied. (d) Both flux and systematic weighting are applied.

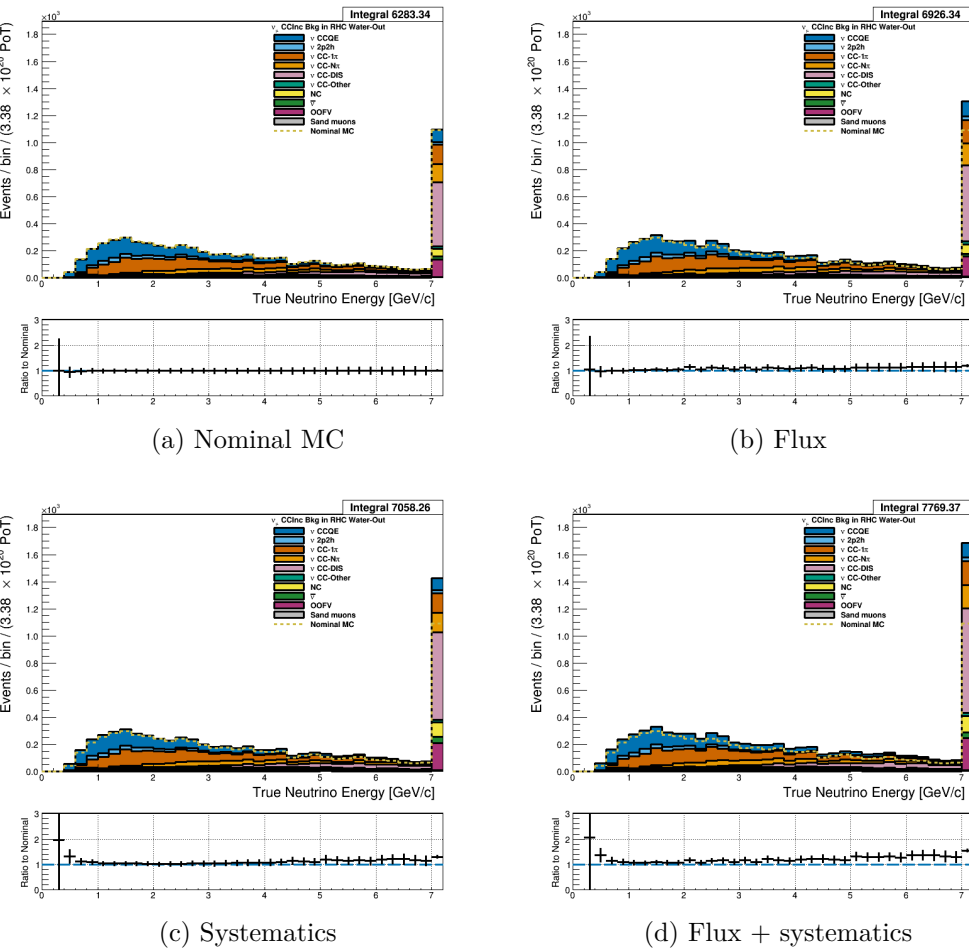


Figure 3.21: True neutrino energy associated with the lepton candidate separated by NEUT model interaction mode for FHC ν_μ CC Inc. events occurring in the PØD in water-out mode. (a) The nominal MC prediction without any weights applied. (b) The flux tuning are applied. (c) The systematic weighting are applied. (d) Both flux and systematic weighting are applied.

548 3.4.2 CC 1-Track (CCQE Enhanced)

549 **ν_μ Selection in FHC Mode:** Shown in

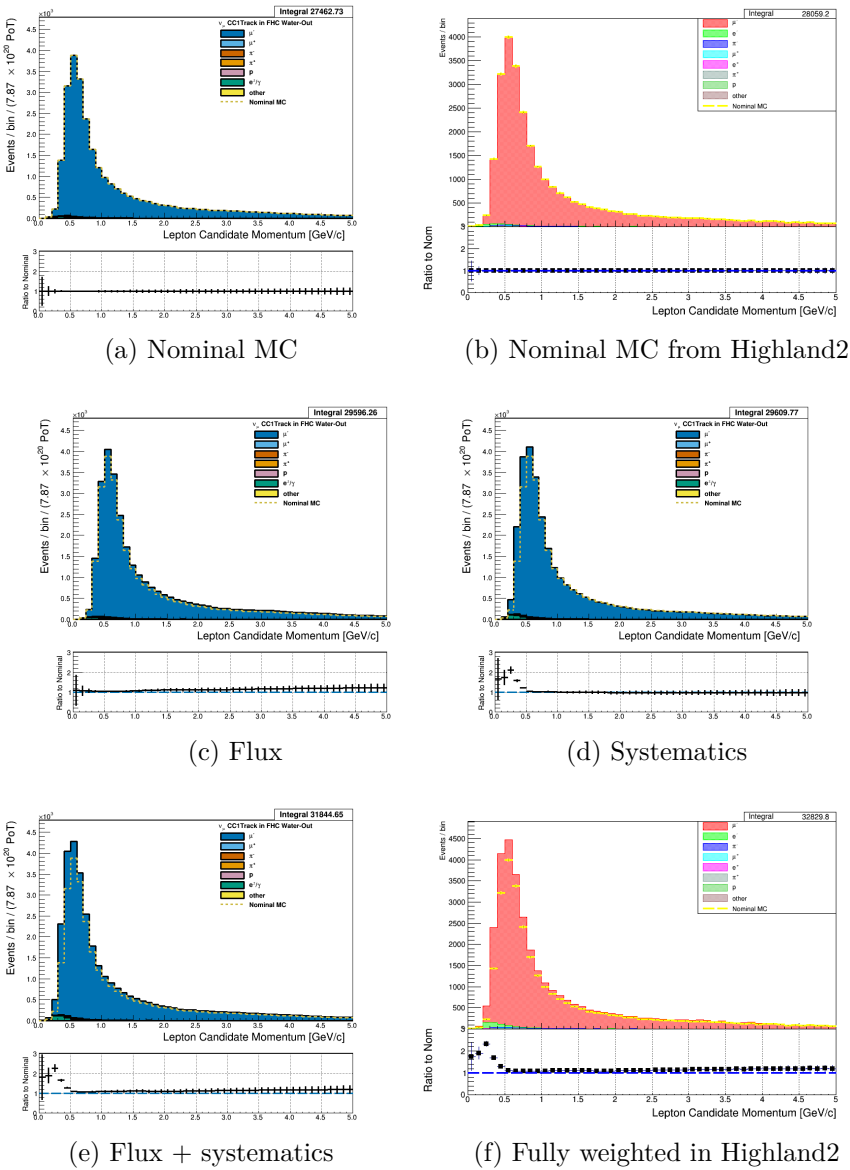


Figure 3.22: Reconstructed lepton candidate momentum separated by true particle species for FHC ν_μ CC 1-Track events occurring in the PØD in water-out mode. (a) The nominal MC prediction without any weights applied. (b) The same POT-normalized plot as (a) using a subset of the water-out MC in Highland. (c) The flux tuning are applied. (d) The systematic weighting are applied. (e) Both flux and systematic weighting are applied. (f) The same POT-normalized plot as (e) using a subset of the water-out MC in Highland. There is a $\sim 1\%$ difference between Highland2 and BANFF since a subset of the MC was used to generate Highland plots.

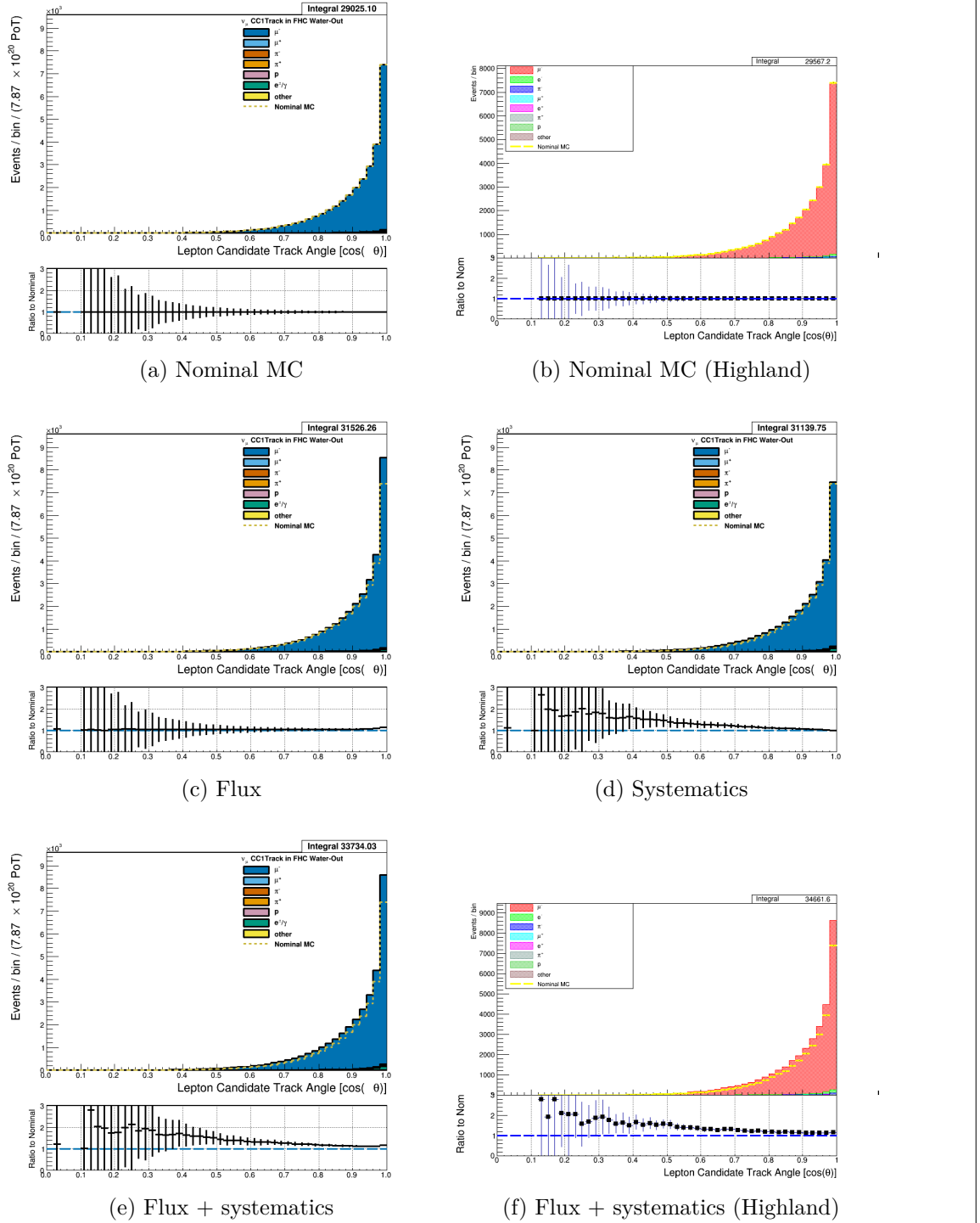


Figure 3.23: Reconstructed lepton candidate angle separated by true particle species for FHC ν_μ CC 1-Track events occurring in the PØD in water-out mode. (a) The nominal MC prediction without any weights applied. (b) The same POT-normalized plot as (a) using a subset of the water-out MC in Highland. (c) The flux tuning are applied. (d) The systematic weighting are applied. (e) Both flux and systematic weighting are applied. (f) The same POT-normalized plot as (e) using a subset of the water-out MC in Highland. There is a ~1% difference between Highland2 and BANFF since a subset of the MC was used to generate Highland plots.

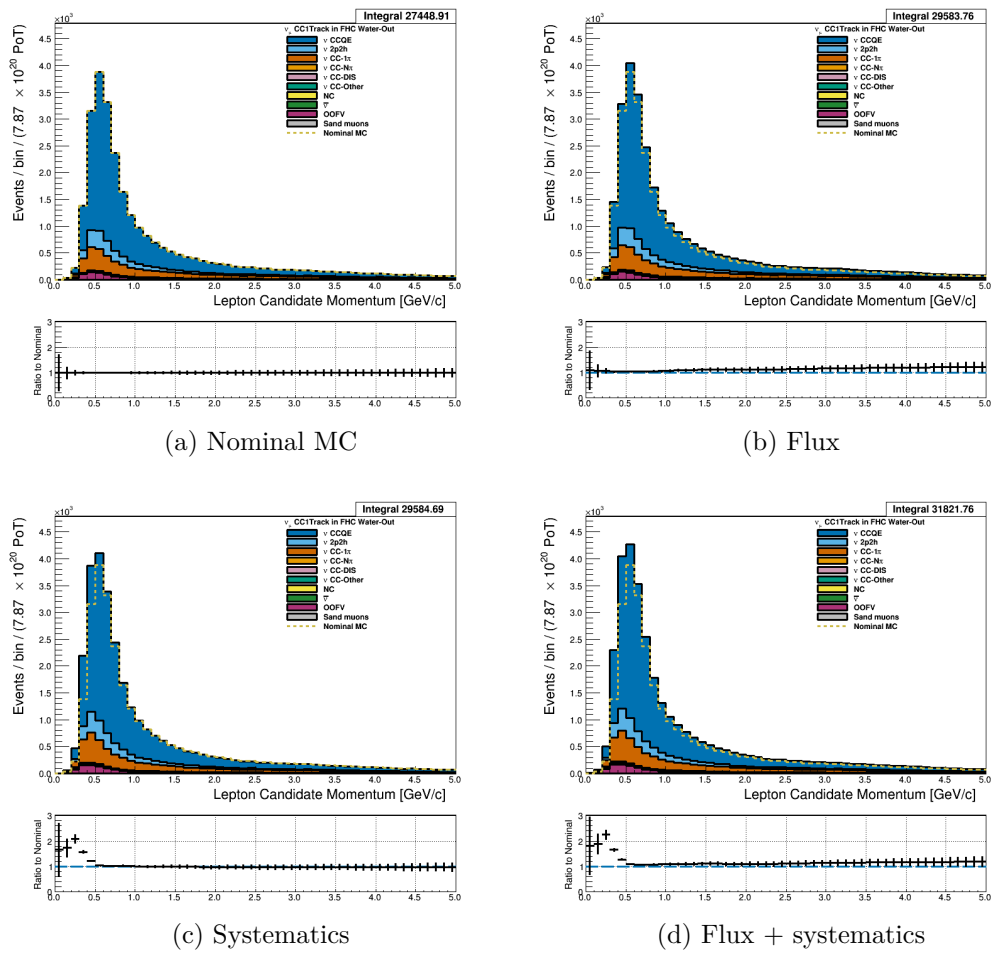


Figure 3.24: Reconstructed lepton candidate momentum separated by NEUT model interaction mode for FHC ν_μ CC 1-Track events occurring in the PØD in water-out mode. (a) The nominal MC prediction without any weights applied. (b) The flux tuning are applied. (c) The systematic weighting are applied. (d) Both flux and systematic weighting are applied.

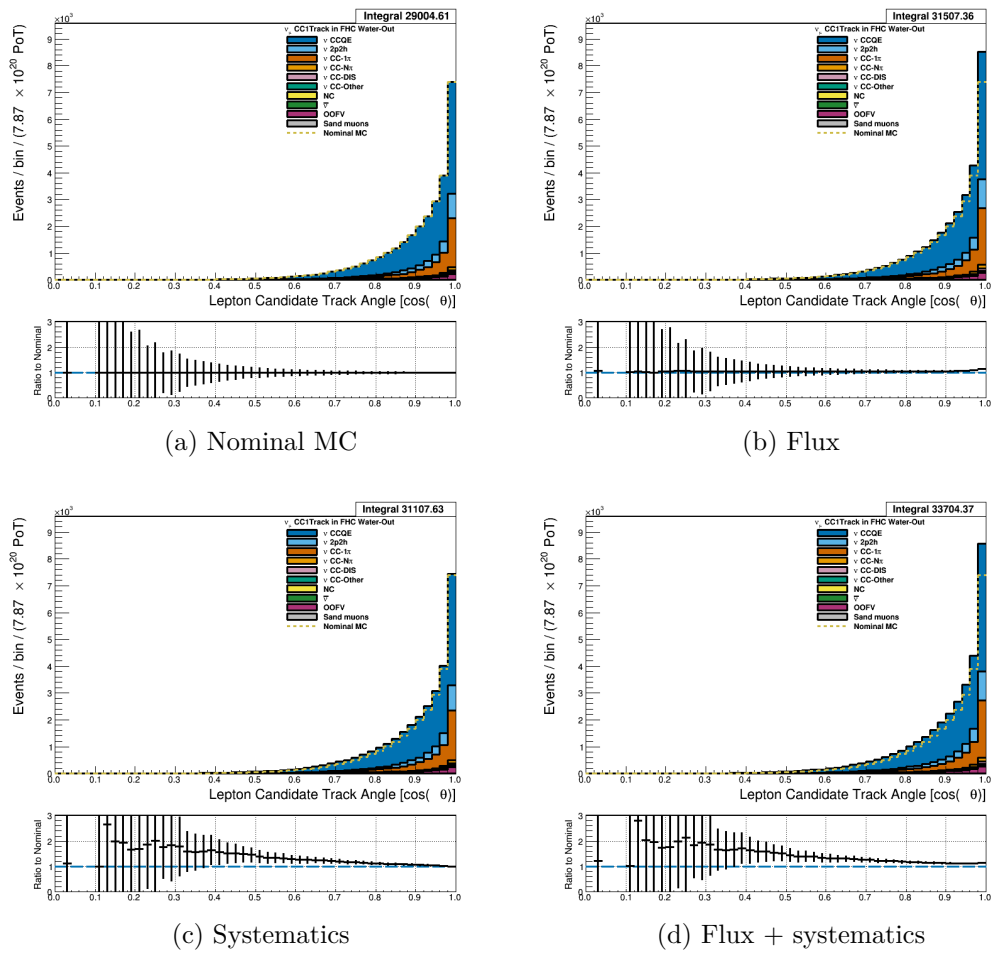


Figure 3.25: Reconstructed lepton candidate $\cos \theta$ separated by NEUT model interaction mode for FHC ν_μ CC 1-Track events occurring in the PØD in water-out mode. (a) The nominal MC prediction without any weights applied. (b) The flux tuning are applied. (c) The systematic weighting are applied. (d) Both flux and systematic weighting are applied.

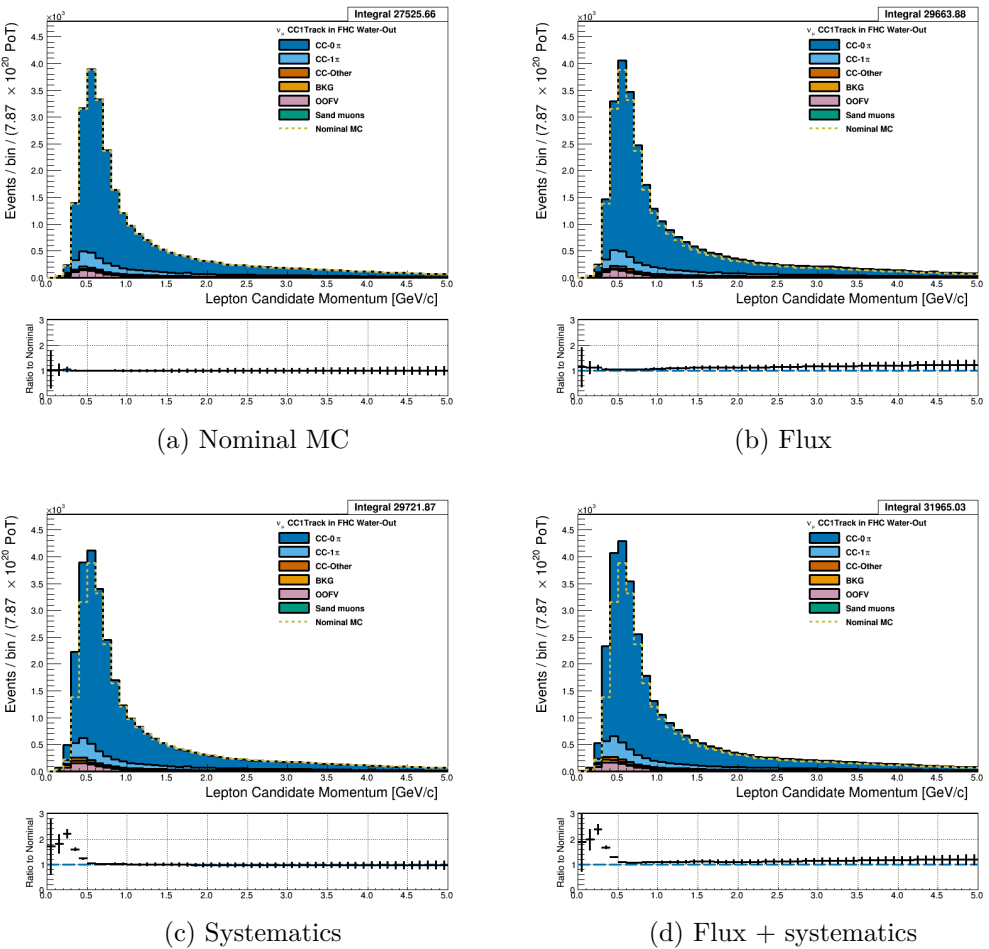


Figure 3.26: Reconstructed lepton candidate momentum separated by topology for FHC ν_μ CC 1-Track events occurring in the PØD in water-out mode. (a) The nominal MC prediction without any weights applied. (b) The flux tuning are applied. (c) The systematic weighting are applied. (d) Both flux and systematic weighting are applied.

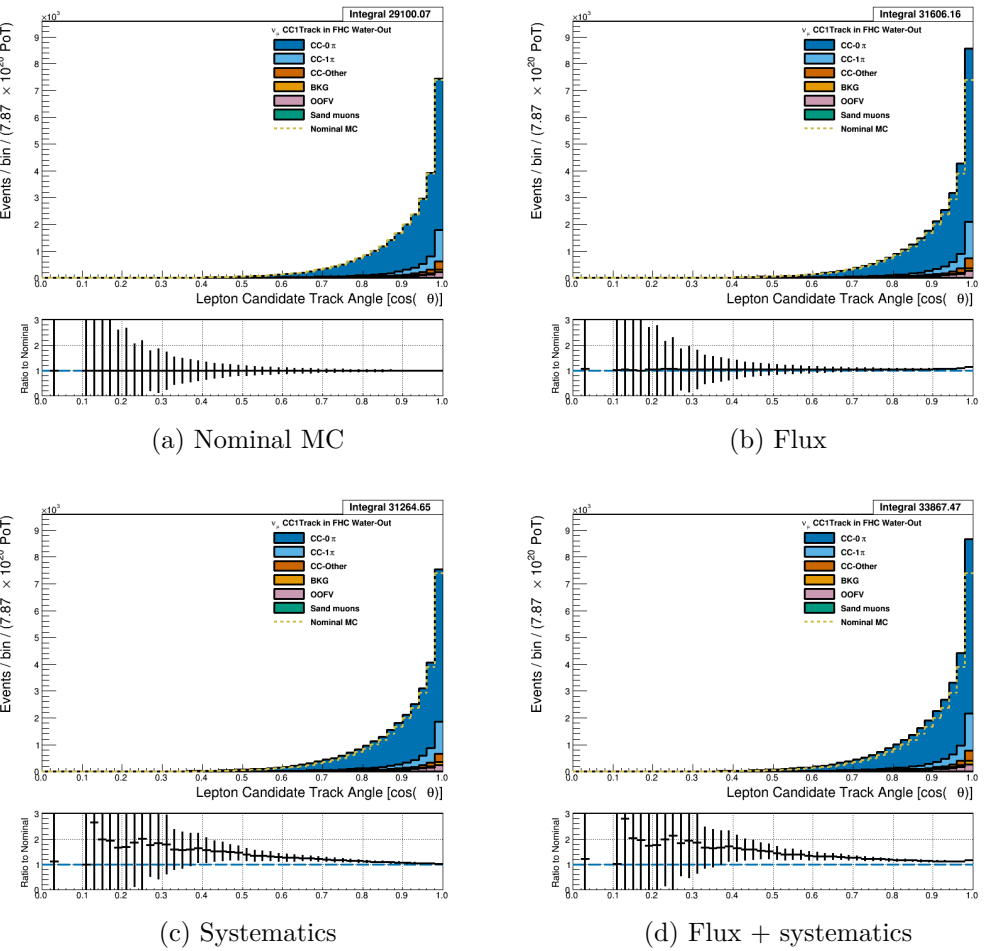


Figure 3.27: Reconstructed lepton candidate $\cos \theta$ separated by topology for FHC ν_μ CC 1-Track events occurring in the PØD in water-out mode. (a) The nominal MC prediction without any weights applied. (b) The flux tuning are applied. (c) The systematic weighting are applied. (d) Both flux and systematic weighting are applied.

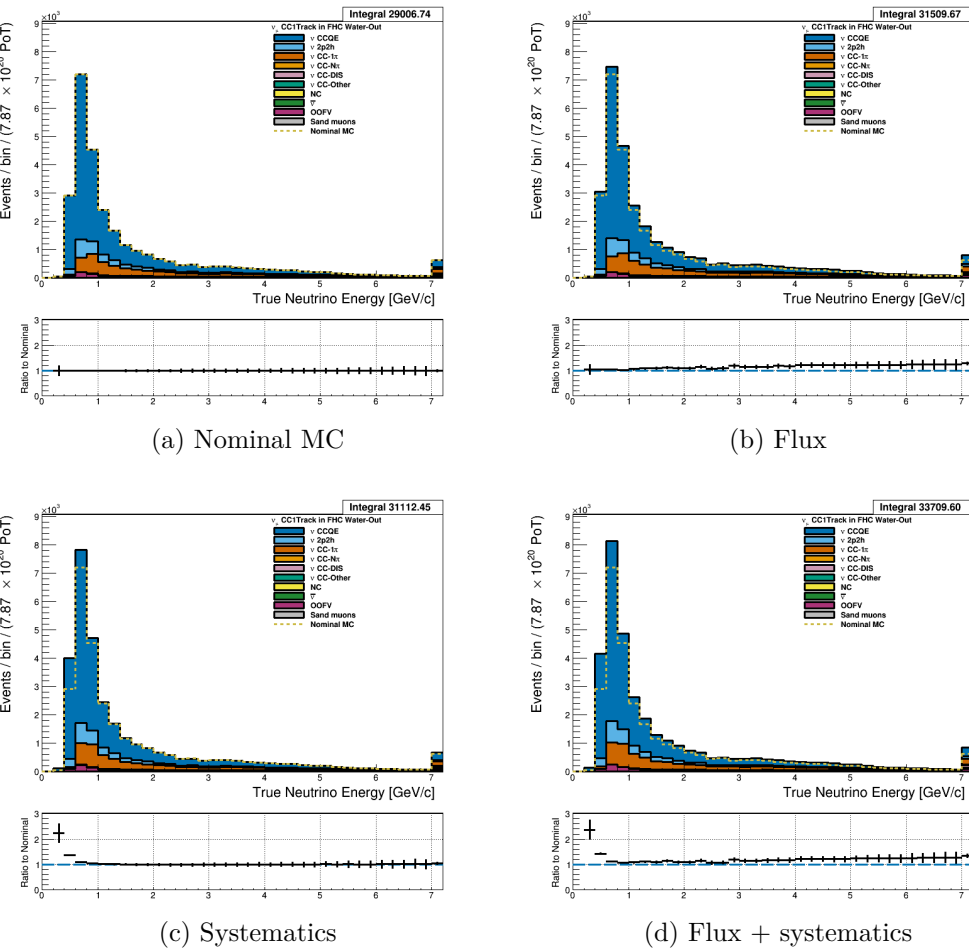


Figure 3.28: True neutrino energy associated with the lepton candidate separated by NEUT model interaction mode for FHC ν_μ CC 1-Track events occurring in the PØD in water-out mode. (a) The nominal MC prediction without any weights applied. (b) The flux tuning are applied. (c) The systematic weighting are applied. (d) Both flux and systematic weighting are applied.

550 3.4.2.2 $\bar{\nu}_\mu$ Selection in RHC Mode: Figures

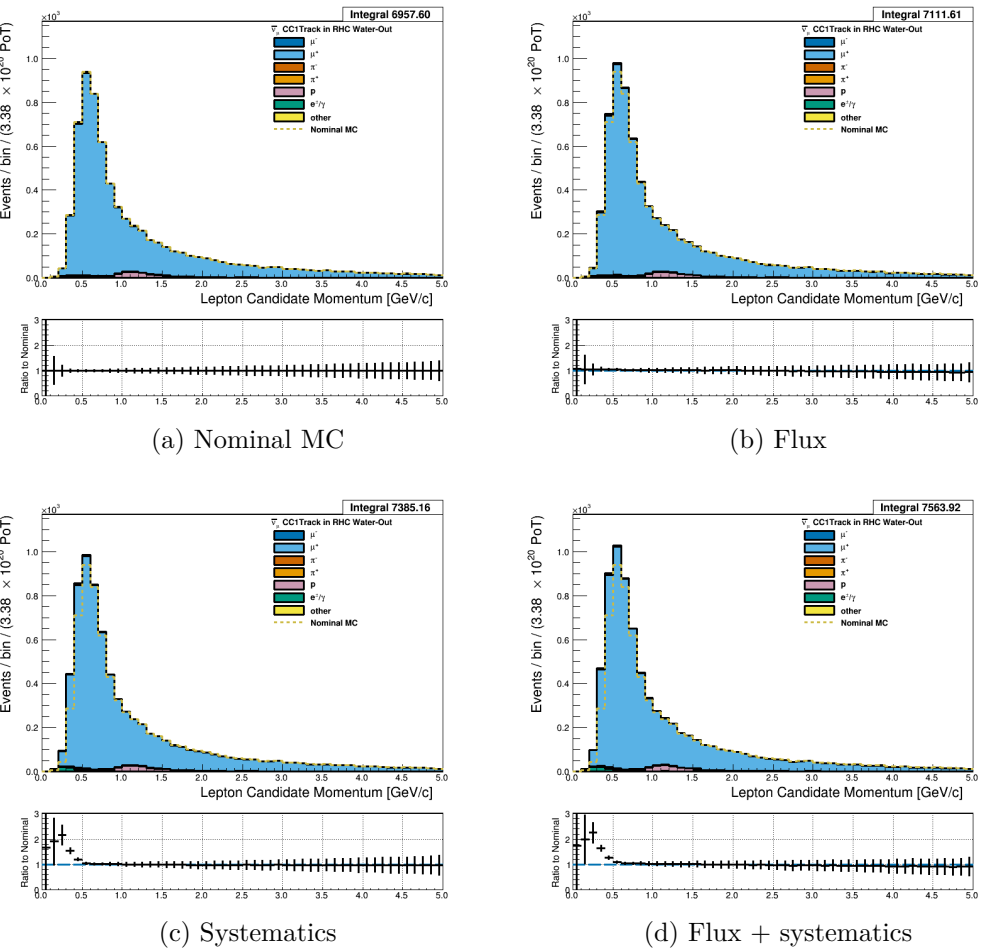


Figure 3.29: Reconstructed lepton candidate momentum separated by true particle species for RHC $\bar{\nu}_\mu$ CC 1-Track events occurring in the PØD in water-out mode. Reconstructed lepton candidate angle separated by true particle species for RHC $\bar{\nu}_\mu$ CC Inc. events occurring in the PØD in water-in mode. (a) The nominal MC prediction without any weights applied. (b) The flux tuning are applied. (c) The systematic weighting are applied. (c) Both flux and systematic weighting are applied.

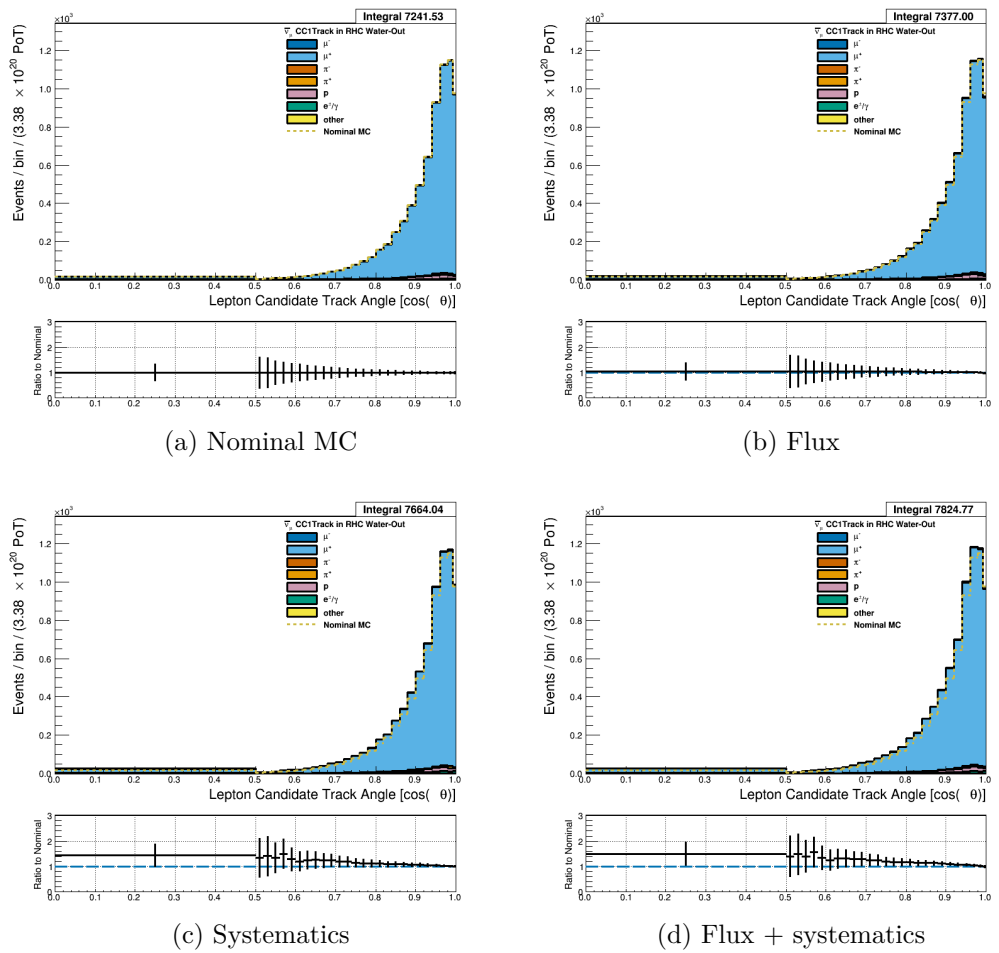


Figure 3.30: Reconstructed lepton candidate angle separated by true particle species for RHC $\bar{\nu}_\mu$ CC 1-Track events occurring in the PØD in water-out mode. (a) The nominal MC prediction without any weights applied. (b) The flux tuning are applied. (c) The systematic weighting are applied. (d) Both flux and systematic weighting are applied.

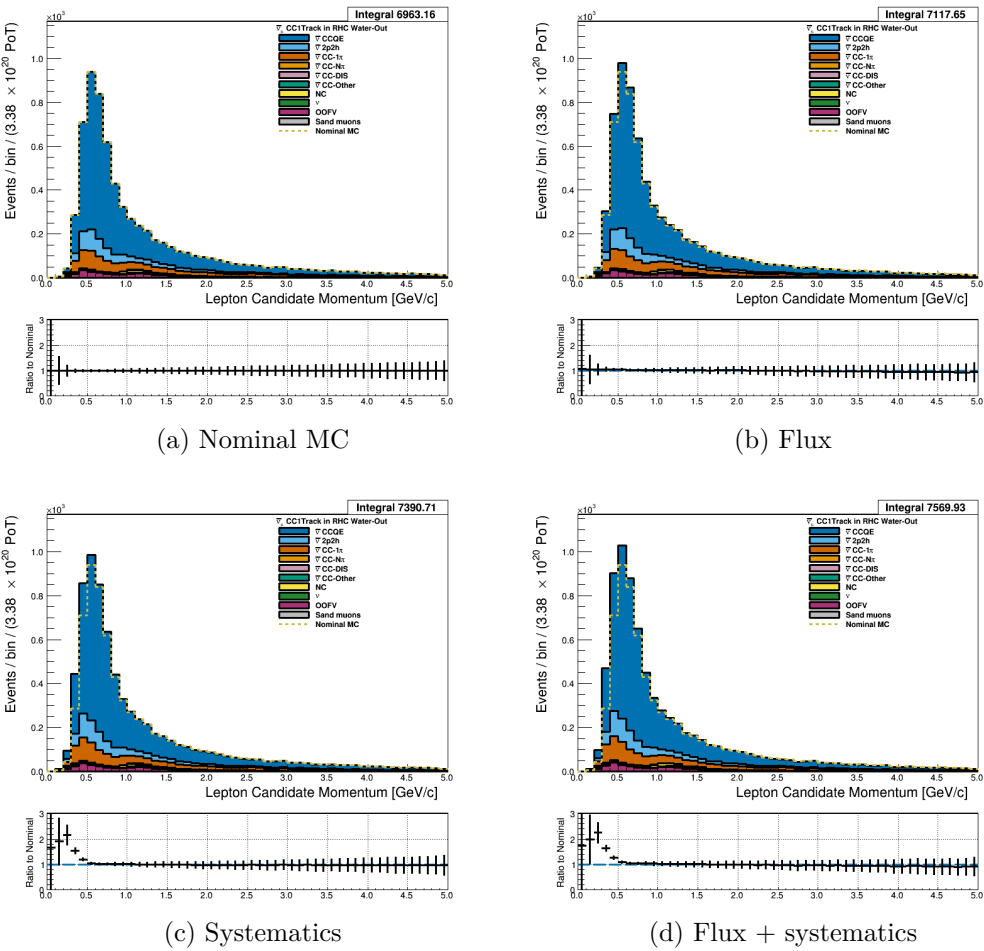


Figure 3.31: Reconstructed lepton candidate momentum separated by NEUT model interaction mode for RHC $\bar{\nu}_\mu$ CC 1-Track events occurring in the PØD in water-out mode. (a) The nominal MC prediction without any weights applied. (b) The flux tuning are applied. (c) The systematic weighting are applied. (d) Both flux and systematic weighting are applied.

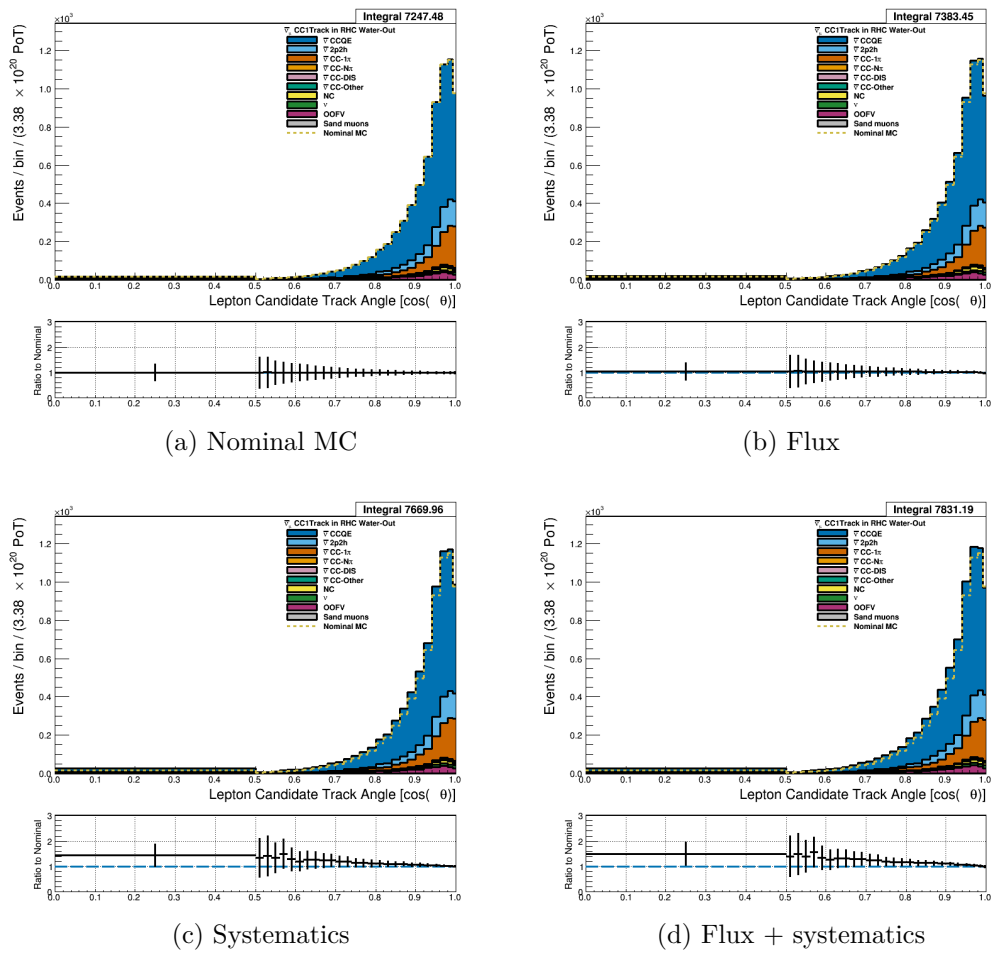


Figure 3.32: Reconstructed lepton candidate $\cos \theta$ separated by NEUT model interaction mode for RHC $\bar{\nu}_\mu$ CC 1-TracI events occurring in the P0D in water-out mode. (a) The nominal MC prediction without any weights applied. (b) The flux tuning are applied. (c) The systematic weighting are applied. (d) Both flux and systematic weighting are applied.

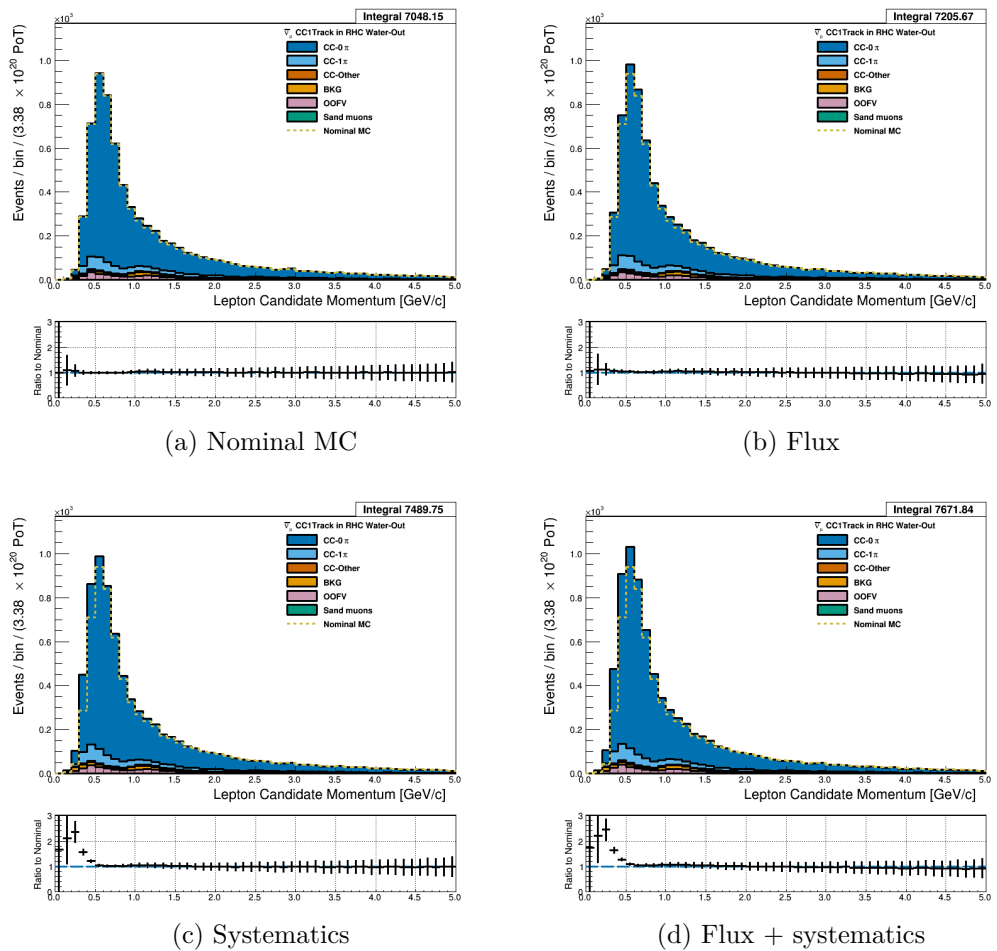


Figure 3.33: Reconstructed lepton candidate momentum separated by topology for RHC $\bar{\nu}_\mu$ CC 1-Track events occurring in the PØD in water-out mode. (a) The nominal MC prediction without any weights applied. (b) The flux tuning are applied. (c) The systematic weighting are applied. (d) Both flux and systematic weighting are applied.

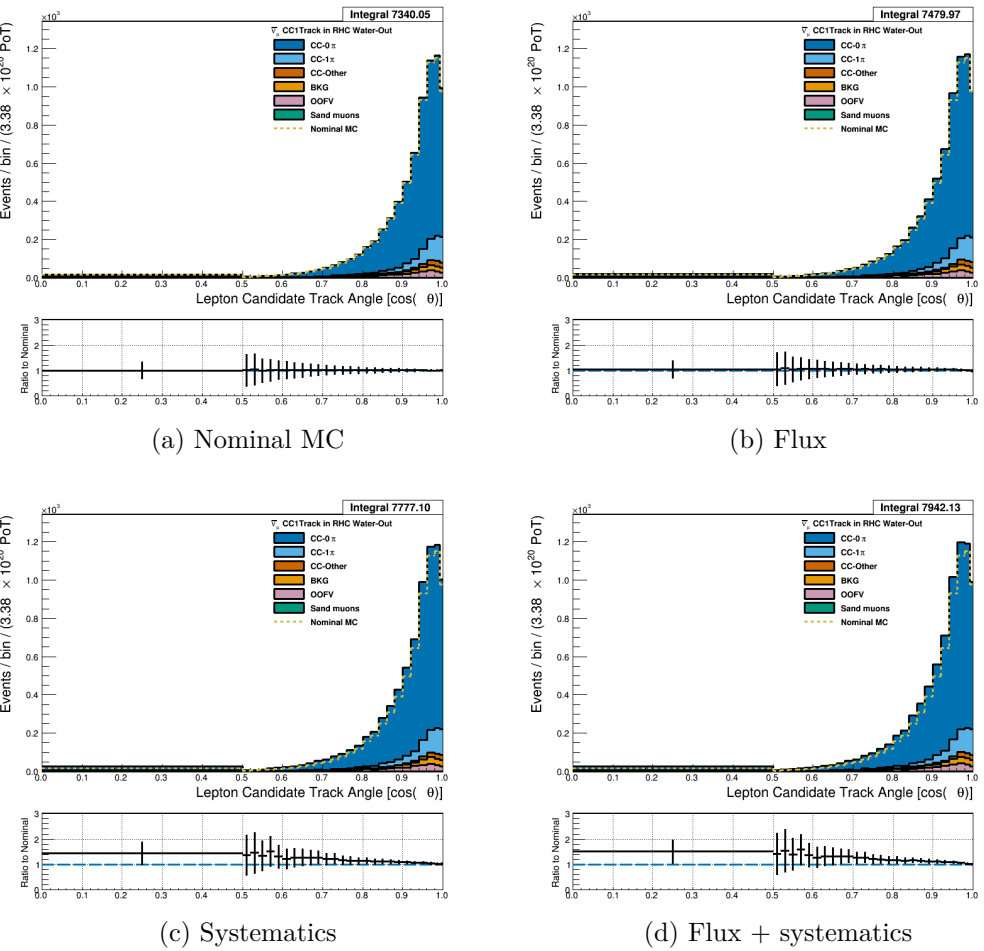


Figure 3.34: Reconstructed lepton candidate $\cos \theta$ separated by topology for RHC $\bar{\nu}_\mu$ CC 1-Track events occurring in the PØD in water-out mode. (a) The nominal MC prediction without any weights applied. (b) The flux tuning are applied. (c) The systematic weighting are applied. (d) Both flux and systematic weighting are applied.

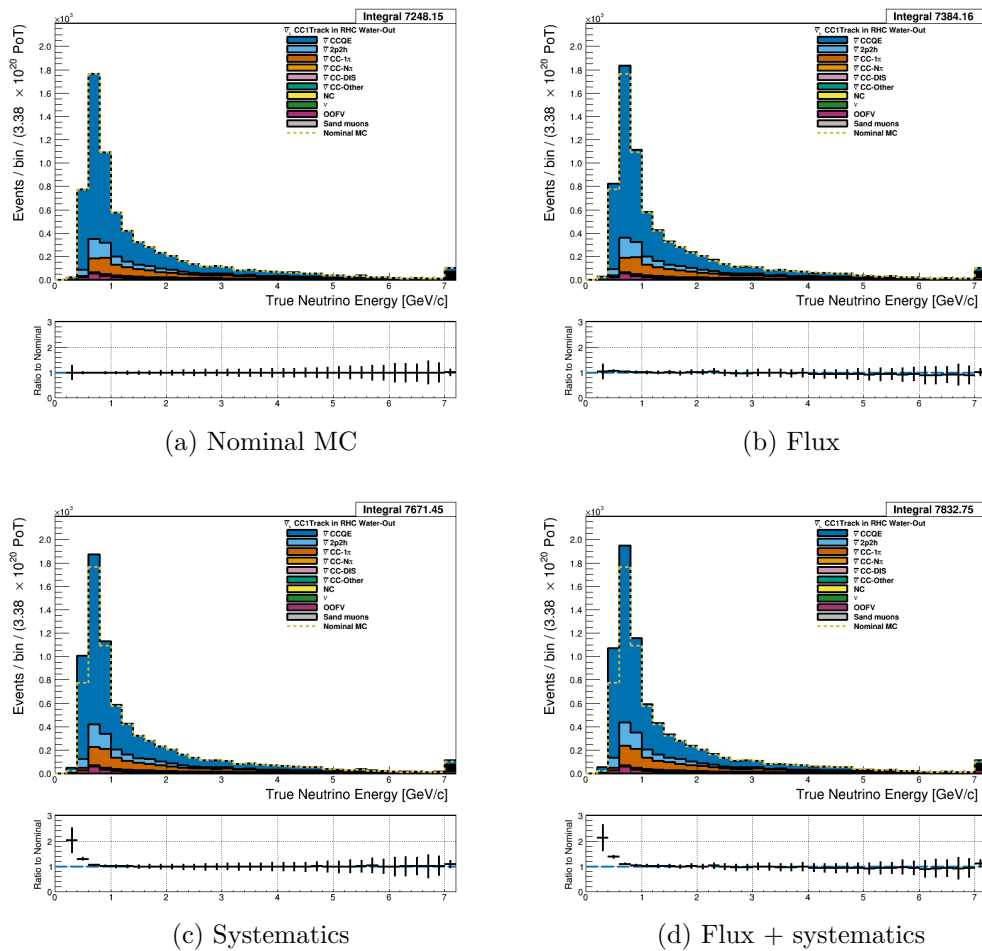


Figure 3.35: True neutrino energy associated with the lepton candidate separated by NEUT model interaction mode for RHC $\bar{\nu}_\mu$ CC 1-Track events occurring in the PØD in water-out mode. (a) The nominal MC prediction without any weights applied. (b) The flux tuning are applied. (c) The systematic weighting are applied. (d) Both flux and systematic weighting are applied.

551 **3.4.2.3 ν_μ Background Selection in RHC Mode:** Text [Add figures here](#)

552 **3.4.3 CC N-Tracks (CCnQE Enhanced)**

553 Text [Add figures here](#)

554 **3.4.3.1 ν_μ Selection in FHC Mode:** Text

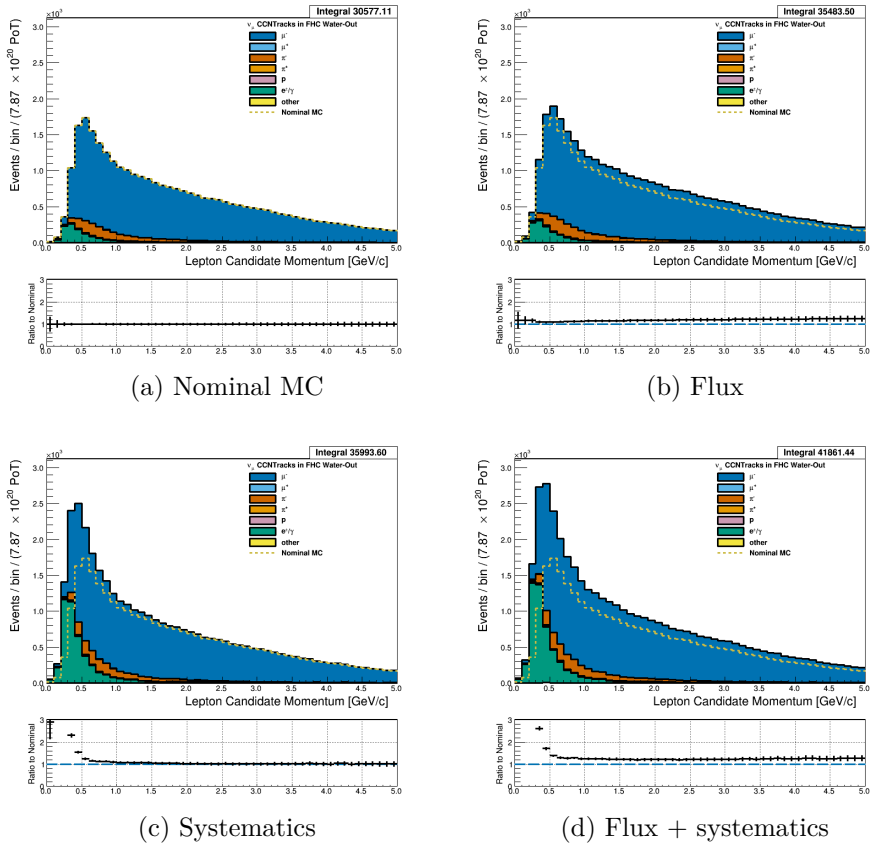


Figure 3.36: Reconstructed lepton candidate momentum separated by true particle species for FHC ν_μ CC N-Tracks events occurring in the PØD in water-out mode. (a) The nominal MC prediction without any weights applied. (b) The flux tuning are applied. (c) The systematic weighting are applied. (e) Both flux and systematic weighting are applied.

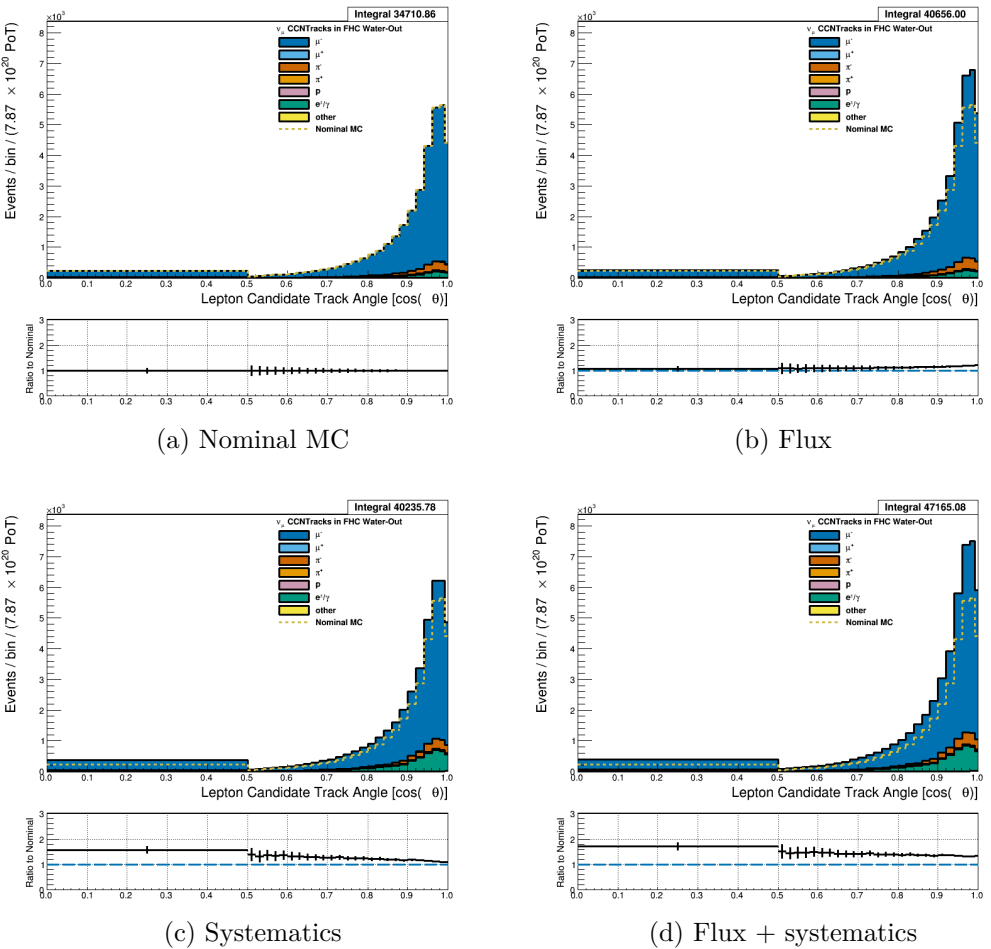


Figure 3.37: Reconstructed lepton candidate angle separated by true particle species for FHC ν_μ CC N-Tracks events occurring in the PØD in water-out mode. (a) The nominal MC prediction without any weights applied. (b) The flux tuning are applied. (c) The systematic weighting are applied. (d) Both flux and systematic weighting are applied.

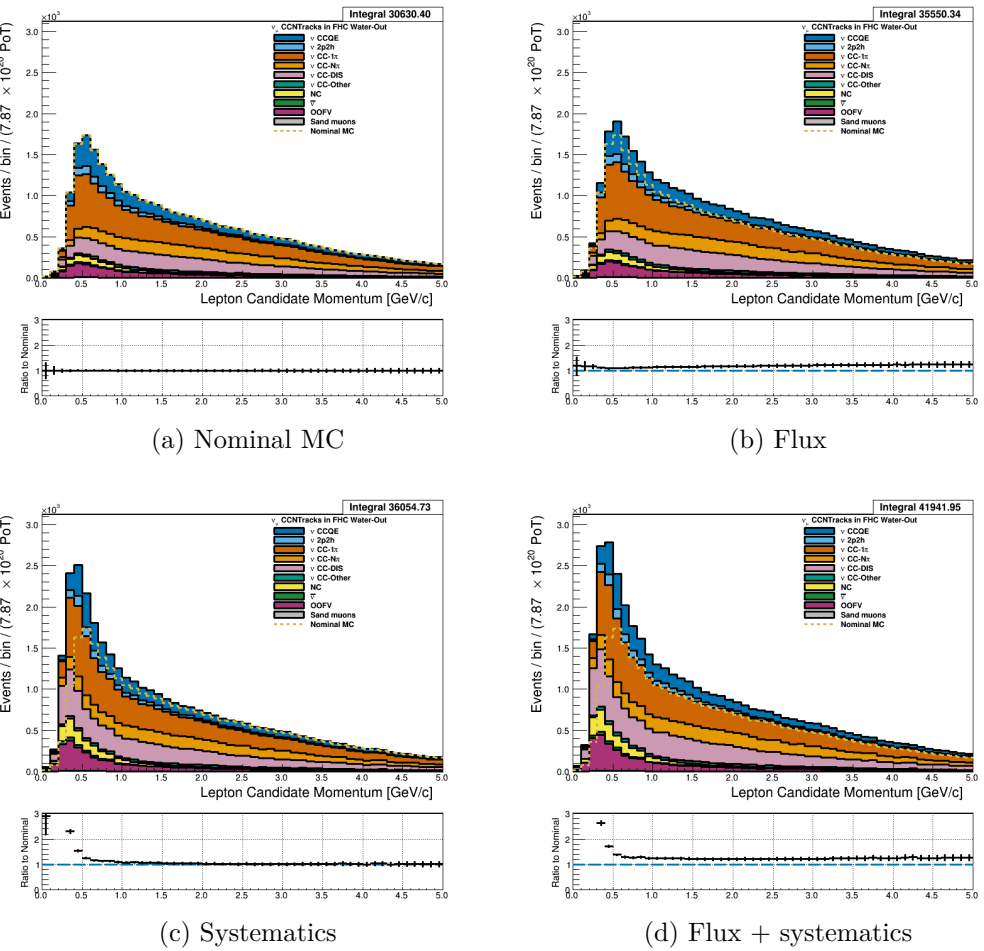


Figure 3.38: Reconstructed lepton candidate momentum separated by NEUT model interaction mode for FHC ν_μ CC N-Tracks events occurring in the PØD in water-out mode. (a) The nominal MC prediction without any weights applied. (b) The flux tuning are applied. (c) The systematic weighting are applied. (d) Both flux and systematic weighting are applied.

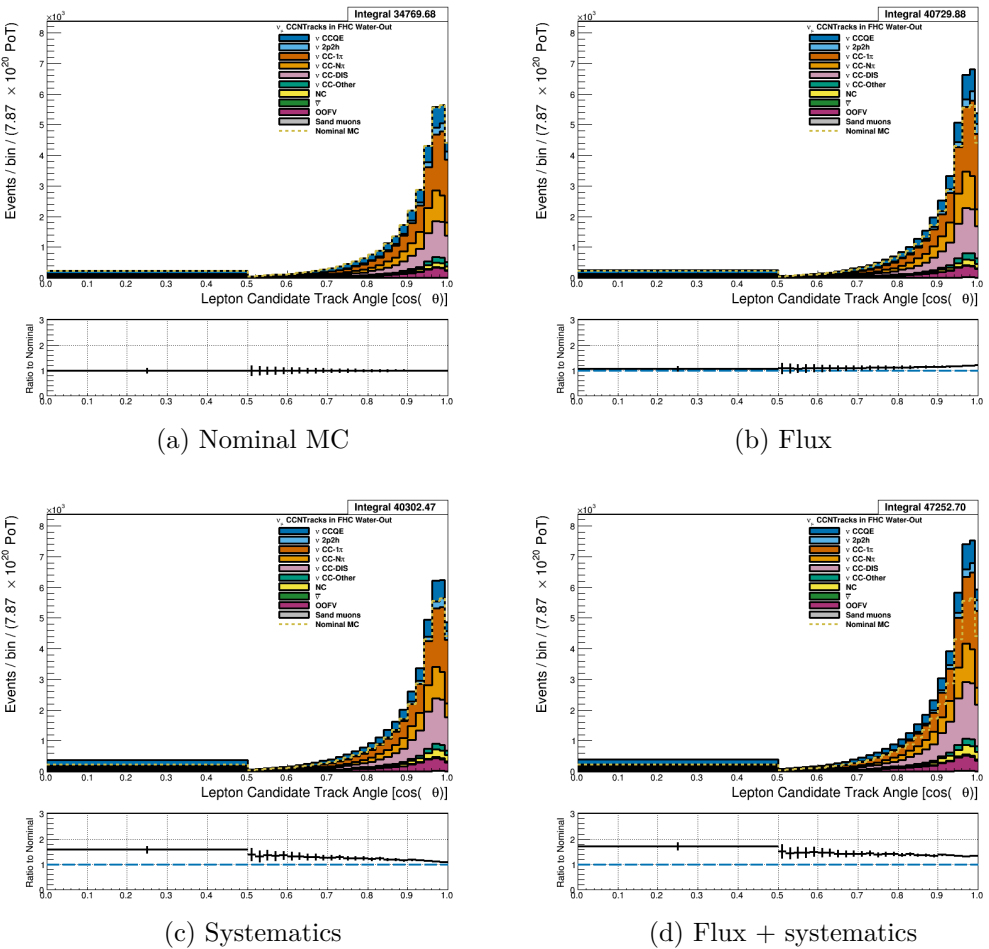


Figure 3.39: Reconstructed lepton candidate $\cos \theta$ separated by NEUT model interaction mode for FHC ν_μ CC N-Tracks events occurring in the PØD in water-out mode. (a) The nominal MC prediction without any weights applied. (b) The flux tuning are applied. (c) The systematic weighting are applied. (d) Both flux and systematic weighting are applied.

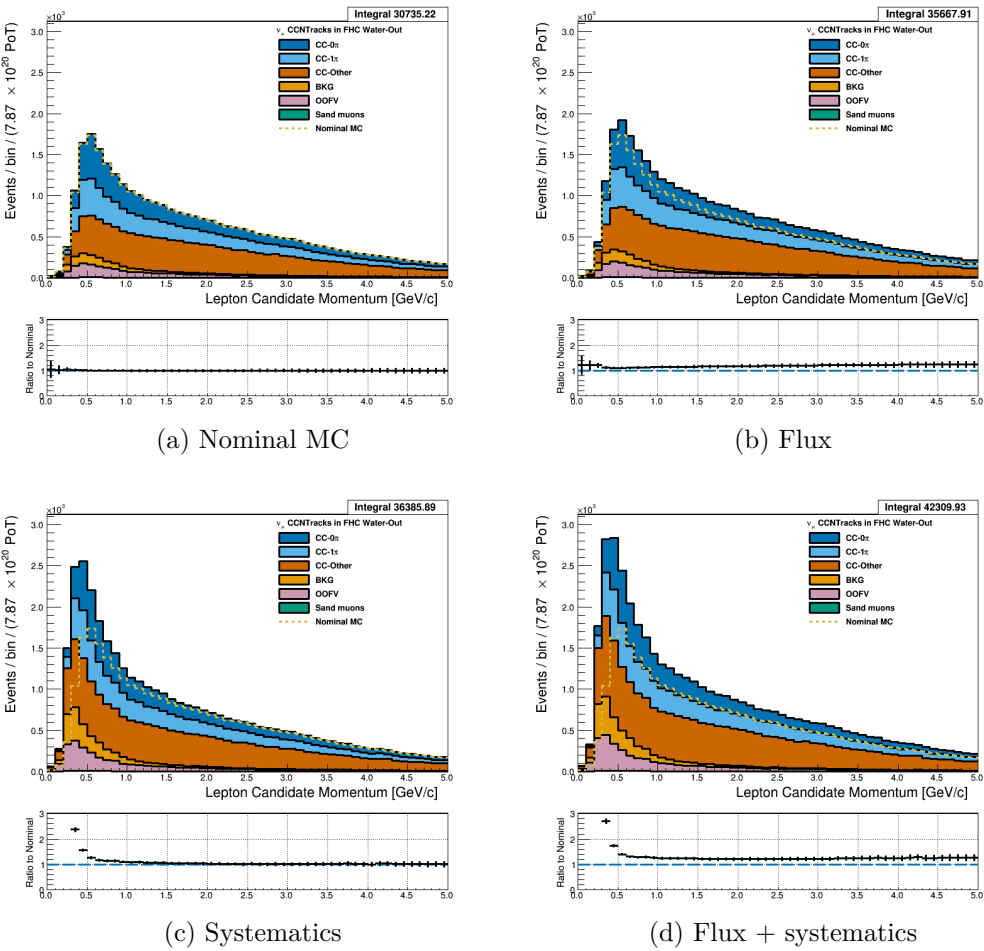


Figure 3.40: Reconstructed lepton candidate momentum separated by topology for FHC ν_μ CC N-Tracks events occurring in the PØD in water-out mode. (a) The nominal MC prediction without any weights applied. (b) The flux tuning are applied. (c) The systematic weighting are applied. (d) Both flux and systematic weighting are applied.

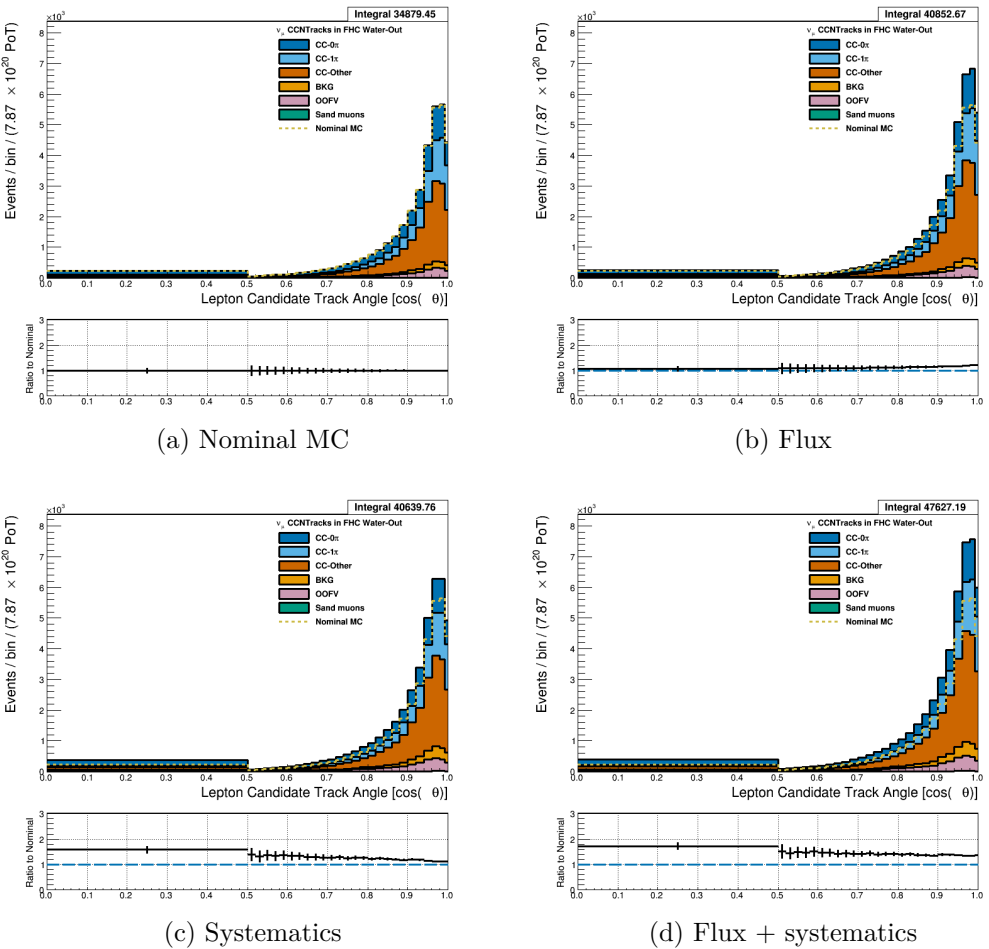


Figure 3.41: Reconstructed lepton candidate $\cos \theta$ separated by topology for FHC ν_μ CC N-Tracks events occurring in the PØD in water-out mode. (a) The nominal MC prediction without any weights applied. (b) The flux tuning are applied. (c) The systematic weighting are applied. (d) Both flux and systematic weighting are applied.

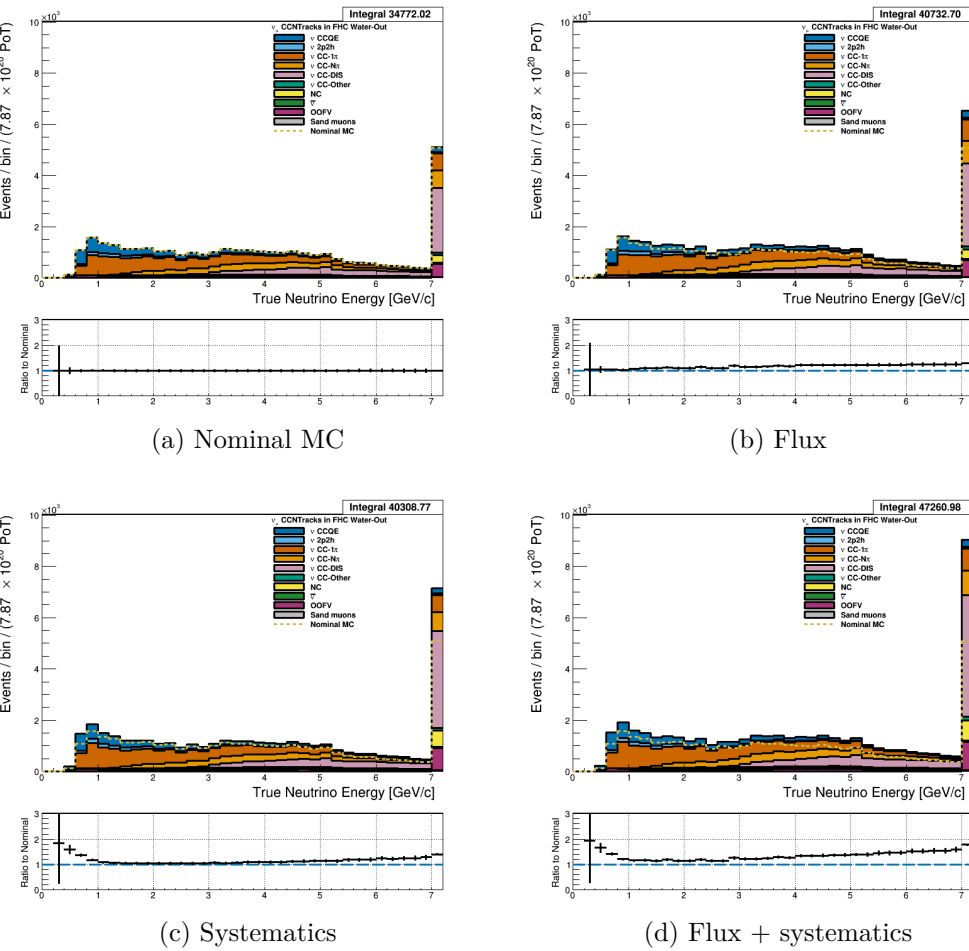


Figure 3.42: True neutrino energy associated with the lepton candidate separated by NEUT model interaction mode for FHC ν_μ CC N-Tracks events occurring in the PØD in water-out mode. (a) The nominal MC prediction without any weights applied. (b) The flux tuning are applied. (c) The systematic weighting are applied. (d) Both flux and systematic weighting are applied.

3.4.3.2 $\bar{\nu}_\mu$ Selection in RHC Mode: Text goes here

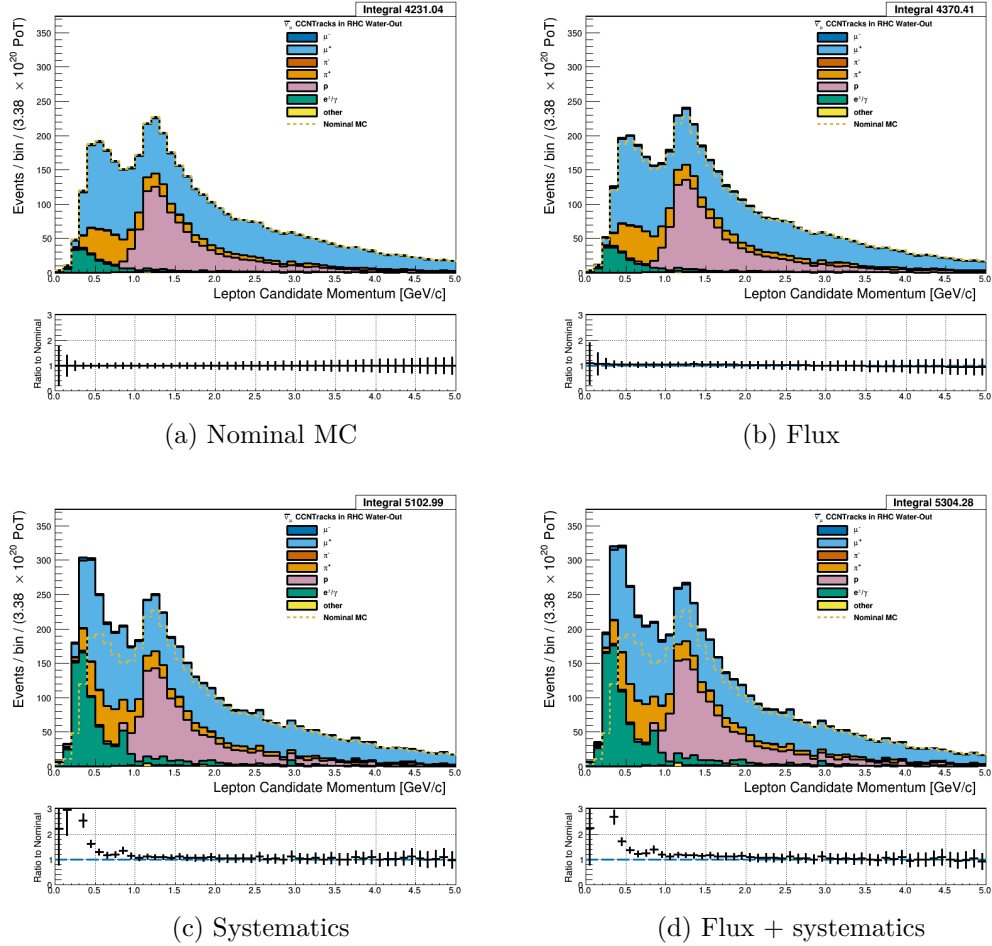


Figure 3.43: Reconstructed lepton candidate momentum separated by true particle species for RHC $\bar{\nu}_\mu$ CC N-Tracks events occurring in the PØD in water-out mode. Reconstructed lepton candidate angle separated by true particle species for RHC $\bar{\nu}_\mu$ CC N-Tracks events occurring in the PØD in water-in mode. (a) The nominal MC prediction without any weights applied. (b) The flux tuning are applied. (c) The systematic weighting are applied. (d) Both flux and systematic weighting are applied.

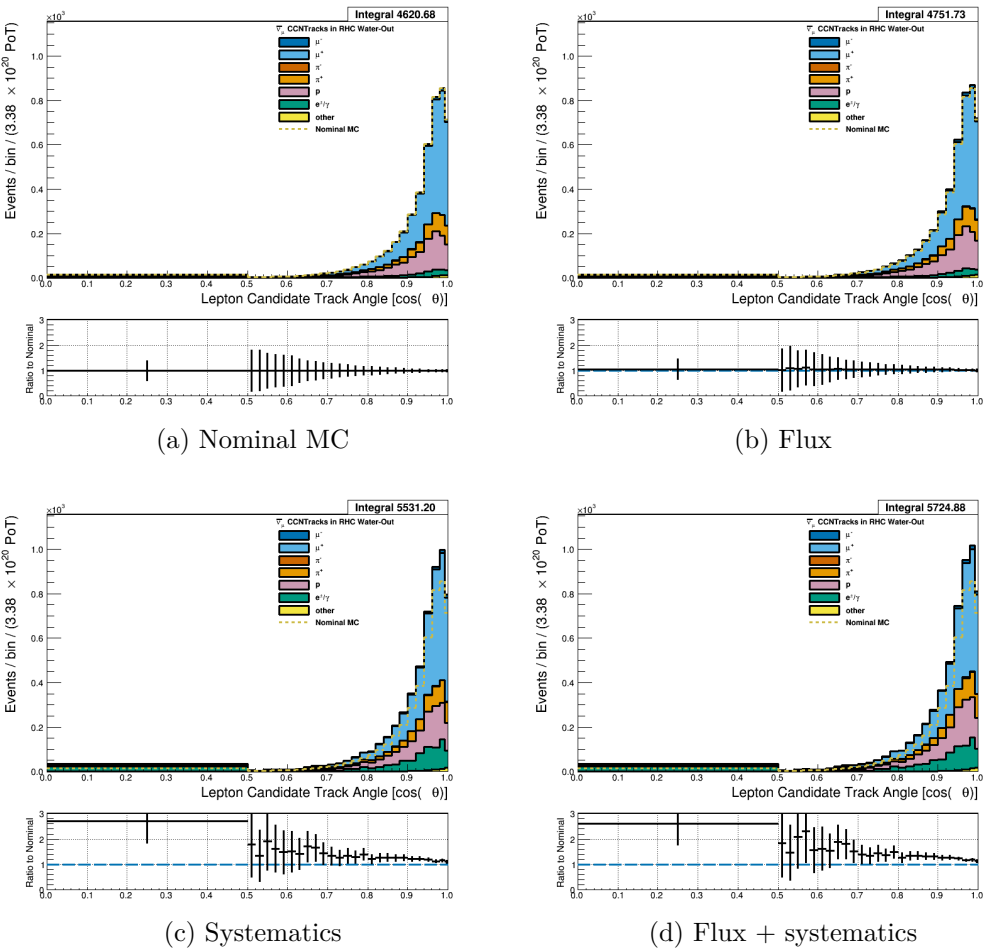


Figure 3.44: Reconstructed lepton candidate angle separated by true particle species for RHC $\bar{\nu}_\mu$ CC N-Tracks events occurring in the PØD in water-out mode. (a) The nominal MC prediction without any weights applied. (b) The flux tuning are applied. (c) The systematic weighting are applied. (d) Both flux and systematic weighting are applied.

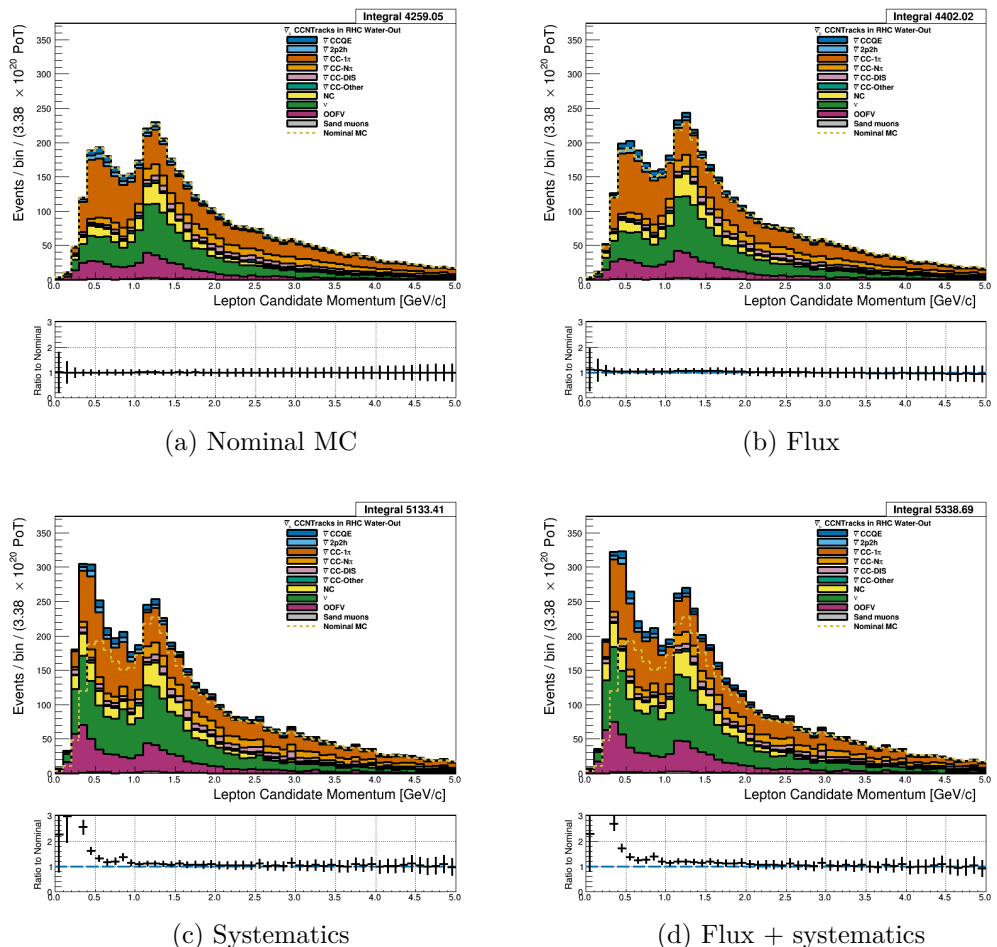


Figure 3.45: Reconstructed lepton candidate momentum separated by NEUT model interaction mode for RHC $\bar{\nu}_\mu$ CC N-Tracks events occurring in the PØD in water-out mode. (a) The nominal MC prediction without any weights applied. (b) The flux tuning are applied. (c) The systematic weighting are applied. (d) Both flux and systematic weighting are applied.

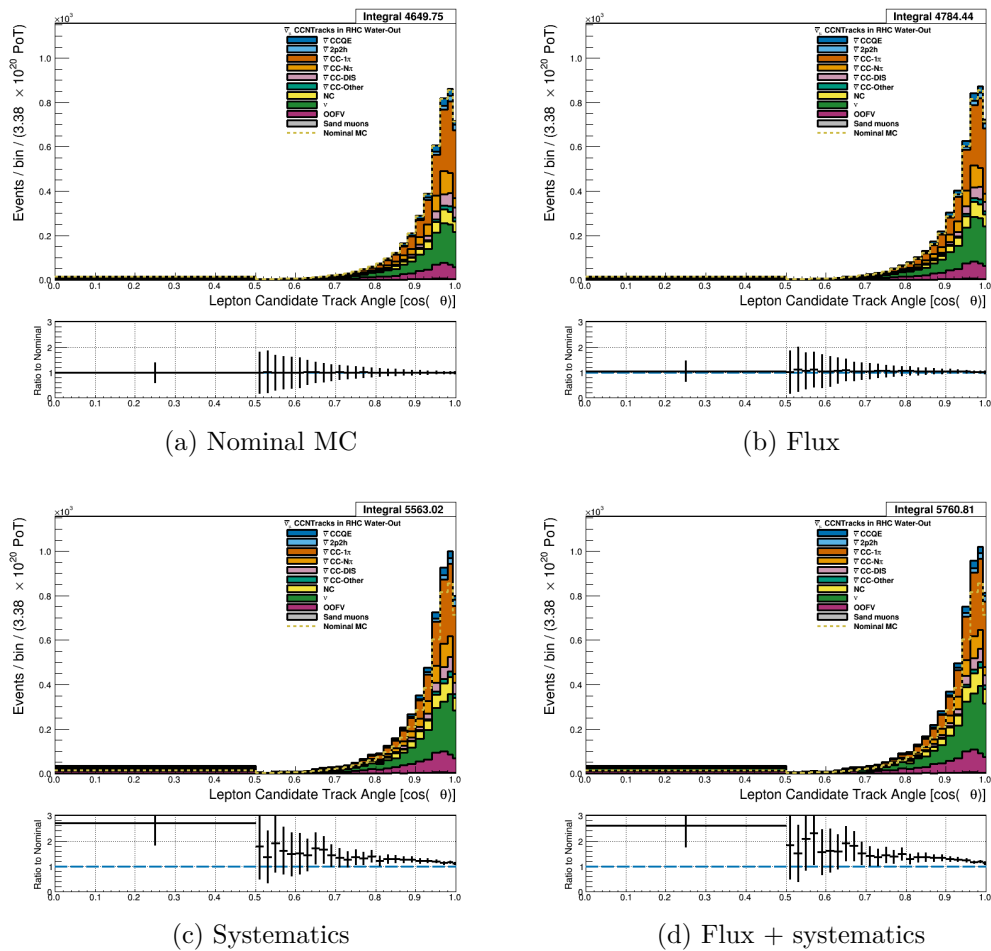


Figure 3.46: Reconstructed lepton candidate $\cos \theta$ separated by NEUT model interaction mode for RHC $\bar{\nu}_\mu$ CC N-Tracks events occurring in the PØD in water-out mode. (a) The nominal MC prediction without any weights applied. (b) The flux tuning are applied. (c) The systematic weighting are applied. (d) Both flux and systematic weighting are applied.

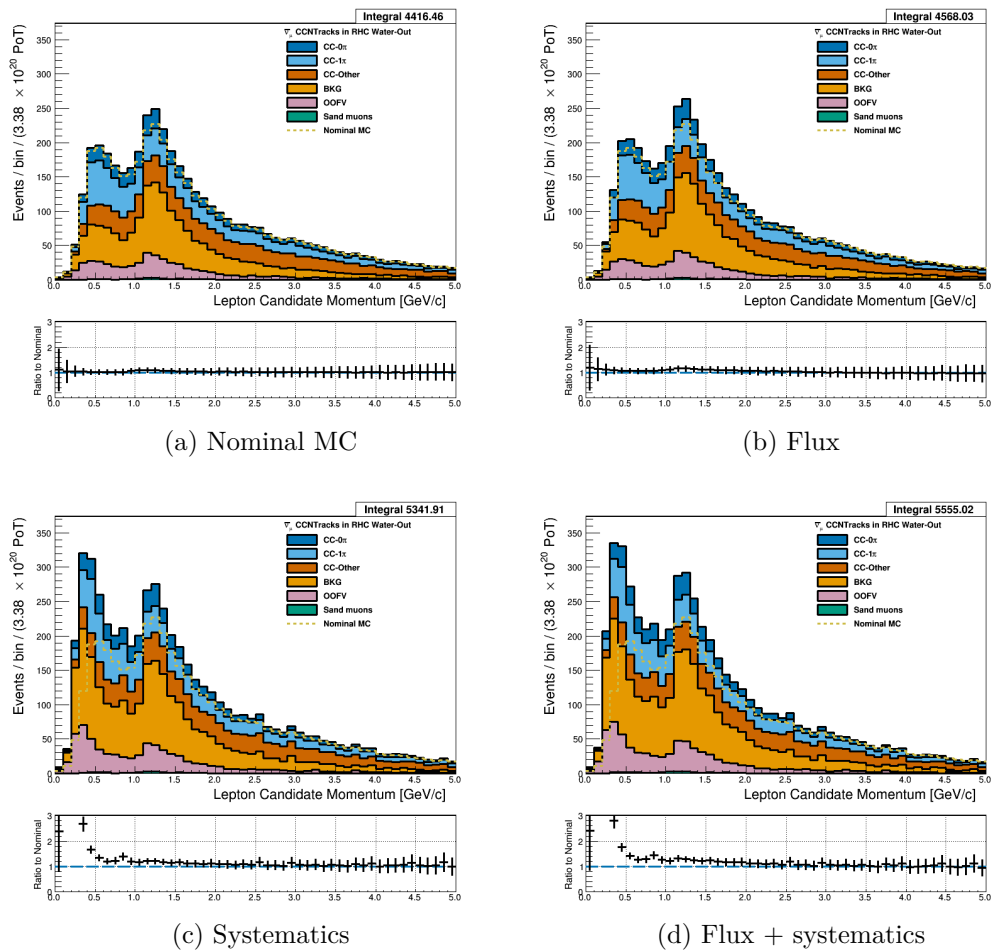


Figure 3.47: Reconstructed lepton candidate momentum separated by topology for RHC $\bar{\nu}_\mu$ CC N-Tracks events occurring in the PØD in water-out mode. (a) The nominal MC prediction without any weights applied. (b) The flux tuning are applied. (c) The systematic weighting are applied. (d) Both flux and systematic weighting are applied.

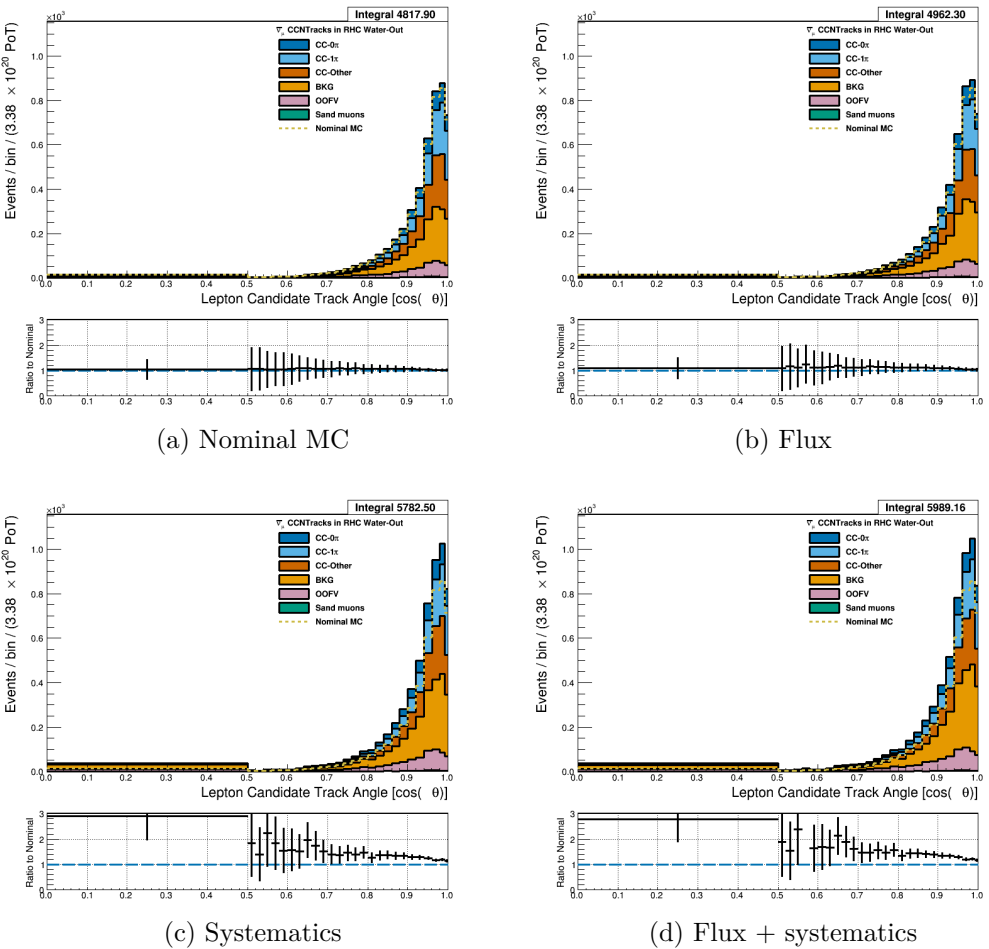


Figure 3.48: Reconstructed lepton candidate $\cos \theta$ separated by topology for RHC $\bar{\nu}_\mu$ CC N-Tracks events occurring in the PØD in water-out mode. (a) The nominal MC prediction without any weights applied. (b) The flux tuning are applied. (c) The systematic weighting are applied. (d) Both flux and systematic weighting are applied.

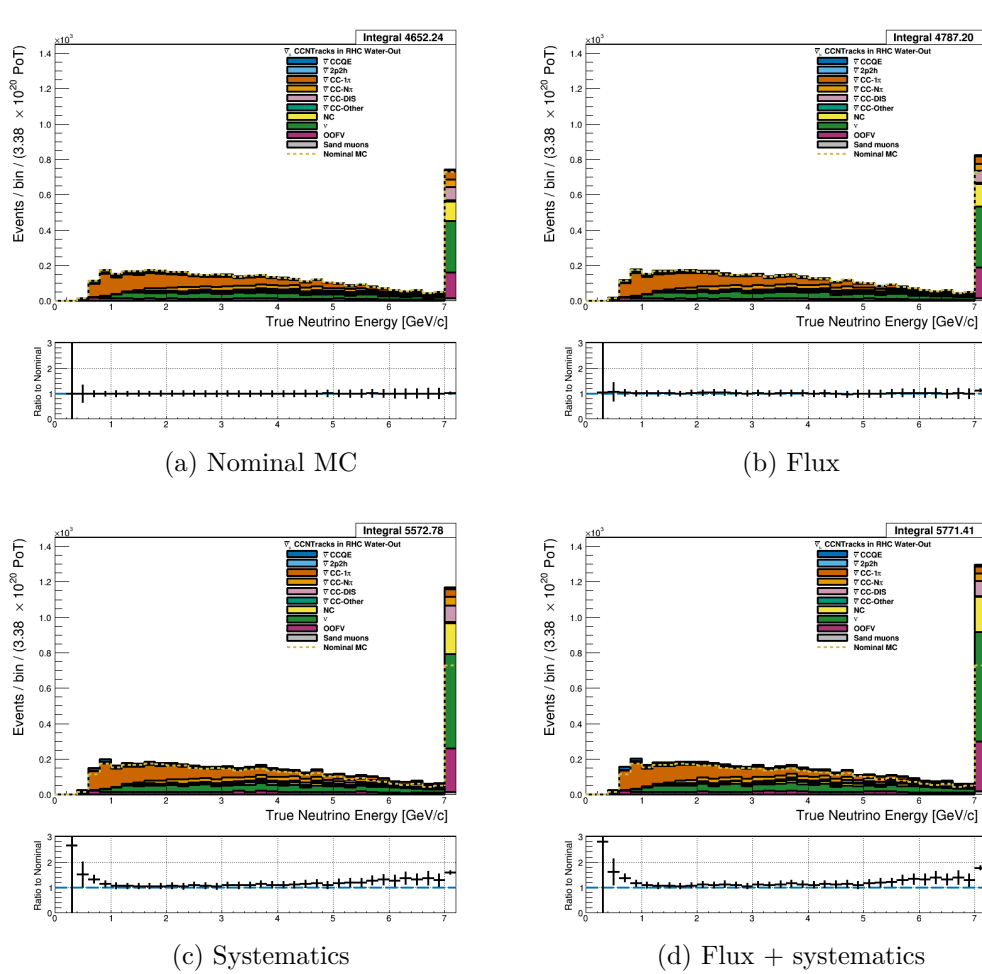


Figure 3.49: True neutrino energy associated with the lepton candidate separated by NEUT model interaction mode for RHC $\bar{\nu}_\mu$ CC N-Tracks events occurring in the PØD in water-out mode. (a) The nominal MC prediction without any weights applied. (b) The flux tuning are applied. (c) The systematic weighting are applied. (d) Both flux and systematic weighting are applied.

556 **3.4.3.3 ν_μ Background Selection in RHC Mode:** Text

557 **3.5 PØD Water-In Samples**

558 This section shows the kinematic distributions for the PØD water-in samples. These samples
 559 will demonstrate the similarities between it and water-out modes. First an examination of
 560 the CC Inclusive samples and the effects of the systematic weights will be explored. The

561 samples are then examined as CC 1-track and CC N-tracks.

562 **3.5.1 CC Inclusive**

563 The CC Inclusive sample cuts are discussed 3.2.1. Since both flux and detector systematic
564 weights are applied to all MC events in BANFF, it is important to validate the event weights.
565 Using neither set of weights is referred to as the nominal MC.

566 **3.5.1.1 ν_μ Selection in FHC Mode:** Shown in Figures 3.50 to 3.56 are the momentum
567 and $\cos\theta$ distributions for ν_μ CC Inclusive events in FHC mode. There are three pairs of
568 P, θ figures with the same truth information break down accompanied by one of neutrino
569 energy. The truth information categories are lepton candidate particle, NEUT reaction, and
570 topology. Each figure consists of a set of four sub-figures which illustrate the application of
571 flux and detector systematic weights.

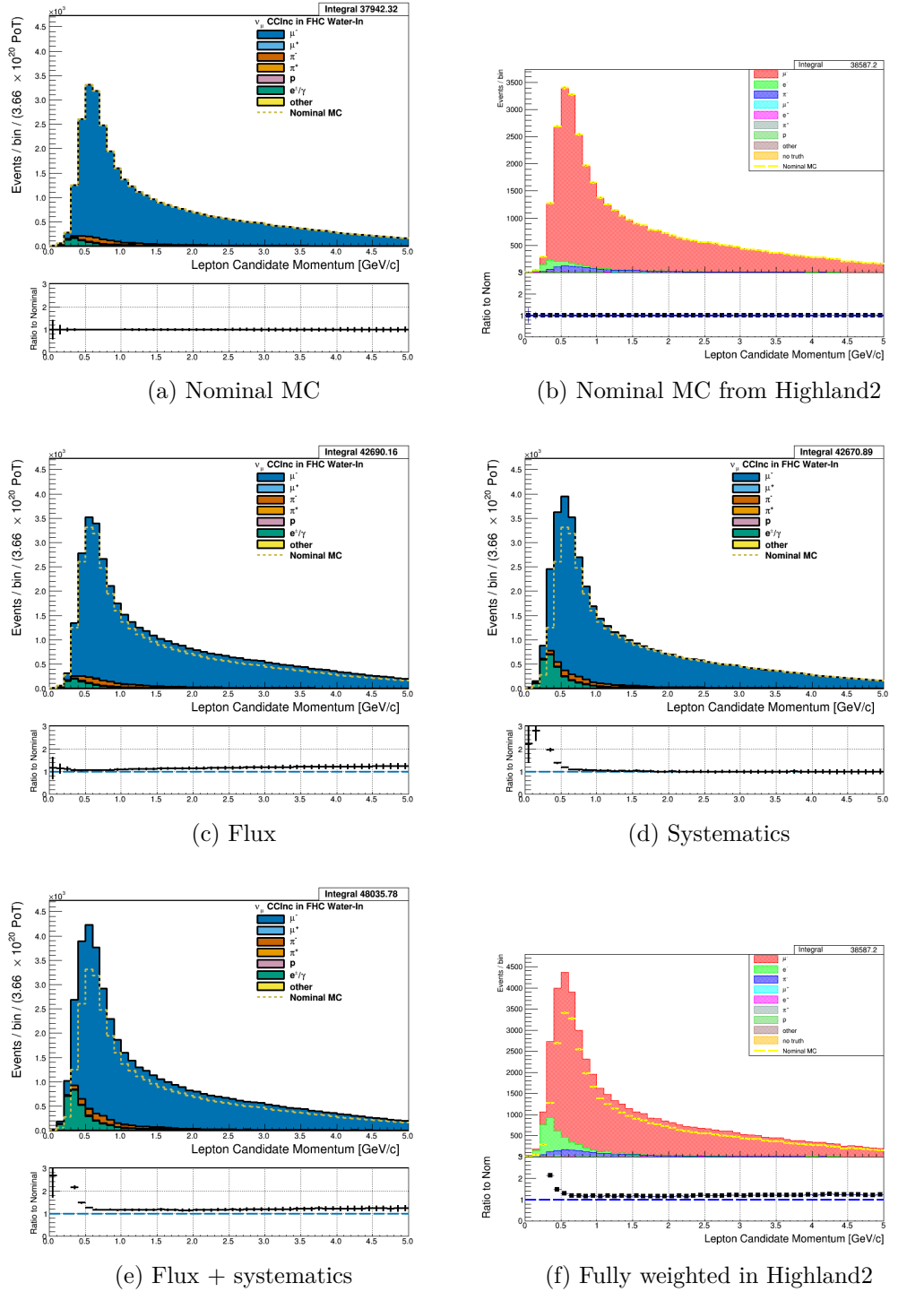


Figure 3.50: Reconstructed lepton candidate momentum separated by true particle species for FHC ν_μ CC Inc. events occurring in the PØD in water-in mode. (a) The nominal MC prediction without any weights applied. (b) Highland2 comparison for (a) without any weights applied using the “NOW” draw option. (c) The flux tuning are applied. (d) The systematic weighting are applied. (e) Both flux and systematic weighting are applied. (f) Highland2 comparison for (e).

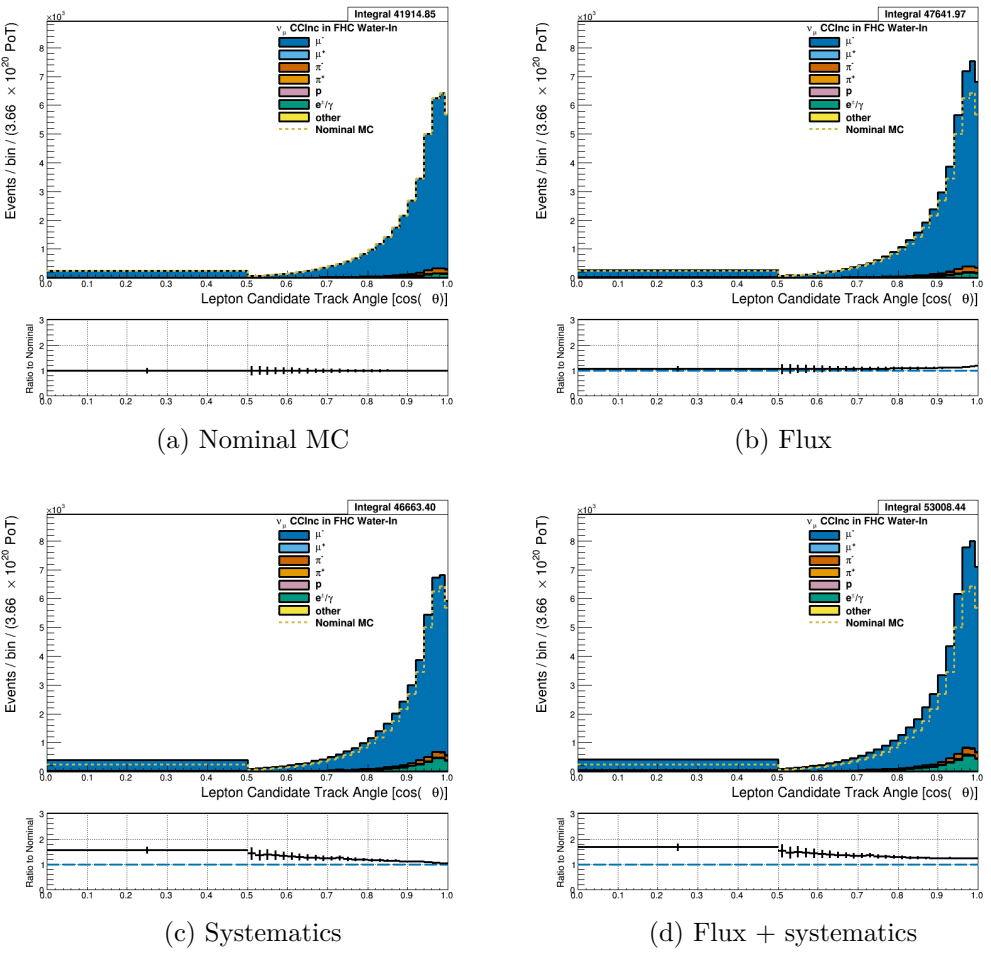


Figure 3.51: Reconstructed lepton candidate angle separated by true particle species for FHC ν_μ CC Inc. events occurring in the PØD in water-in mode. (a) The nominal MC prediction without any weights applied. (b) The flux tuning are applied. (c) The systematic weighting are applied. (d) Both flux and systematic weighting are applied.

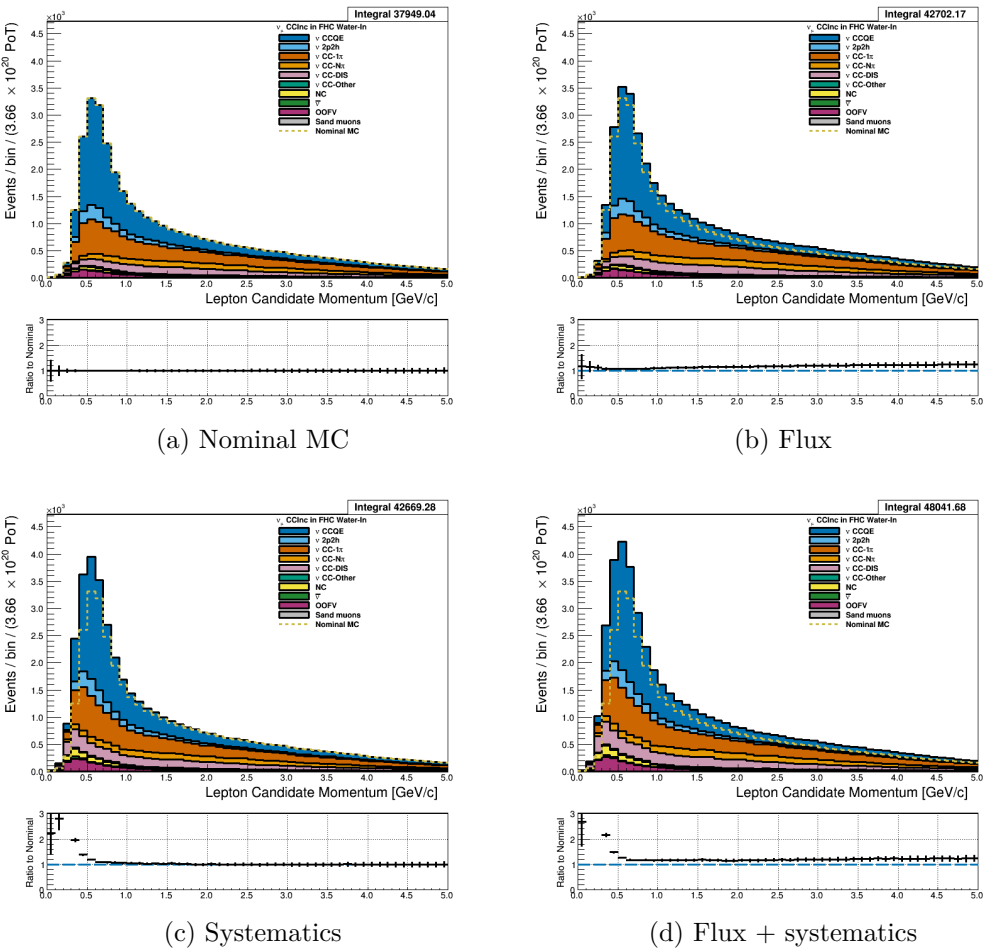


Figure 3.52: Reconstructed lepton candidate momentum separated by NEUT model interaction mode for FHC ν_μ CC Inc. events occurring in the PØD in water-in mode. (a) The nominal MC prediction without any weights applied. (b) The flux tuning are applied. (c) The systematic weighting are applied. (d) Both flux and systematic weighting are applied.

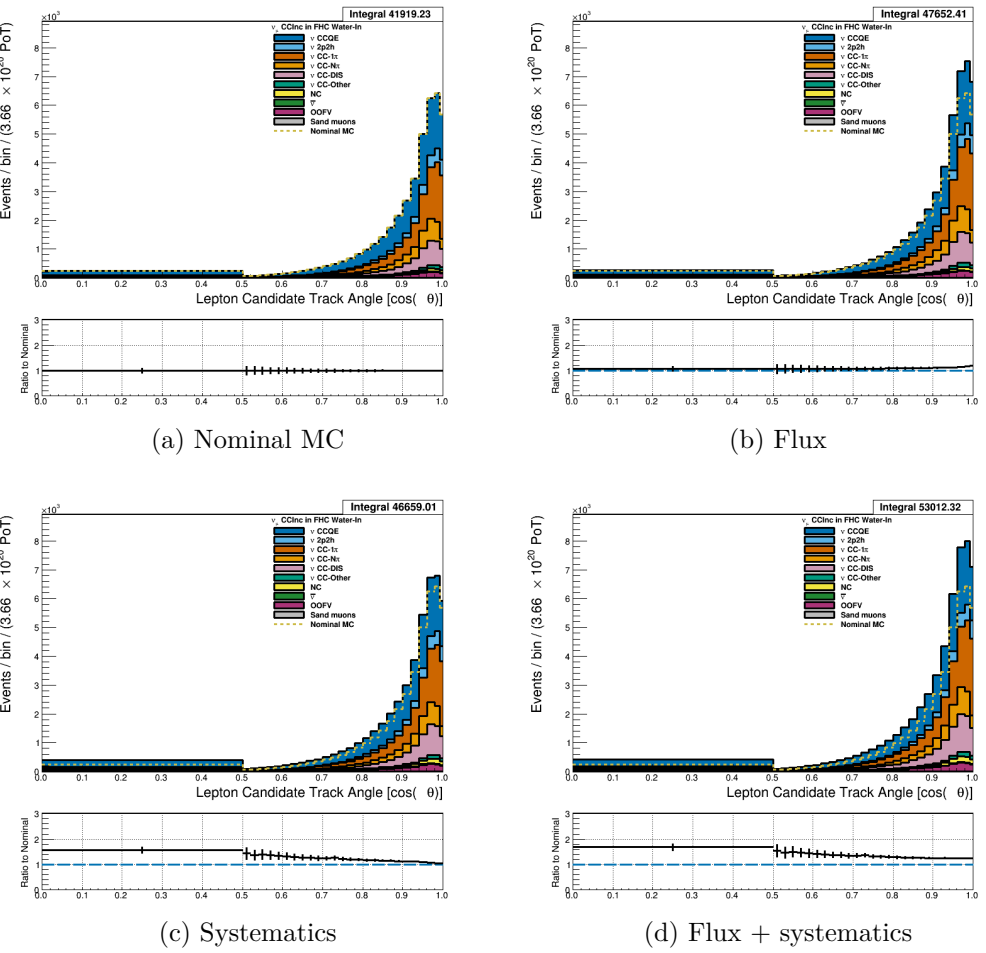


Figure 3.53: Reconstructed lepton candidate $\cos \theta$ separated by NEUT model interaction mode for FHC ν_μ CC Inc. events occurring in the PØD in water-in mode. (a) The nominal MC prediction without any weights applied. (b) The flux tuning are applied. (c) The systematic weighting are applied. (d) Both flux and systematic weighting are applied.

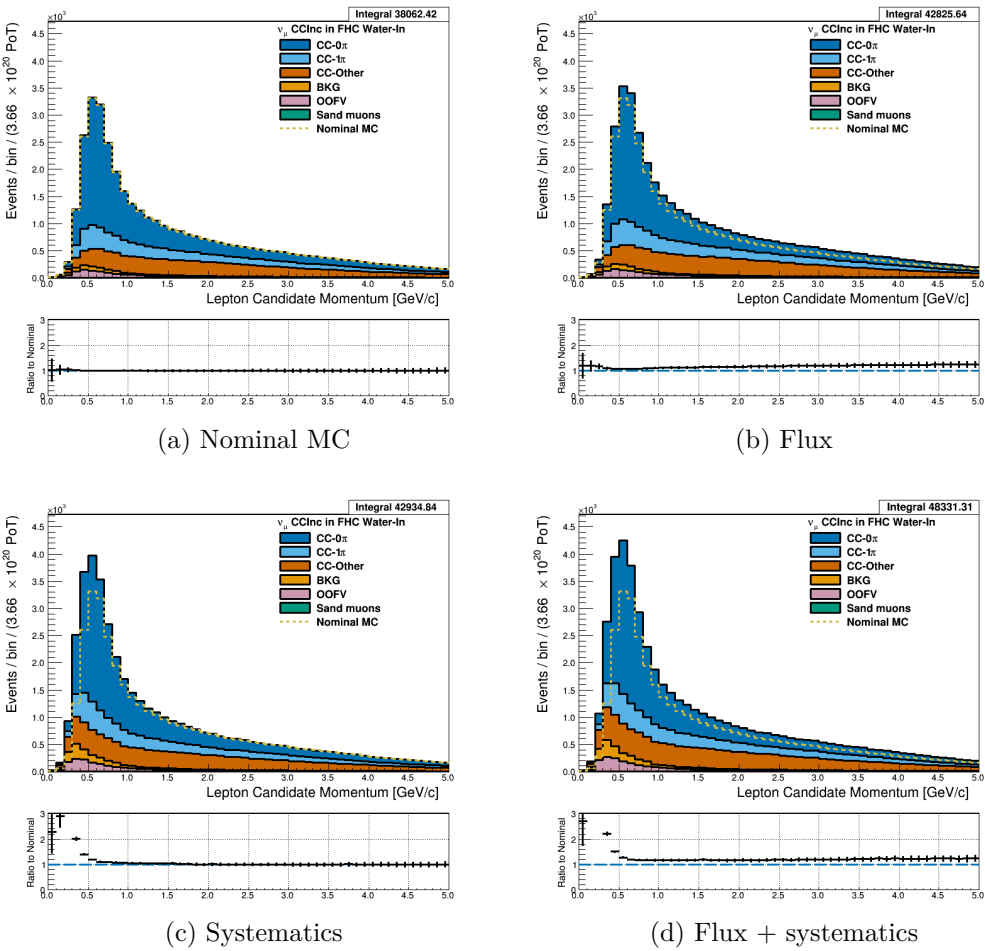


Figure 3.54: Reconstructed lepton candidate momentum separated by topology for FHC ν_μ CC Inc. events occurring in the PØD in water-in mode. (a) The nominal MC prediction without any weights applied. (b) The flux tuning are applied. (c) The systematic weighting are applied. (d) Both flux and systematic weighting are applied.

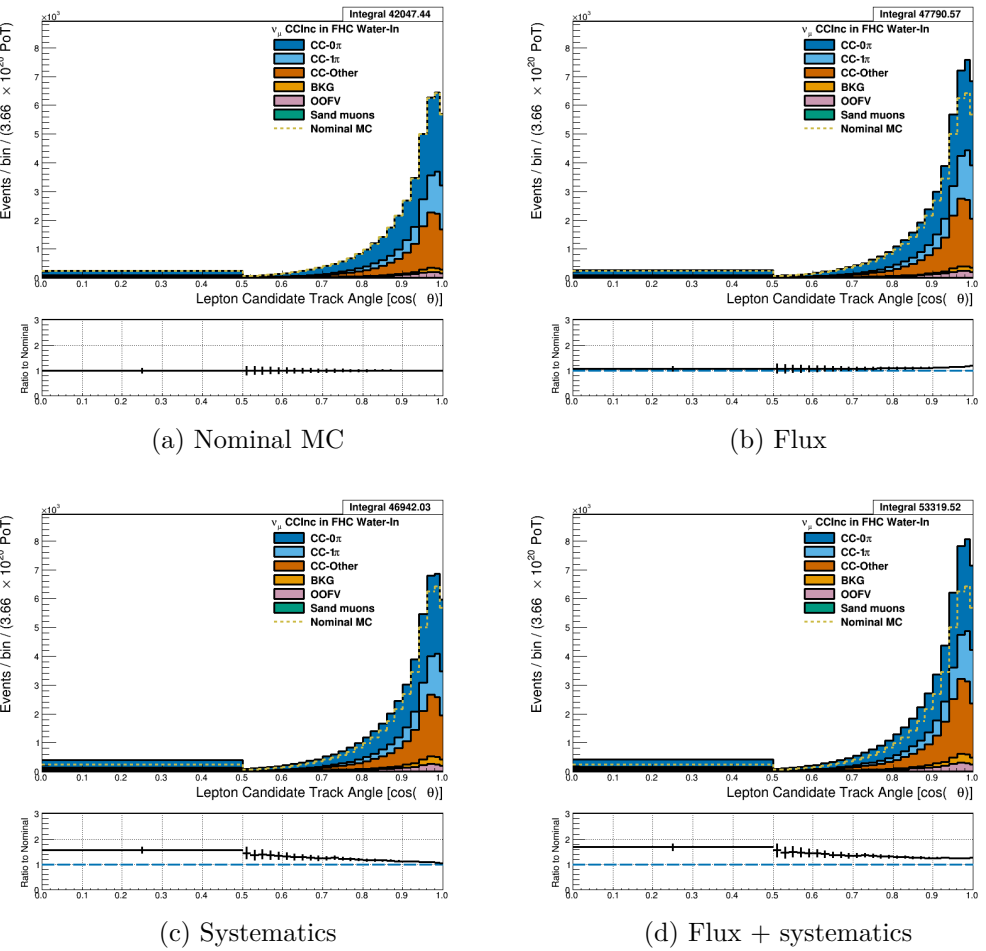


Figure 3.55: Reconstructed lepton candidate $\cos \theta$ separated by topology for FHC ν_μ CC Inc. events occurring in the PØD in water-in mode. (a) The nominal MC prediction without any weights applied. (b) The flux tuning are applied. (c) The systematic weighting are applied. (d) Both flux and systematic weighting are applied.

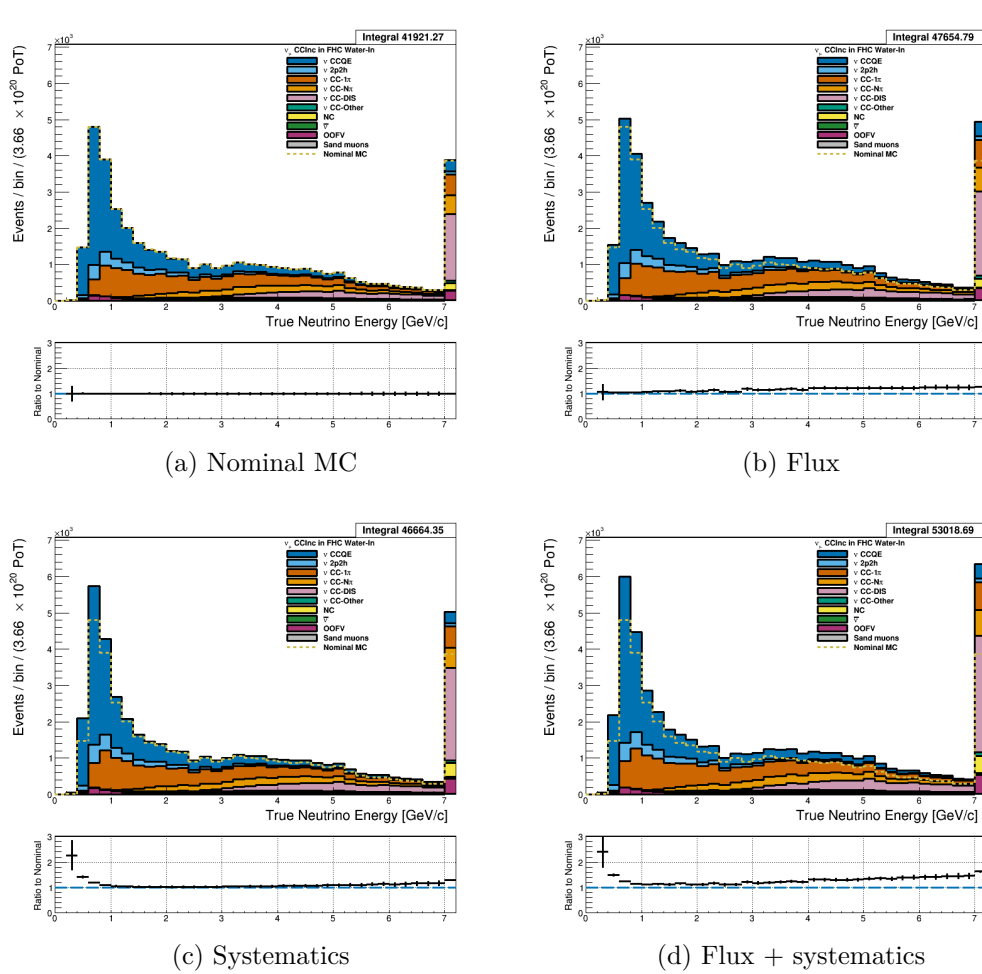


Figure 3.56: True neutrino energy associated with the lepton candidate separated by NEUT model interaction mode for FHC ν_μ CC Inc. events occurring in the PØD in water-out mode. (a) The nominal MC prediction without any weights applied. (b) The flux tuning are applied. (c) The systematic weighting are applied. (d) Both flux and systematic weighting are applied.

572 **3.5.1.2 $\bar{\nu}_\mu$ Selection in RHC Mode:** Shown in Figures 3.57 to 3.63 for $\bar{\nu}_\mu$ CC Inclusive
 573 events in RHC mode. There are three pairs of P, θ figures with the same truth information
 574 break down accompanied by one of neutrino energy. The truth information categories are
 575 lepton candidate particle, NEUT reaction, and topology. Each figure consists of a set of four
 576 sub-figures which illustrate the application of flux and detector systematic weights.

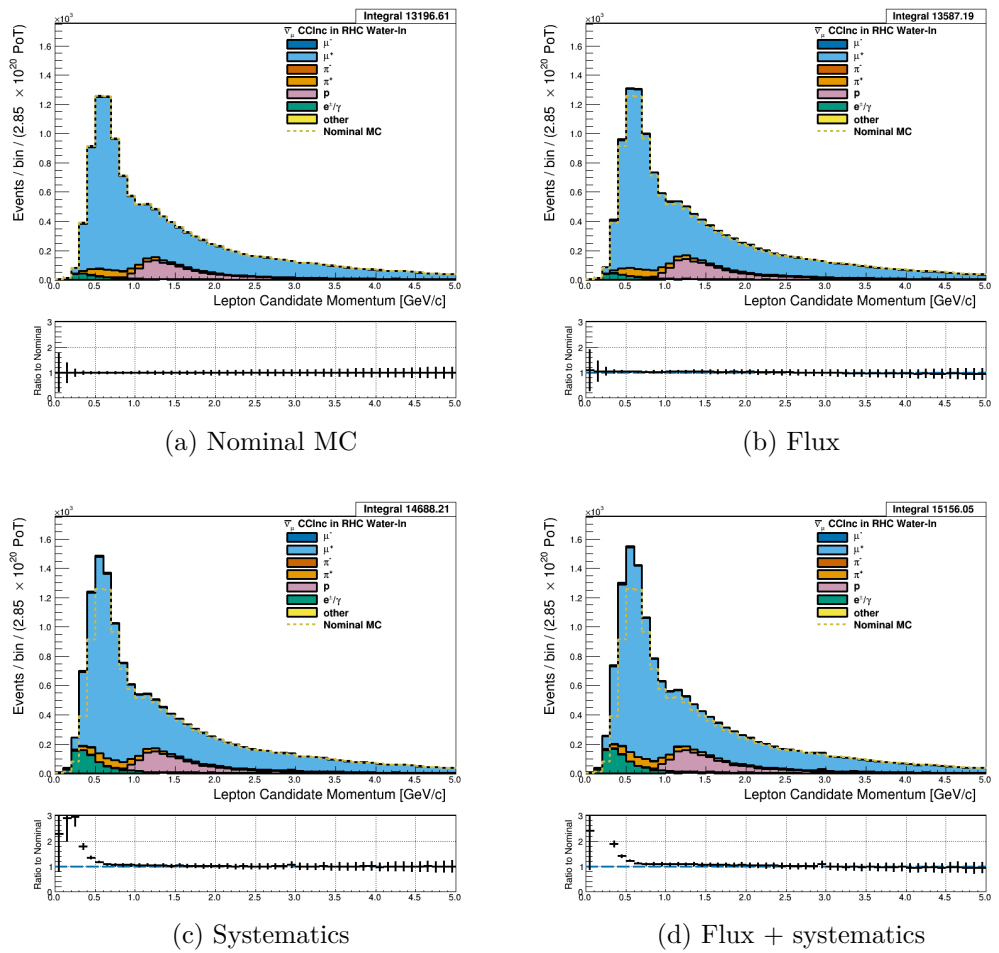


Figure 3.57: Reconstructed lepton candidate momentum separated by true particle species for RHC $\bar{\nu}_\mu$ CC Inc. events occurring in the PØD in water-out mode. (a) The nominal MC prediction without any weights applied. (b) The flux tuning are applied. (c) The systematic weighting are applied. (d) Both flux and systematic weighting are applied.

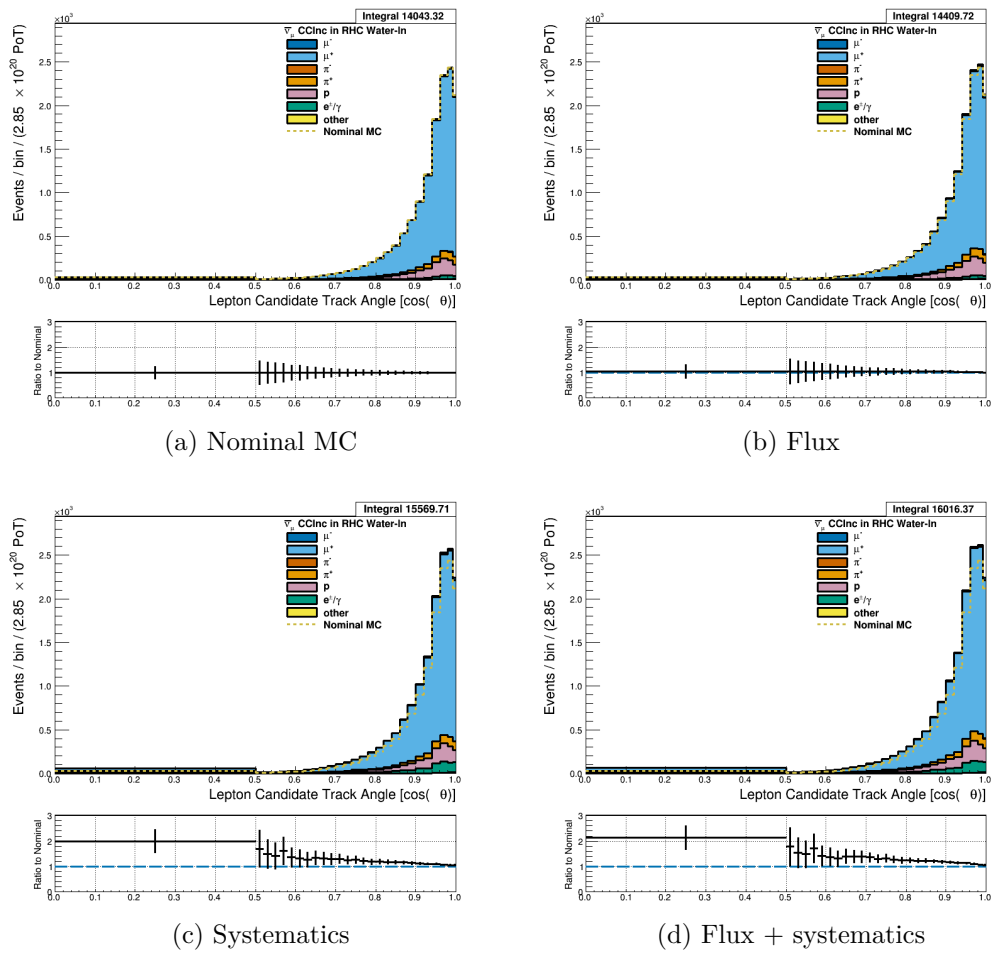


Figure 3.58: Reconstructed lepton candidate angle separated by true particle species for RHC $\bar{\nu}_\mu$ CC Inc. events occurring in the PØD in water-in mode. (a) The nominal MC prediction without any weights applied. (b) The flux tuning are applied. (c) The systematic weighting are applied. (d) Both flux and systematic weighting are applied.

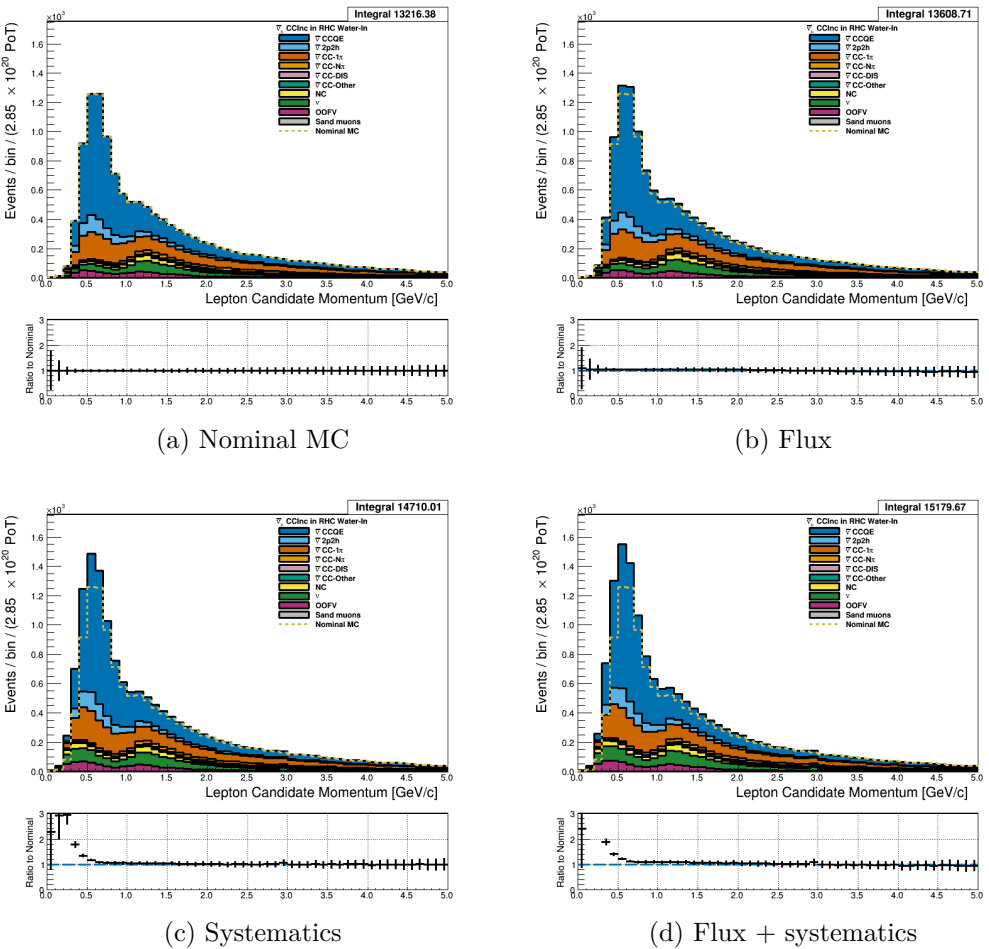


Figure 3.59: Reconstructed lepton candidate momentum separated by NEUT model interaction mode for RHC $\bar{\nu}_\mu$ CC Inc. events occurring in the PØD in water-out mode. (a) The nominal MC prediction without any weights applied. (b) The flux tuning are applied. (c) The systematic weighting are applied. (d) Both flux and systematic weighting are applied.

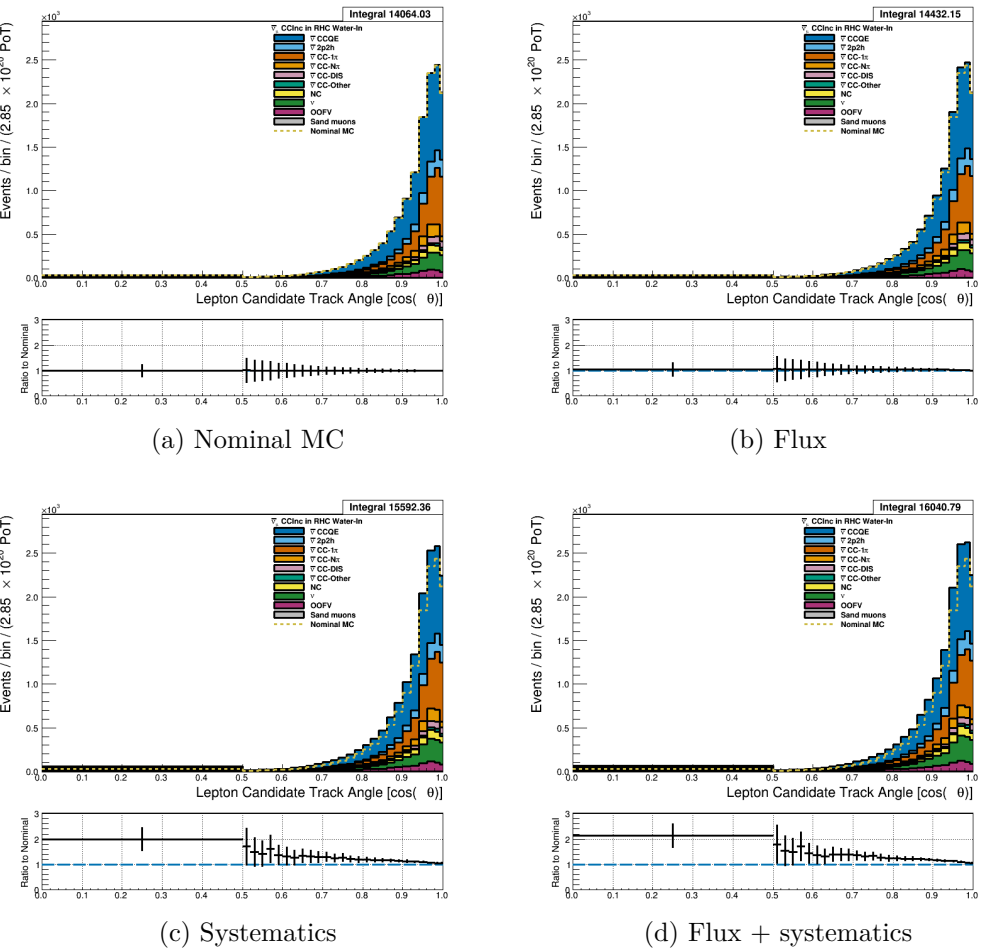


Figure 3.60: Reconstructed lepton candidate $\cos \theta$ separated by NEUT model interaction mode for RHC $\bar{\nu}_\mu$ CC Inc. events occurring in the PØD in water-out mode. (a) The nominal MC prediction without any weights applied. (b) The flux tuning are applied. (c) The systematic weighting are applied. (d) Both flux and systematic weighting are applied.

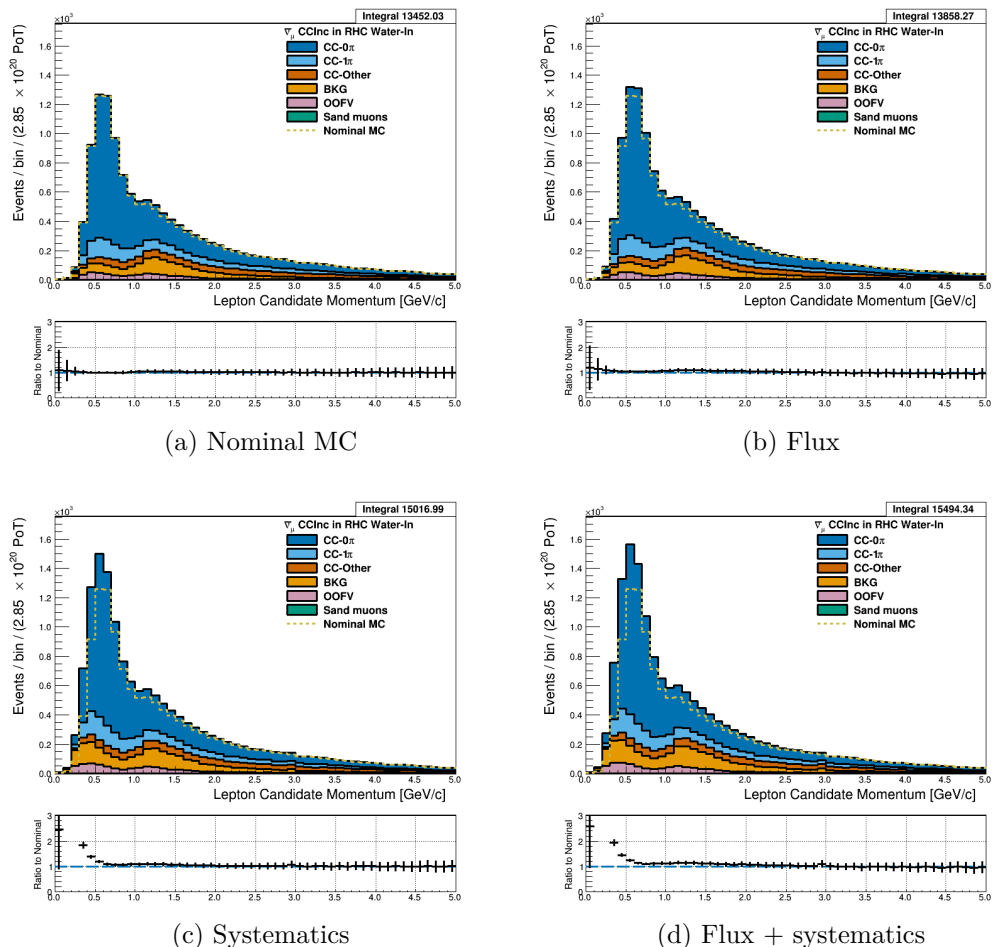


Figure 3.61: Reconstructed lepton candidate momentum separated by topology for RHC $\bar{\nu}_\mu$ CC Inc. events occurring in the PØD in water-out mode. (a) The nominal MC prediction without any weights applied. (b) The flux tuning are applied. (c) The systematic weighting are applied. (d) Both flux and systematic weighting are applied.

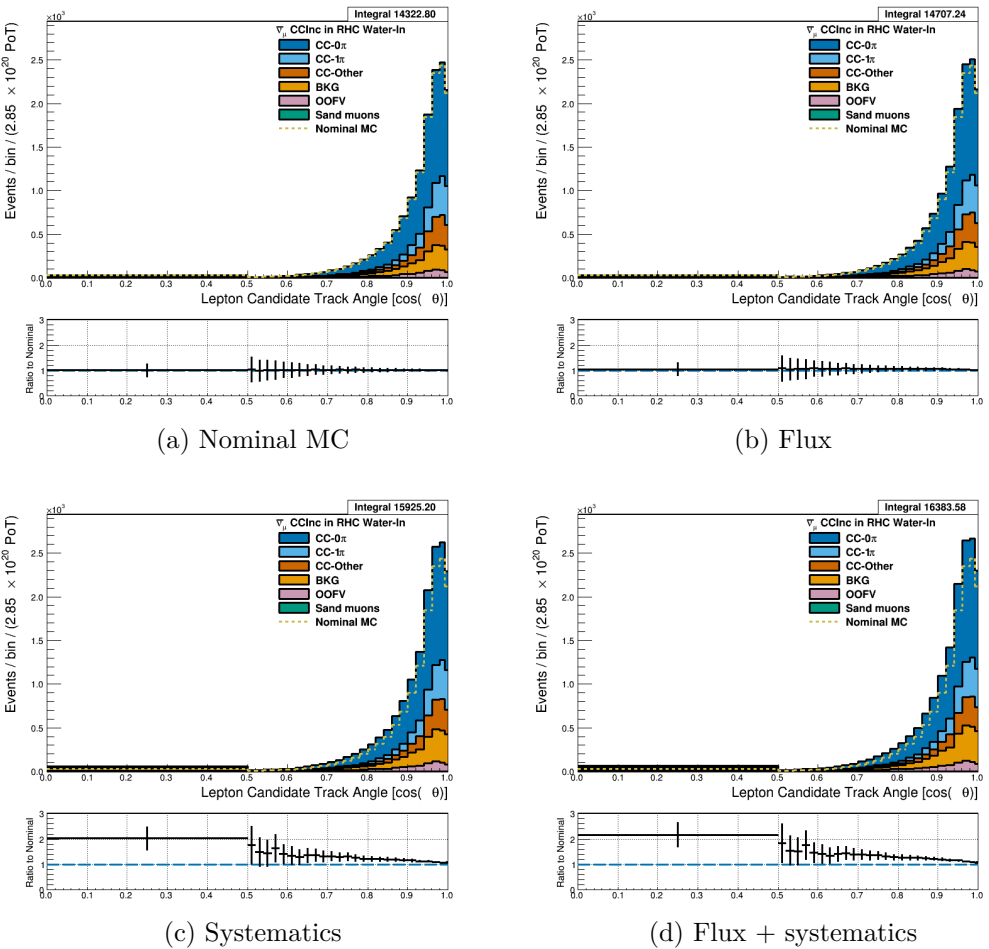


Figure 3.62: Reconstructed lepton candidate $\cos \theta$ separated by topology for RHC $\bar{\nu}_\mu$ CC Inc. events occurring in the PØD in water-out mode. (a) The nominal MC prediction without any weights applied. (b) The flux tuning are applied. (c) The systematic weighting are applied. (d) Both flux and systematic weighting are applied.

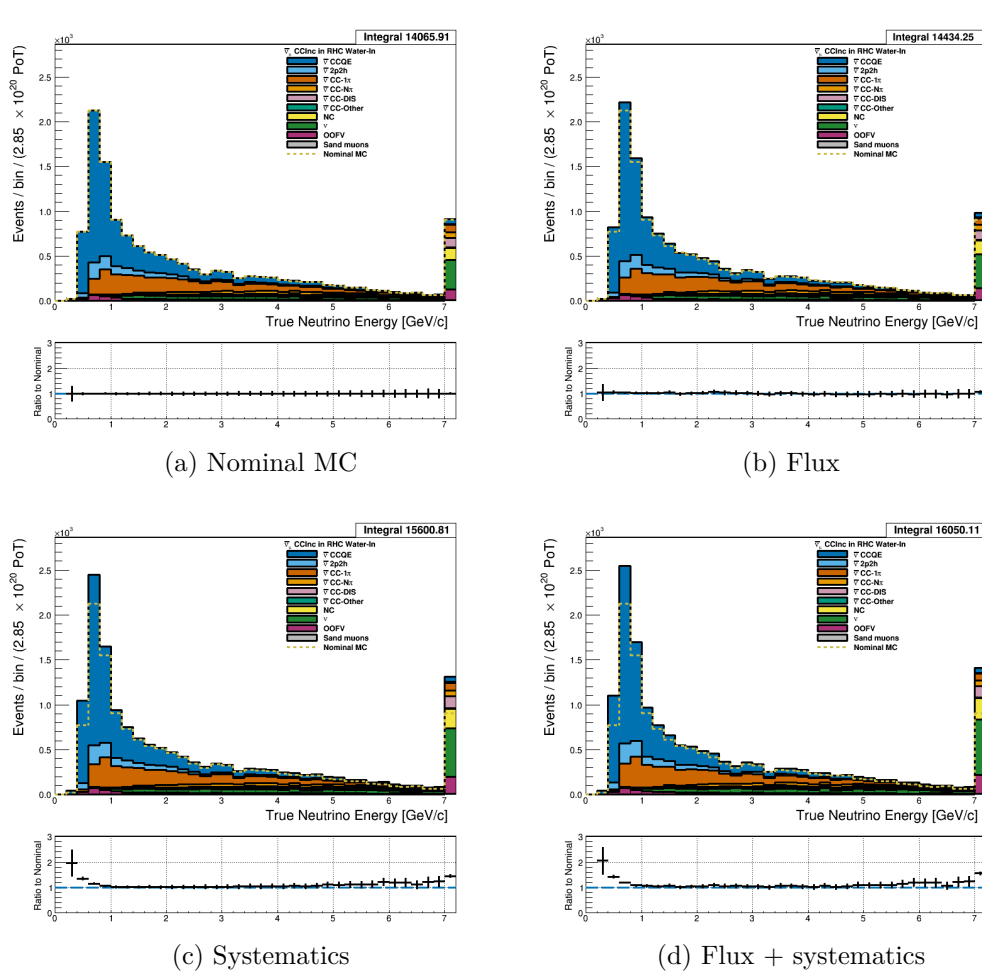


Figure 3.63: True neutrino energy associated with the lepton candidate separated by NEUT model interaction mode for RHC $\bar{\nu}_\mu$ CC Inc. events occurring in the PØD in water-out mode. (a) The nominal MC prediction without any weights applied. (b) The flux tuning are applied. (c) The systematic weighting are applied. (d) Both flux and systematic weighting are applied.

577 **3.5.1.3 ν_μ Background Selection in RHC Mode:** Add figures here

578 **3.5.2 CC 1-Track (CCQE Enhanced)**

579 Text

580 **3.5.2.1 ν_μ Selection in FHC Mode:** Text

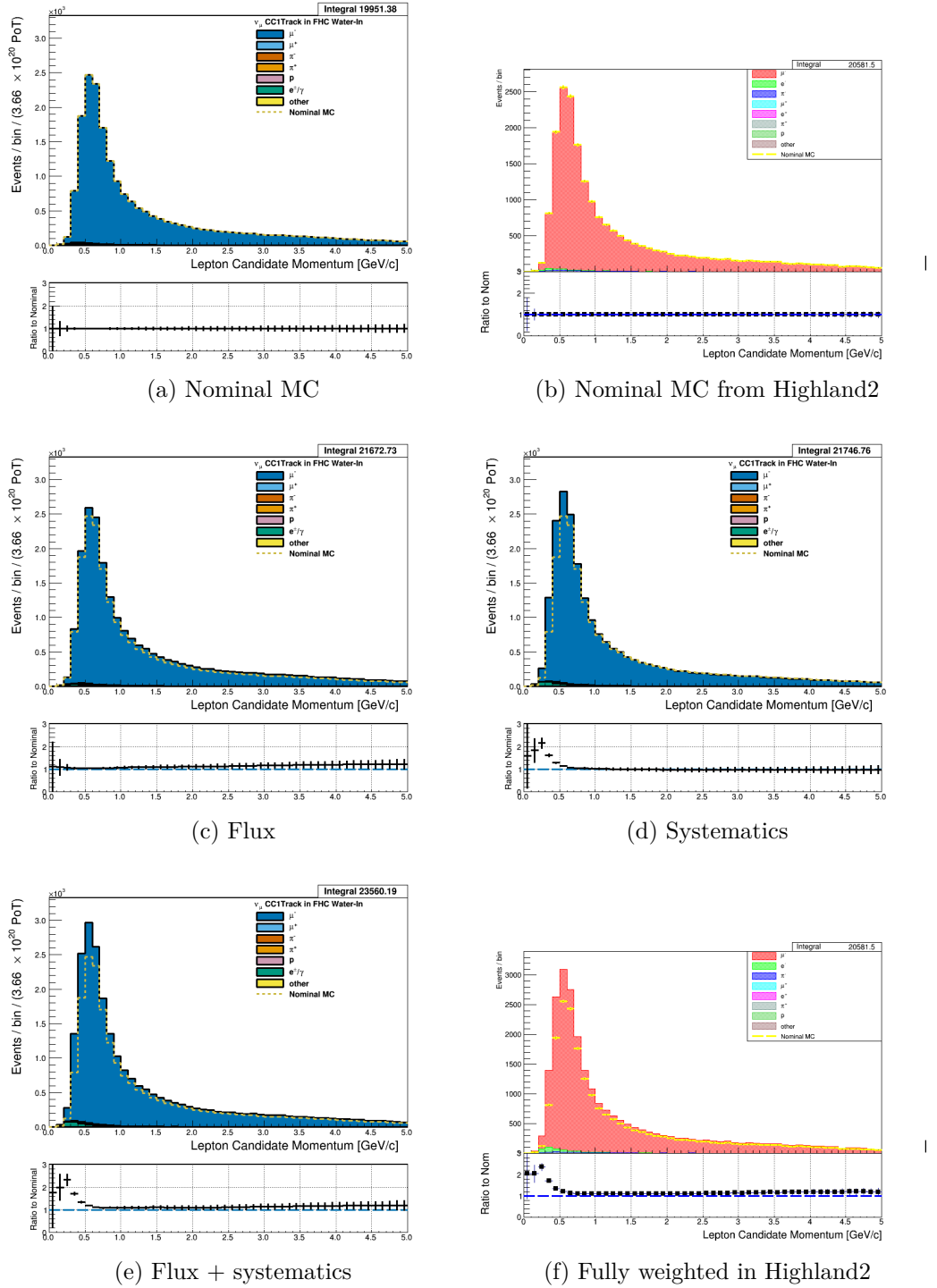


Figure 3.64: Reconstructed lepton candidate momentum separated by true particle species for FHC ν_μ CC 1-Track events occurring in the PØD in water-in mode. (a) The nominal MC prediction without any weights applied. (b) Highland2 comparison for (a) without any weights applied using the “NOW” draw option. (c) The flux tuning are applied. (d) The systematic weighting are applied. (e) Both flux and systematic weighting are applied. (f) Highland2 comparison for (e).

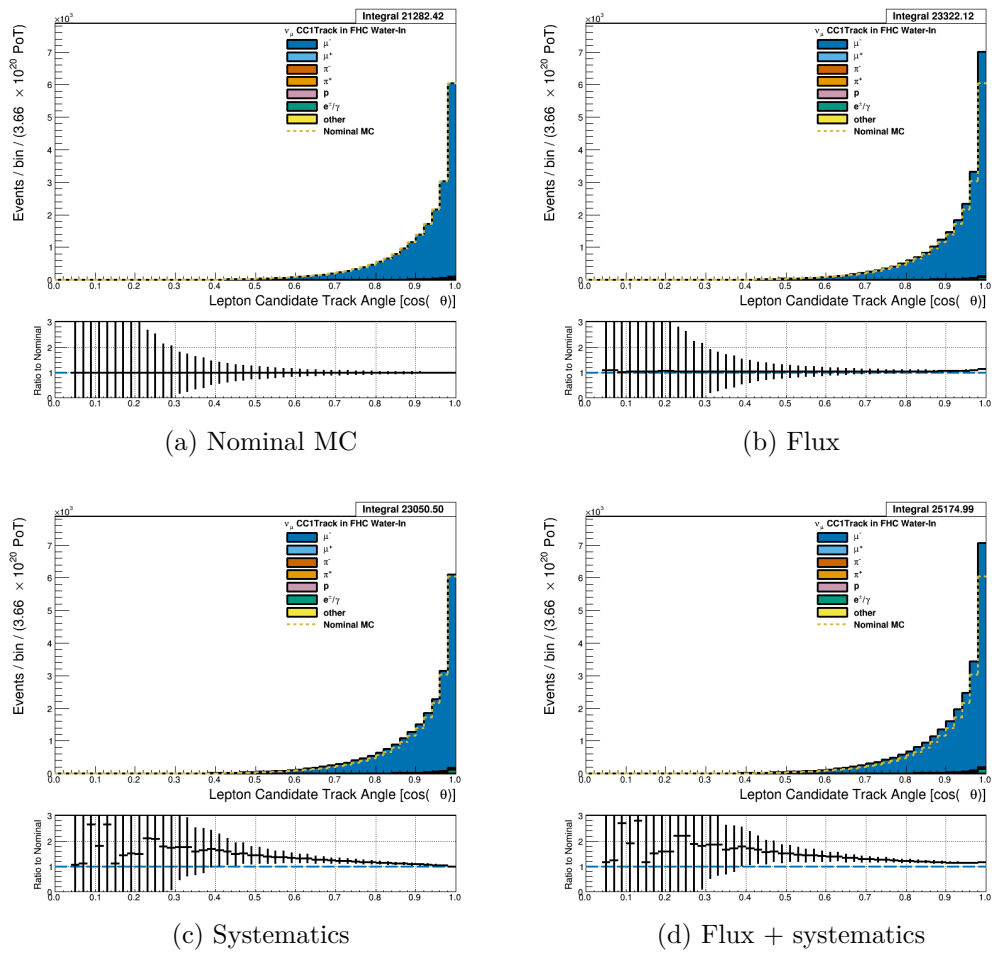


Figure 3.65: Reconstructed lepton candidate angle separated by true particle species for FHC ν_μ CC 1-Track events occurring in the PØD in water-in mode. (a) The nominal MC prediction without any weights applied. (b) The flux tuning are applied. (c) The systematic weighting are applied. (d) Both flux and systematic weighting are applied.

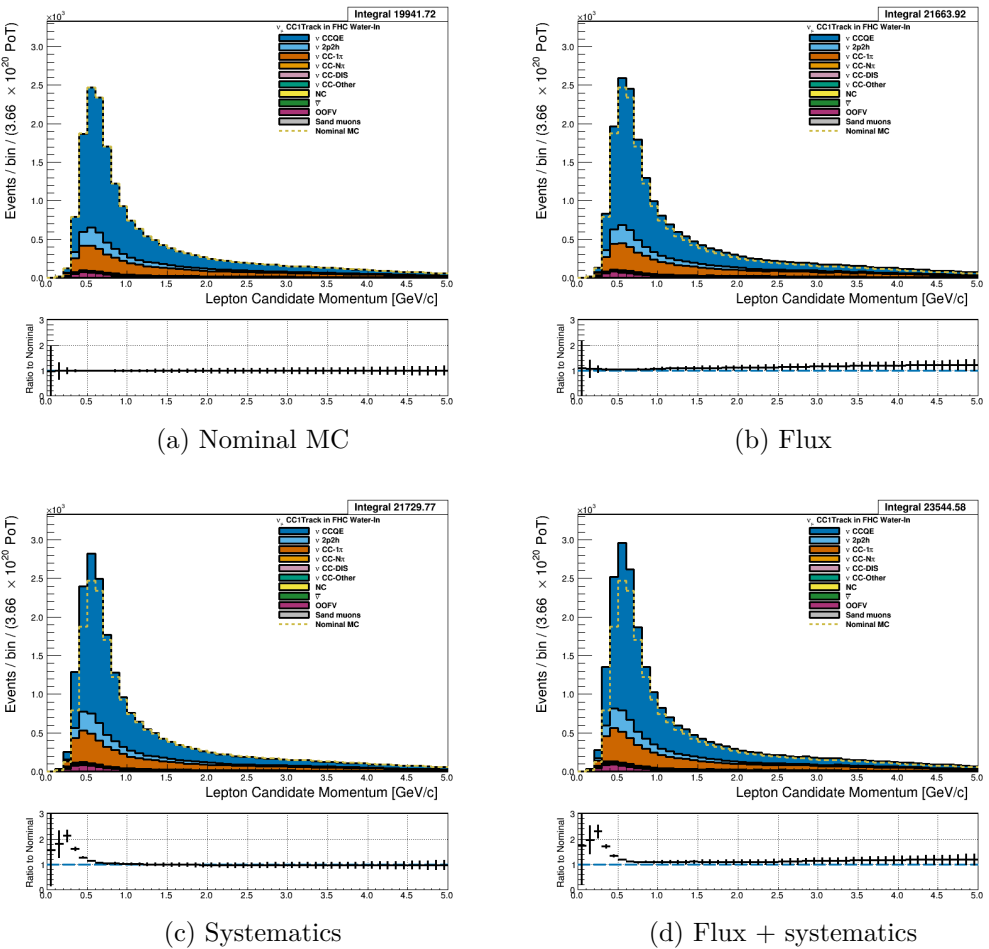


Figure 3.66: Reconstructed lepton candidate momentum separated by NEUT model interaction mode for FHC ν_μ CC 1-Track events occurring in the PØD in water-in mode. (a) The nominal MC prediction without any weights applied. (b) The flux tuning are applied. (c) The systematic weighting are applied. (d) Both flux and systematic weighting are applied.

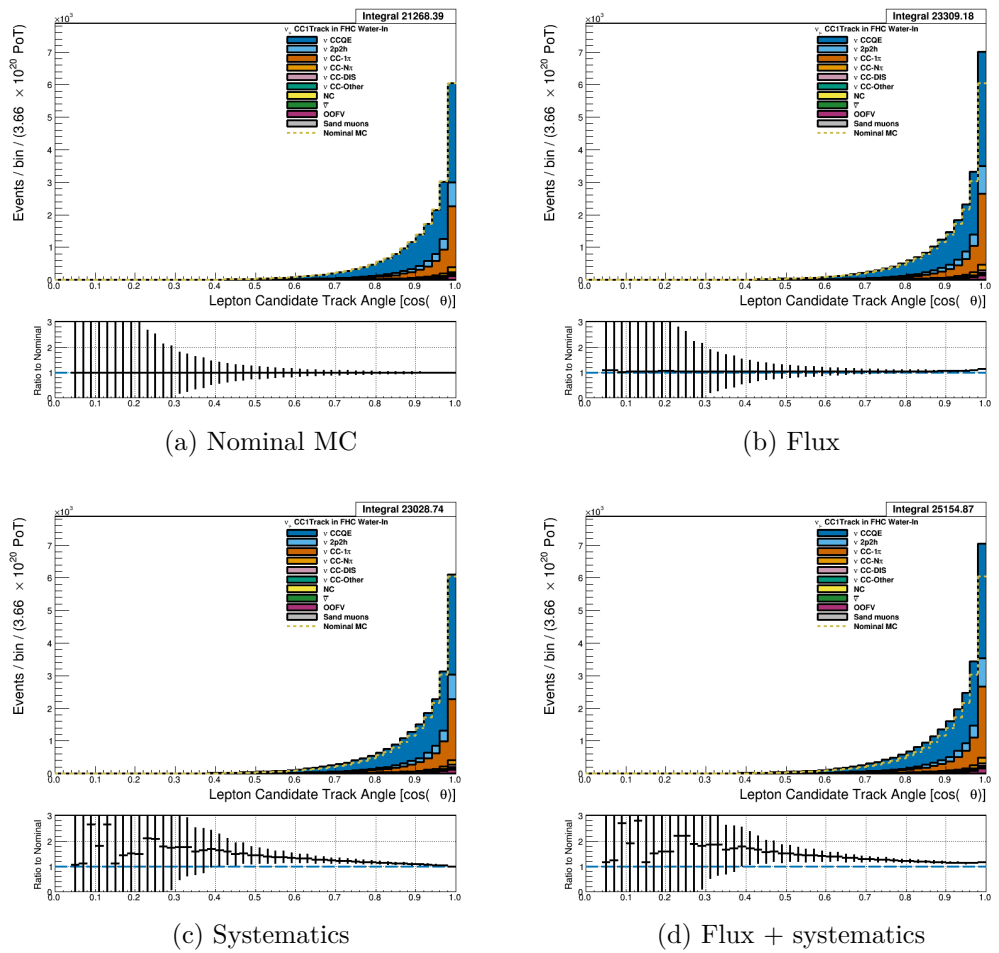


Figure 3.67: Reconstructed lepton candidate $\cos \theta$ separated by NEUT model interaction mode for FHC ν_μ CC 1-Track events occurring in the PØD in water-in mode. (a) The nominal MC prediction without any weights applied. (b) The flux tuning are applied. (c) The systematic weighting are applied. (d) Both flux and systematic weighting are applied.

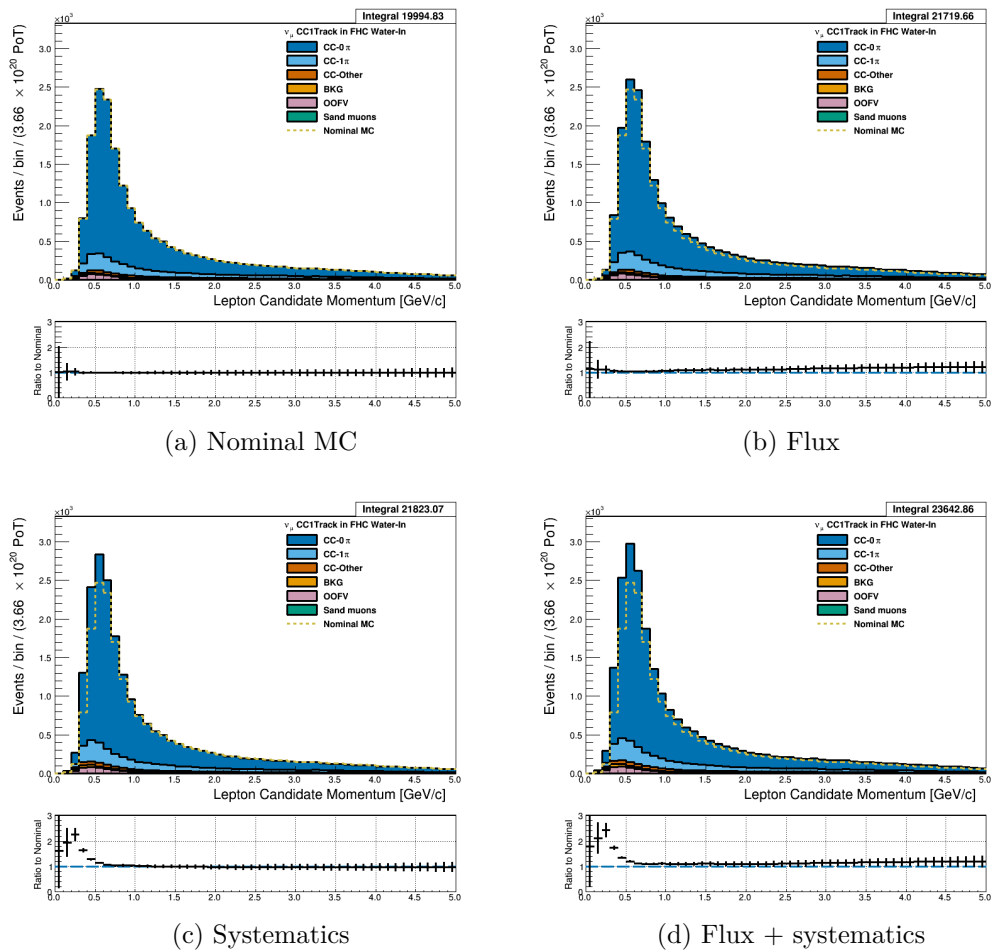


Figure 3.68: Reconstructed lepton candidate momentum separated by topology for FHC ν_μ CC 1-Track events occurring in the PØD in water-in mode. (a) The nominal MC prediction without any weights applied. (b) The flux tuning are applied. (c) The systematic weighting are applied. (d) Both flux and systematic weighting are applied.

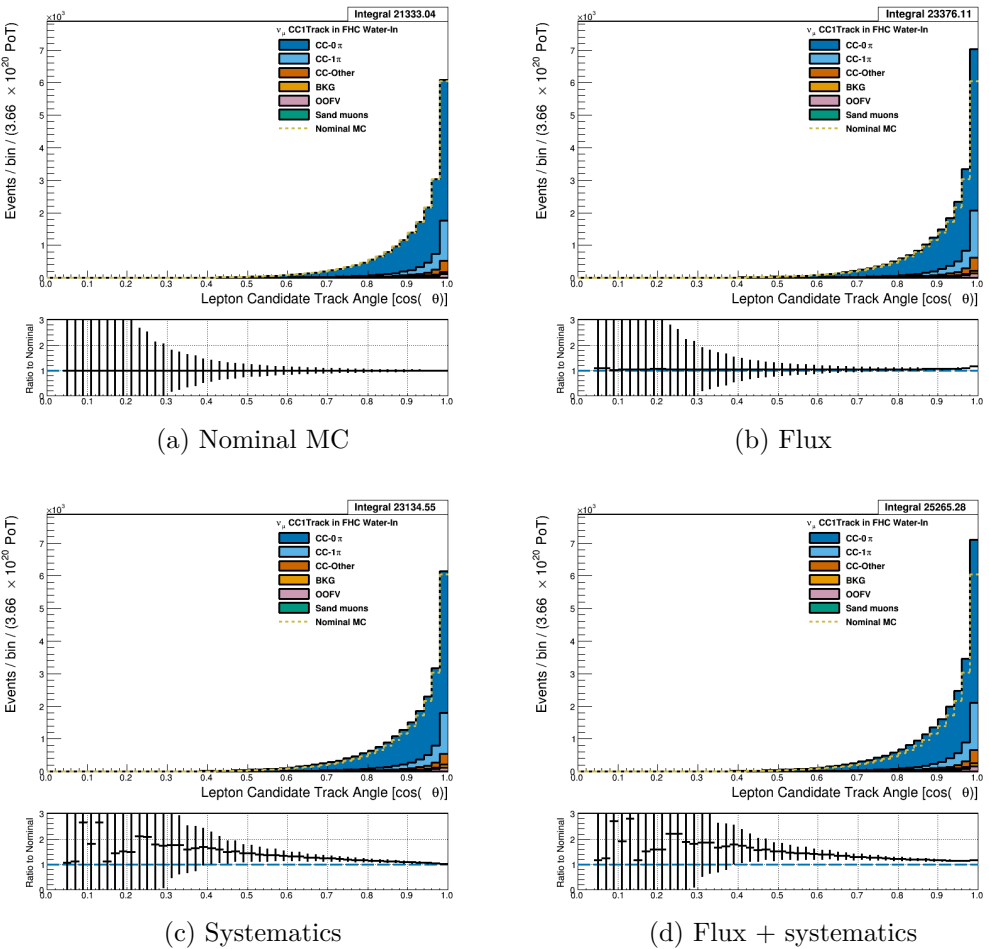


Figure 3.69: Reconstructed lepton candidate $\cos \theta$ separated by topology for FHC ν_μ CC 1-Track events occurring in the PØD in water-in mode. (a) The nominal MC prediction without any weights applied. (b) The flux tuning are applied. (c) The systematic weighting are applied. (d) Both flux and systematic weighting are applied.

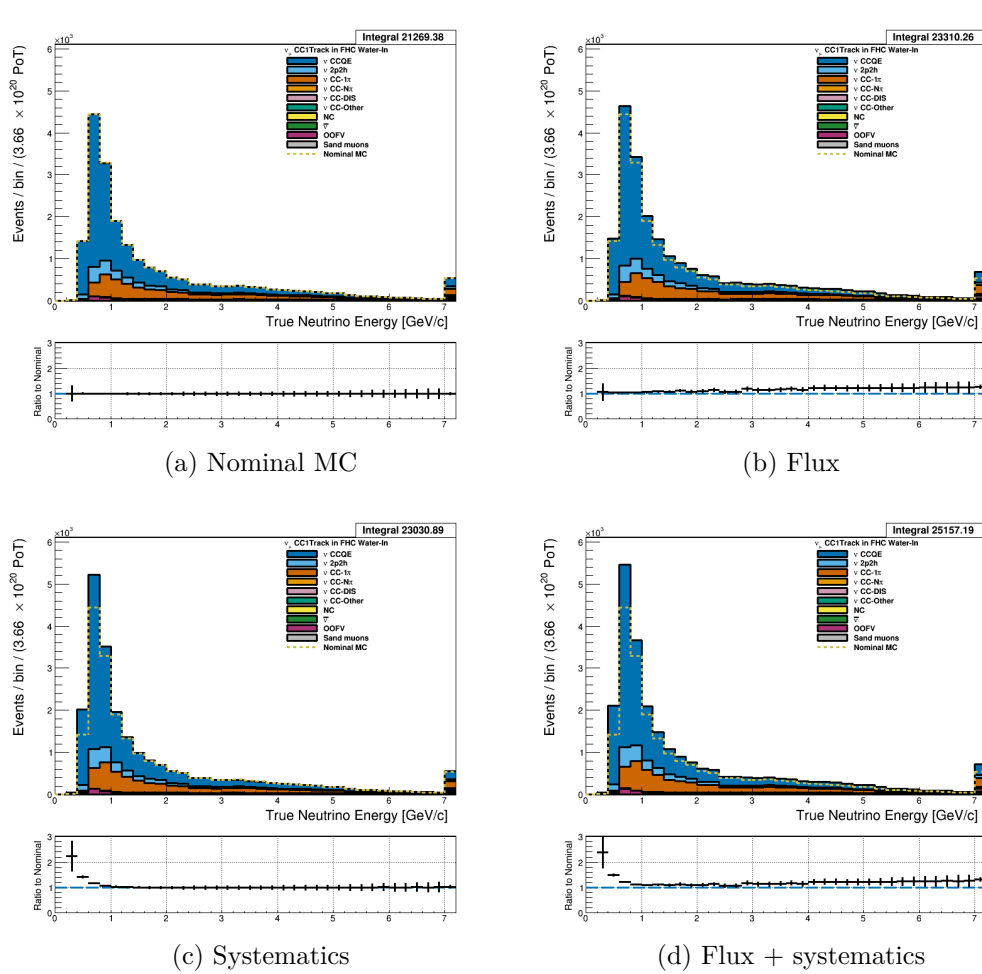


Figure 3.70: True neutrino energy associated with the lepton candidate separated by NEUT model interaction mode for FHC ν_μ CC 1-Track events occurring in the PØD in water-out mode. (a) The nominal MC prediction without any weights applied. (b) The flux tuning are applied. (c) The systematic weighting are applied. (d) Both flux and systematic weighting are applied.

581 3.5.2.2 $\bar{\nu}_\mu$ Selection in RHC Mode: Text

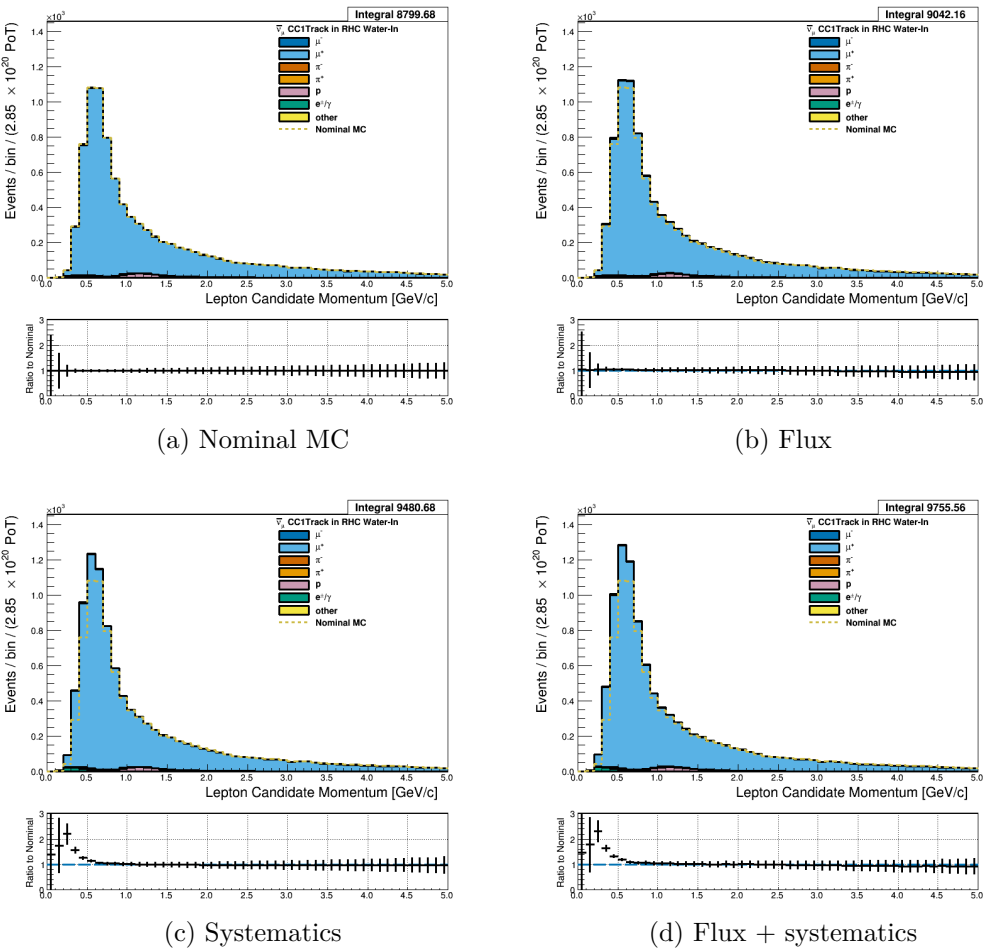


Figure 3.71: Reconstructed lepton candidate momentum separated by true particle species for RHC $\bar{\nu}_\mu$ CC 1-Track events occurring in the PØD in water-out mode. (a) The nominal MC prediction without any weights applied. (b) The flux tuning are applied. (c) The systematic weighting are applied. (d) Both flux and systematic weighting are applied.

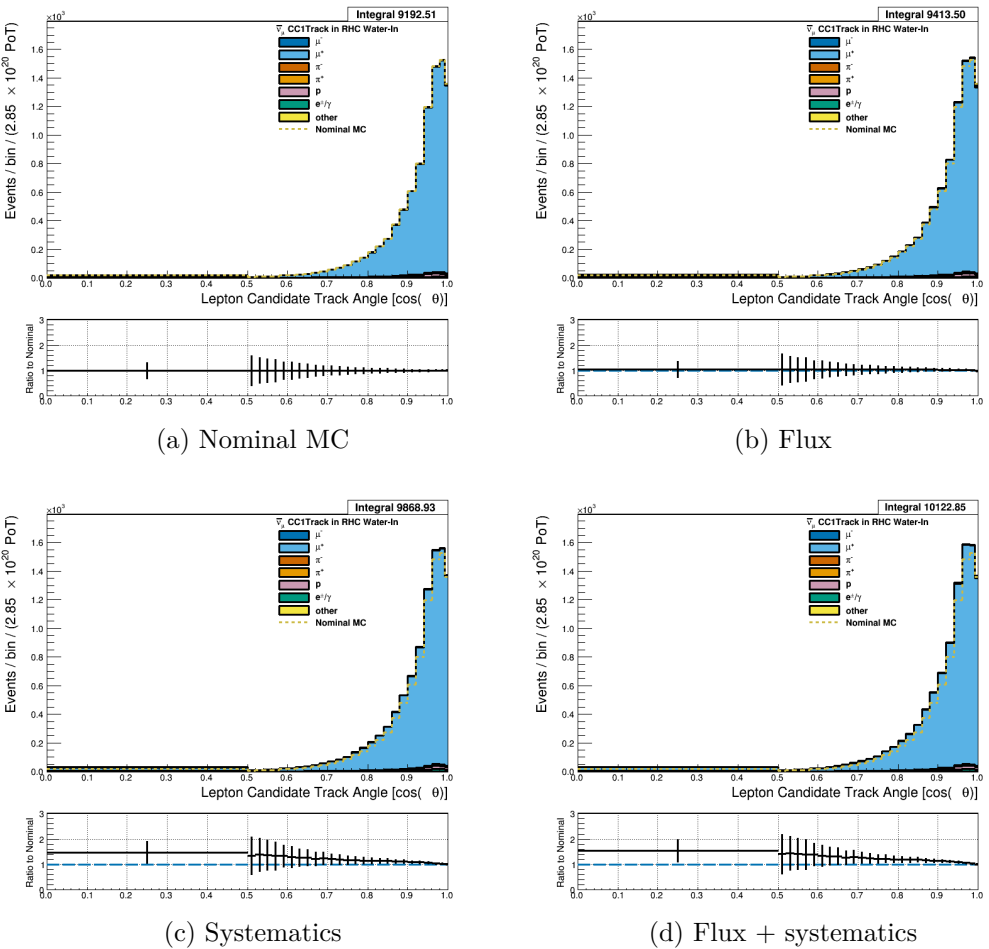


Figure 3.72: Reconstructed lepton candidate angle separated by true particle species for RHC $\bar{\nu}_\mu$ CC 1-Track events occurring in the PØD in water-in mode. (a) The nominal MC prediction without any weights applied. (b) The flux tuning are applied. (c) The systematic weighting are applied. (d) Both flux and systematic weighting are applied.

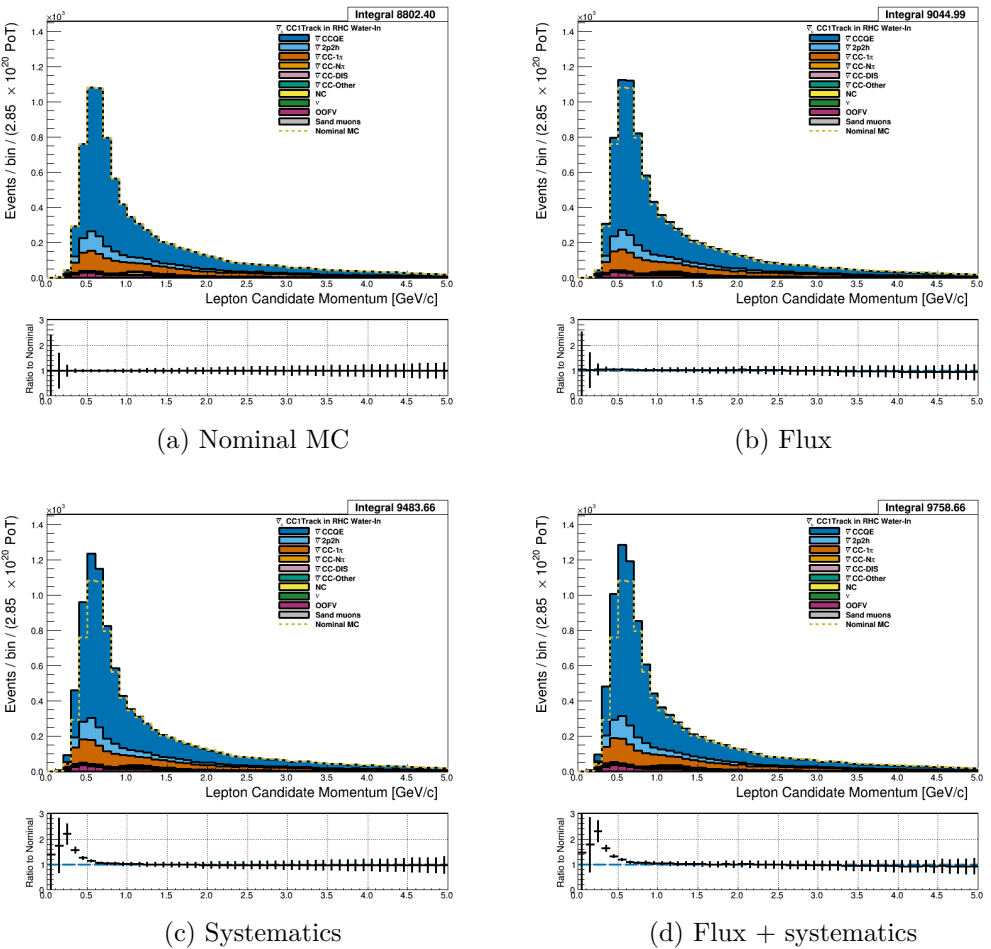


Figure 3.73: Reconstructed lepton candidate momentum separated by NEUT model interaction mode for RHC $\bar{\nu}_\mu$ CC 1-Track events occurring in the PØD in water-out mode. (a) The nominal MC prediction without any weights applied. (b) The flux tuning are applied. (c) The systematic weighting are applied. (d) Both flux and systematic weighting are applied.

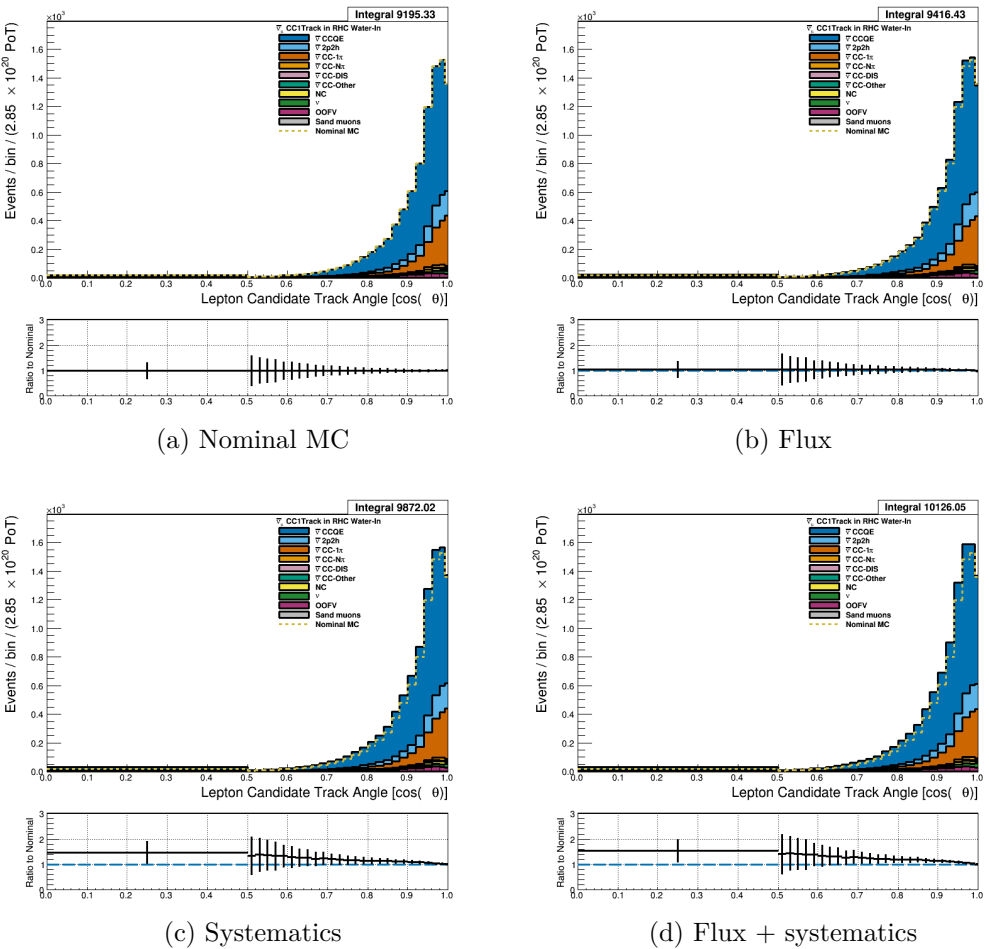


Figure 3.74: Reconstructed lepton candidate $\cos \theta$ separated by NEUT model interaction mode for RHC $\bar{\nu}_\mu$ CC 1-Track events occurring in the PØD in water-out mode. (a) The nominal MC prediction without any weights applied. (b) The flux tuning are applied. (c) The systematic weighting are applied. (d) Both flux and systematic weighting are applied.

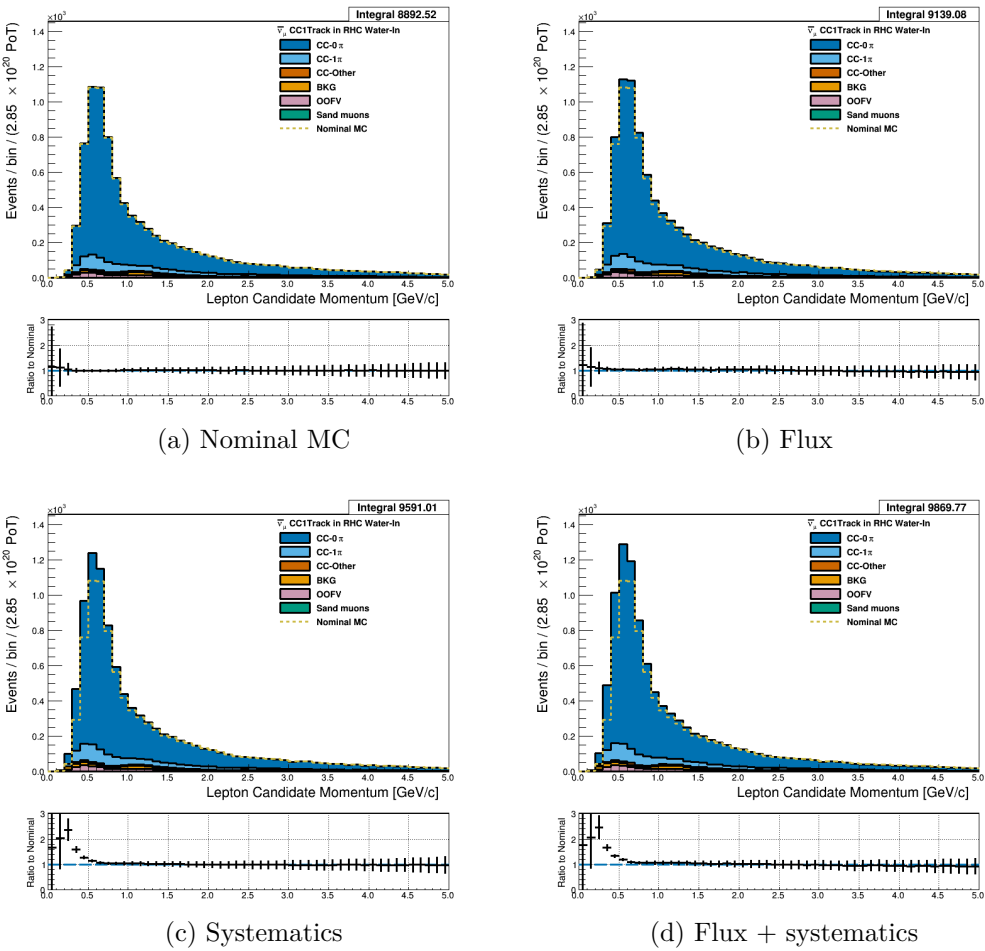


Figure 3.75: Reconstructed lepton candidate momentum separated by topology for RHC $\bar{\nu}_\mu$ CC 1-Track events occurring in the PØD in water-out mode. (a) The nominal MC prediction without any weights applied. (b) The flux tuning are applied. (c) The systematic weighting are applied. (d) Both flux and systematic weighting are applied.

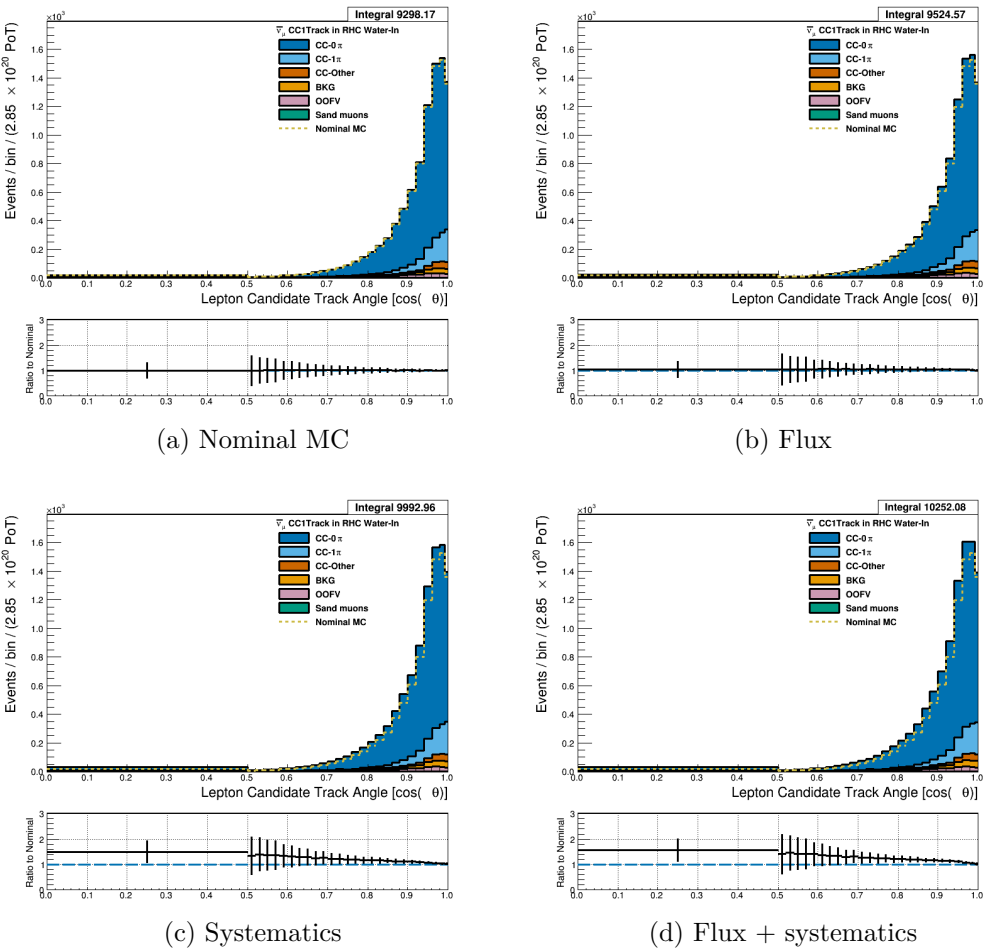


Figure 3.76: Reconstructed lepton candidate $\cos \theta$ separated by topology for RHC $\bar{\nu}_\mu$ CC 1-Track events occurring in the PØD in water-out mode. (a) The nominal MC prediction without any weights applied. (b) The flux tuning are applied. (c) The systematic weighting are applied. (d) Both flux and systematic weighting are applied.

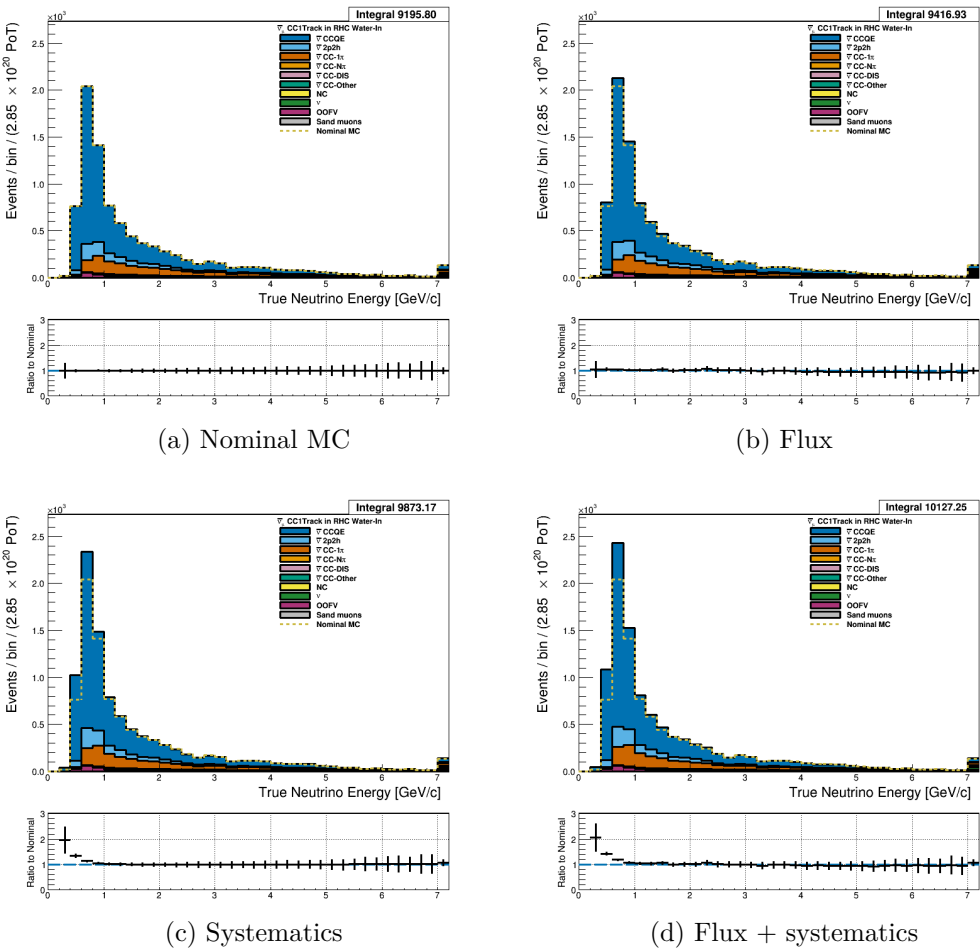


Figure 3.77: True neutrino energy associated with the lepton candidate separated by NEUT model interaction mode for RHC $\bar{\nu}_\mu$ CC 1-Track events occurring in the PØD in water-out mode. (a) The nominal MC prediction without any weights applied. (b) The flux tuning are applied. (c) The systematic weighting are applied. (d) Both flux and systematic weighting are applied.

3.5.2.3 ν_μ Background Selection in RHC Mode: Text

3.5.3 CC N-Tracks (CCnQE Enhanced)

Text

3.5.3.1 ν_μ Selection in FHC Mode: Text

586 **3.5.3.2 $\bar{\nu}_\mu$ Selection in RHC Mode:** Text

587 **3.5.3.3 ν_μ Background Selection in RHC Mode:** Text

588 **3.5.4 Differences Between Water-Out and Water-In Samples**

589 **4 PØD-Only BANFF Parameterization**

590 **4.1 PØD Samples Fit Binning**

591 The PØD ND280 BANFF fit uses the samples described in 3. The bin edges are tabulated
592 below.

- 593 • FHC ν_μ CC 1-Track bin edges:

594 p [GeV/c]: 0, 0.3, 0.4, 0.5, 0.6, 0.7, 0.8, 1, 1.25, 1.5, 2, 3, 4, 5.5, 30

595 $\cos\theta$: -1, 0.7, 0.8 , 0.88, 0.94, 0.96, 0.975, 0.99, 1

- 596 • FHC ν_μ CC N-Tracks bin edges:

597 p [GeV/c]: 0, 0.4, 0.5, 0.6, 0.7, 0.8, 1, 1.2, 1.5, 1.8, 2.2, 2.7, 3.5, 5, 10, 30

598 $\cos\theta$: -1, 0.65, 0.77, 0.85, 0.9, 0.94, 0.97, 0.99, 1

- 599 • RHC $\bar{\nu}_\mu$ CC 1-Track bin edges:

600 p [GeV/c]: 0, 0.4, 0.5, 0.6, 0.7, 0.8, 1, 1.25, 1.5, 2, 3, 30

601 $\cos\theta$: -1, 0.82, 0.87, 0.9, 0.93, 0.95, 0.97, 0.99, 1

- 602 • RHC $\bar{\nu}_\mu$ CC N-Tracks bin edges:

603 p [GeV/c]: 0, 0.5, 0.9, 1.25, 1.6, 2, 3, 8, 30

604 $\cos\theta$: -1, 0.8, 0.89, 0.95, 0.97, 0.99, 1

- 605 • RHC ν_μ CC 1-Track bin edges:

606 p [GeV/c]: 0, 0.4, 0.6, 0.8, 1.1, 2, 10

607 $\cos\theta$: -1, 0.78, 0.84, 0.89, 0.92, 0.95, 0.97, 0.98, 0.99, 1

- 608 • RHC ν_μ CC N-Tracks bin edges:

609 p [GeV/c]:0, 0.4, 0.6, 0.8, 1, 1.5, 2, 3, 10

610 $\cos\theta$: -1, 0.7, 0.8, 0.85, 0.9, 0.94, 0.965, 0.98, 0.99, 1

611 **4.1.1 Fit Binning Determination**

612 The fit binning is designed to optimized to ensure at least 1 predicted Monte Carlo (MC)
613 event in each bin when scaled to the collected data POT. The fit bins must also account
614 for detector smearing effects. In order to mitigate smearing and event migration, the recon-
615 structed kinematics were examined to their MC truth value using only correctly identified
616 leptons in one-dimensional kinematic slices. Since the MC provides about $10\times$ the data
617 statistics, the statistical uncertainty for each bin should be negligible for high statistics re-
618 gions. The kinematics are scanned across their full relevant spaces in order to understand the
619 needed width for a fit bin. The first fit bin is always defined from the kinematic maximum.

620 For the momentum bins, the momentum resolution is compared to MC truth . The
621 momentum resolution is defined as

$$R(r, t) = \frac{r - t}{t},$$

622 where r is the reconstructed momentum and t is the true value. The momentum was scanned
623 in finite bin widths with the mean and standard deviation of the resolution R extracted. The
624 mean and standard deviation are used as a proxy for the true bias and true resolution, re-
625 spectively. In addition, a bootstrapping algorithm was employed to understand the accuracy
626 of the sample estimates. Bootstrapping in this context is sampling over all relevant values
627 of true momentum and randomly replacing the values. For each scanned bin, at least 1000
628 bootstrapping sampling with replacement was performed. In the case of large variances in
629 the bootstrapping samples, additional 10000 sampling with replacement were performed.
630 The results for analyzing the FHC ν_μ CC 1-Track selection is shown in Figure 4.1 on page

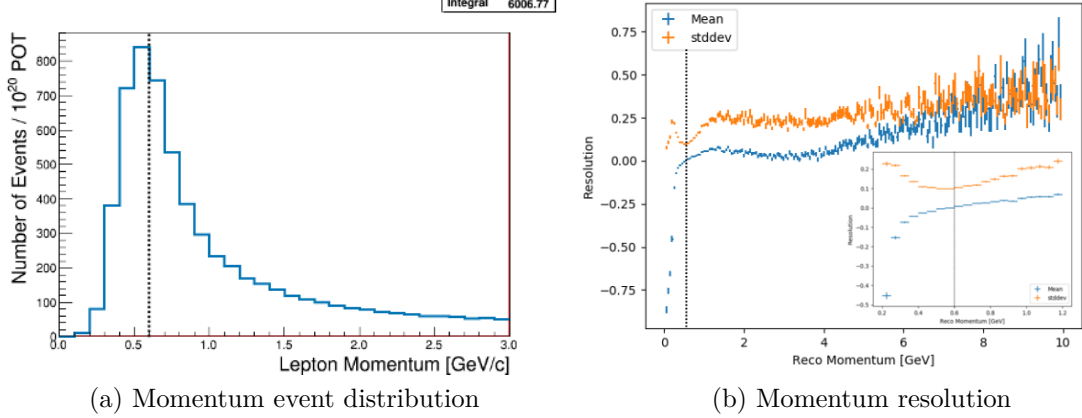


Figure 4.1: The momentum event distribution and uncertainty for FHC ν_μ CC 1-Track events is shown above. Only correctly identified muons are shown. (a) The number of events per unit momentum is scaled to 10^{20} POT which is the approximate scale for all the samples in this analysis. A dashed line indicates the maximum of the peak. (b) The resolution of the momentum measurement is shown for a wide region of momenta. In the inset is the resolution zoomed near the momentum distribution maximum. Like in (a), a dashed line shows the momentum maximum.

631 115.

632 The angle bins are treated in an almost identical manner. While the fit bins and physics
 633 parameterized in $\cos \theta$, the angle with respect to the z-axis, the detector smearing is a
 634 function of the angle θ . In addition, since the angle can be nearly zero for the most forward-
 635 going tracks, the resolution was not used to characterize the angular uncertainties. Instead,
 636 the difference between the true and reconstructed angle were analyzed as shown in . The
 637 mean and standard deviation were studied. Bootstrapping was again used to quantify the
 638 accuracy of the mean and standard deviation.

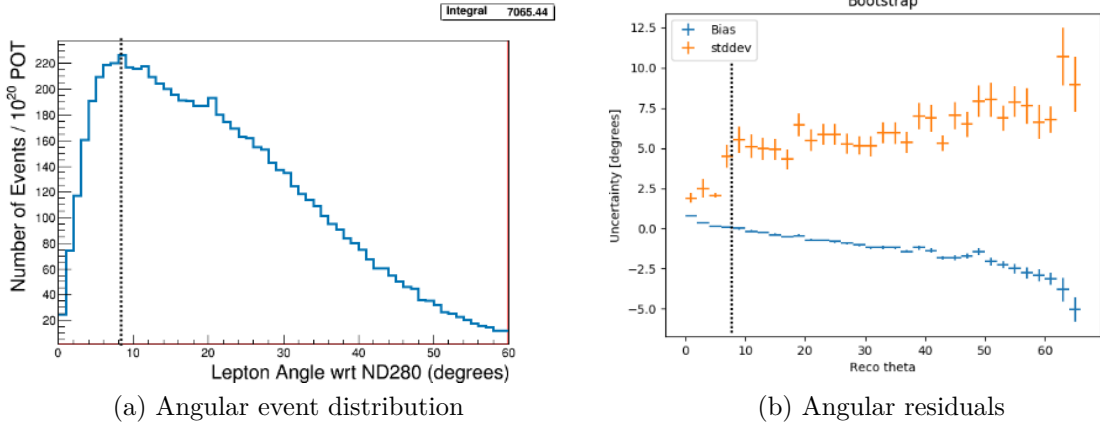


Figure 4.2: The angular event distribution and uncertainty for FHC ν_μ CC 1-Track events is shown above. Only correctly identified muons are shown. (a) The number of angular events is scaled to 10^{20} POT which is the approximate scale for all the samples in this analysis. A dashed line indicates the maximum of the peak. (b) The residual of the angular measurement is shown up to where there are sufficient statistics. Like in (a), a dashed line shows the momentum maximum.

639 **5 Detector Systematics**

640 Sources of systematic uncertainties, hitherto referred to as systematics, must be evaluated in
641 order to understand their effect on any analysis. The BANFF fit utilizes a set of canonical
642 systematics

643 **5.1 Detector Systematic Uncertainties**

644 All the detector systematics in BANFF are evaluated as either observable variations or
645 weights. An observable variation affects the physical observables of selected events. The most
646 important variation is the energy loss in the PØD of the outgoing muon in CC interactions.

647 **5.1.1 Efficiency-like Systematics**

648 Efficiency-like systematics are treated as weights to the MC predictions in order to evaluate
649 the uncertainty the systematic has on an analysis. They are based on studies comparing
650 data and MC predictions in well known control samples (CS). A CS is designed to provide a
651 reliable measurement with minimal influence from other dependent and independent factors.

652 An example of a well established CS is a collection of single, isolated cosmic ray (muon) tracks
653 to measure the energy loss in a detector. In general, a CS may have different properties than
654 the analysis sample like event topology. In particular the cosmic ray CS cannot account for
655 efficiency effects of other tracks present. Therefore a model extrapolation is needed to map
656 the CS to the analysis sample. The model used in psyche/BANFF is that the efficiency of
657 the data and MC is the same in both analysis sample and CS

$$\epsilon_{\text{Data}}(x) = \left(\frac{\epsilon_{\text{Data}}(x)}{\epsilon_{\text{MC}}(x)} \right)_{\text{CS}} \epsilon_{\text{MC}}(x)$$

658 where $\epsilon_{\text{MC}} / \epsilon_{\text{Data}}$ denotes the mean efficiency of the MC/data as a function of some observable
659 x . We need to update this model to account for statistical uncertainties in the CS. The

660 updated model, with x dependence assumed, is now

$$\epsilon'_{\text{Data}} = \left(\frac{\epsilon_{\text{Data}} + \delta_{\text{Data}} \cdot \sigma_{\epsilon_{\text{Data}}}}{\epsilon_{\text{MC}} + \delta_{\text{MC}} \cdot \sigma_{\epsilon_{\text{MC}}}} \right)_{\text{CS}} \epsilon_{\text{MC}}$$

661 where $\sigma_{\epsilon_{\text{MC}/\text{Data}}}$ is the standard deviation of the efficiency of the MC/Data and $\delta_{\text{MC}/\text{Data}}$ is
662 a random, normally distributed number $\mathcal{N}(\mu = 0, \sigma^2 = 1)$.

$$w_{\text{eff}} = \frac{\epsilon'_{\text{Data}}}{\epsilon_{\text{MC}}}$$
$$w_{\text{ineff}} = \frac{1 - \epsilon'_{\text{Data}}}{1 - \epsilon_{\text{MC}}}$$

663 **5.1.2 Observable Variation Systematics**

$$x' = x_{\text{Nom}} + \Delta x + \delta_{\sigma} \cdot \sigma_{\Delta x}$$

664 **5.1.3 Normalization Systematics**

$$w = w_0 (1 + \delta \cdot \sigma_w)$$

Systematic effect	Treatment
TPC cluster eff.	efficiency
TPC tracking eff.	efficiency
TPC charge misassignment	efficiency
TPC particle ID	observable variation
TPC momentum resol.	observable variation
TPC momemtum scale	observable variation
B field distortion	observable variation
FGD “hybrid” tracking eff.	efficiency
Michel election eff.	efficiency
FGD particle ID	observable variation
FGD mass	normalization
Pion secondary interactions	efficiency
Proton secondary interactions	efficiency
TPC-FGD track matching eff.	efficiency
FGD OOFV	efficiency
FGD TOF resol.	observable variation
FGD sand muon eff.	efficiency
FGD event pile up	normalization
PØD energy loss scale	observable variation
PØD energy loss resol.	observable variation
PØD OOFV	efficiency
PØD track veto	efficiency

Table 5.1: [2]

665 **6 Fitter Validation**

666 Fitter validation

667

7 Fitter Results

668

Fitter results

669 **8 Discussion**

670 Discussion

671 **References**

- 672 [1] K. Abe et al. The T2K Experiment. *Nucl. Instrum. Meth.*, A659:106–135, 2011. 25
- 673 [2] K. Abe and Others. Measurements of neutrino oscillation in appearance and disappearance channels by the t2k experiment with 6.6×10^{20} protons on target. *Phys. Rev. D*,
674 91:072010, Apr 2015. 9, 119
- 675 [3] S. Baker and R. D. Cousins. Clarification of the use of Chi-Square and Likelihood
676 Functions in Fits to Histograms. *Nucl. Instrum. Meth.*, A221:437–442, 1983. 16
- 677 [4] S. Bienstock et al. Assessing the effect of cross-section model uncertainties on the T2K
678 oscillation analyses with simulated data studies using the BANFF, MaCh3, P-Theta
679 and VALOR frameworks, May 2018. T2K-TN-331 v5. 14
- 680 [5] S. Bienstock and Others. Constraining the Flux and Cross Section Models with Data
681 from the ND280 Detector using FGD1 and FGD2 for the 2017 Joint Oscillation Analysis,
682 August 2017. T2K-TN-324 v3. 14, 21
- 683 [6] S. Bolognesi and Others. Niwg model and uncertainties for 2017 oscillation analysis,
684 April 2017. T2K-TN-315 v5. 21
- 685 [7] T. Campbell. Measurement of the ν_μ cc-0π double differential cross section on water in
686 the pød, February 2018. T2K-TN-328. 24
- 687 [8] T. Campbell and Others. Analysis of ν_μ charged current inclusive events in the pød in
688 runs 1+2+3+4, Mar 2014. T2K-TN-80 v4. 24, 26, 27
- 689 [9] R. Das and Others. Measurement of induced charged current cross section on water
690 using the pød and tpc, November 2014. T2K-TN-100. 24
- 691

- 692 [10] K. Gilje. Geometry and mass of the π^0 detector in the nd280 basket, Apr 2012. T2K-
693 TN-73 v3.1. 27
- 694 [11] M. Hartz and Others. Constraining the flux and cross section models with data from
695 the nd280 detector for the 2014/15 oscillation analysis, May 2015. T2K-TN-220 v4. 14,
696 16
- 697 [12] M. Hartz and Others. Constraining the Flux and Cross Section Models with Data from
698 the ND280 Detector using FGD1 and FGD2 for the 2016 Joint Oscillation Analysis,
699 June 2016. T2K-TN-230 v3. 14
- 700 [13] A. Hillairet and Others. Nd280 reconstruction, Nov 2011. T2K-TN-72 v1. 27
- 701 [14] T. Koga. Comparison between banff post fit results and on-axis detectors, 2017. 10
- 702 [15] K. Mahn and Others. Implementation of new cross section parameters for the 2017
703 oscillation analysis, 2017. T2K-TN-307. 21
- 704 [16] G. Wikström and A. Finch. Global kalman vertexing in nd280, Feb 2018. T2K-TN-46
705 v3. 26
- 706 [17] T. Yuan and Others. Double differential measurement of the flux averaged ν_μ cc0pi
707 cross section on water, Aug 2016. T2K-TN-258 v4.6.1. 24, 26

708 **Nomenclature**

- 709 BANFF The **beam and near detector task force** is the group responsible for providing near
710 detector constraints on cross section and flux model parameters.
- 711 CC- 0π A **charged current zero pion** selection is an exclusive selection that selects neutrino
712 interaction topologies only one MIP-like particle.
- 713 CC-Inclusive A **charged current event** selection that selects all neutrino interaction topolo-
714 gies with an outgoing charged lepton.
- 715 FD The **far detector** refers to the particle detector in a long baseline neutrino oscilla-
716 tion experiment that is located far away from the neutrino production source where
717 oscillated neutrinos are observed.
- 718 FGD A **fine grain detector** is a detector made of closely spaced, small scintillating bars
719 designed to provide precise resolution of charged particle tracks
- 720 FHC The **forward horn current** beam configuration that focuses positively charged particles
721 into the particle decay pipe. This configuration produces a very pure ν_μ neutrino beam
- 722 HMNT The **highest momentum negatively-charged track** in the bunch
- 723 HMPT The **highest momentum positively-charged track** in the bunch
- 724 MIP A **minimum ionizing particle**
- 725 ND280 The **Near Detector** of T2K which is **280** meters away from the neutrino source.
- 726 ND The **near detector** refers to the particle detector in a long baseline neutrino oscillation
727 experiment that is located close to the neutrino production source before neutrino
728 oscillations occur.

729 CECal The **Central ECal** detector which is a part of the PØD inside ND280

730 PØD The π^0 detector (**pi-Q** detector)

731 PØDule A collection of two active scintillator bar layers inside the PØD

732 RHC The **reverse horn current** beam configuration that focuses negatively charged particles
733 into the particle decay pipe. This configuration produces a $\bar{\nu}_\mu$ enriched neutrino beam
734 with a significant ν_μ contribution.

735 FV The **fiducial volume** of a detector is the region where the detector response is well
736 understood

737 TPC A **time projection chamber** is a device that detects and tracks charged particles with
738 the application of strong electric fields

739 Tracker The region of ND280 consisting of two FGDs and TPCs

740 Global The **Global reconstruction module** responsible for making joined tracks between the
741 subdetectors inside ND280

742 USECal The **Upstream ECal** which is a part of the PØD inside ND280